Report No. FAA-RD-71-90

0004900

SONIC BOOM MINIMIZATION THROUGH AIR STREAM ALTERATION

F.W. Lipfert

GENERAL APPLIED SCIENCE LABORATORIES, INC.

An Affiliate of CCI Corporation

Merrick and Stewart Avenues

Westbury, New York 11590

transpo 72

U.S. International Transportation Exposition
Dulles International Airport
Washington, D.C.
May 27-June 4, 1972

JULY 1971

FINAL REPORT

Availability is unlimited. Document may be released to the National Technical Information Service, Springfield, Virginia 22151, for sale to the public.

Prepared for

DEPARTMENT OF TRANSPORTATION

FEDERAL AVIATION ADMINISTRATION

Systems Research & Development Service

Washington, D.C. 20591

This report has been prepared by General Applied Science Laboratories, Inc., for the Systems Research and Development Service, Federal Aviation Agency, under Contract No. DOT-FA70-WA-2320. The contents of this report reflect the views of the contractor, who is responsible for the facts and the accuracy of the data presented herein, and do not necessarily reflect the official views or policy of the FAA. This report does not constitute a standard, specification, or regulation.

TECHNICAL REPORT STANDARD TITLE PAGE

1. Report No. FAA-RD-71-90	2. Government Accession No.	3. Recipient's Catalog No.
4. Title and Subtitle SONIC BOOM MINIMIZATION THROUGH AIR STREAM ALTERATION		5. Report Date July 1971
		6. Performing Organization Code –
7. Author(s) F. W. Lipfert		8. Performing Organization Report No. TR-760
9. Performing Organization Name and Address General Applied Science Laboratories, Inc. Merrick & Stewart Avenues Westbury, New York 11590		10. Work Unit No. –
		11. Contract or Grant No. FA70-WA-2320
12. Sponsoring Agency Name and Address Department of Transportation Federal Aviation Administration Washington, D. C.		13. Type of Report and Period Covered Final Report March 1970-July 1971
		14. Sponsoring Agency Code
15. Supplementary Notes		

16. Abstract The potential of modifying supersonic aircraft sonic boom signatures by means of altering the flow field in the vicinity of the aircraft has been investigated theoretically. A specific airplane, the NASA SCAT-15F, was selected as a basis, and a cruise flight condition of Mach 2.7, 62,000 feet was chosen. Signatures were computed using real (1962) atmospheric properties. Finite rise times, reduced overpressures, and reduced shock pressure rises were among the sginature improvements investigated.

Flow field alteration mechanisms considered included free combustion, boundary layer mass addition, force fields, and laser-generated heat fields.

Weight penalties of the order of the baseline aircraft gross weight were found for all attempts to modify the complete baseline aircraft signature. If this additional weight were borne by the baseline aircraft, an additional overpressure would result which would, in many cases, negate the effect of the signature improvement.

Considerably smaller weight penalties (by factors of 4-5) were found to be required to create a precursor signal that would warn of the impending sonic boom. However, the merit of such a scheme must be established through testing of human subjects.

Finally, the concept of a separate "penalty aircraft" was put forth. This would be an aircraft, presumably carrying no payload, that would fly in close proximity (so that the sonic booms interfere) to the baseline aircraft and relieve the necessity of increasing the baseline aircraft gross weight because of sonic boom alleviation schemes. The additional weight would be borne by the penalty aircraft, and its lift distribution would be tailored to provide, in part, the desired combined signature.

17. Key Words Sonic boom theory Flow fields Free combustion Boundary layer mass addition Laser application		18. Distribution Statement Availability is unlimited. Document may be released to the National Tech. Information Service, Springfield, Virginia 22151. Available to the public.	
19. Security Classif. (of this report) Unclassified	20. Security Classif. (of this page) Unclassified	21. No. of Pages 129	22. Price $3.00 P.C. $ .95 M.F.

Form DOT F 1700.7 (8-69)

TECHNICAL REPORT DISCLAIMER TITLE PAGE

1. Report No. FAA-RD-71-90	2. Government Accession No.	3. Recipient's Catalog No.
4. Title and Subtitle SONIC BOOM MINIMIZATION THROUGH AIR STREAM ALTERATION		5. Report Date July 1971
		6. Performing Organization Code
7. Author(s) F. W. Lapiere		8. Performing Organization Report No. TED-70-7
9. Performing Organization Name and Address Central Applied Science Laboratories, Inc. Merrick & Stewart Avenues Westbury, New York 11590		10. Work Unit No.
		11. Contract or Grant No. FA70-WA-2320
12. Sponsoring Agency Name and Address Department of Transportation Federal Aviation Administration Washington, D. C.		13. Type of Report and Period Covered Final Report March 1970-July 1971
		14. Sponsoring Agency Code

15. Supplementary Notes

16. Abstract The potential of modifying supersonic aircraft-sonic boom characteristics by means of altering the flow field in the vicinity of the aircraft has been investigated theoretically. A specific airplane, the NASA SCAT-15F, was selected as a basis, and a cruise flight condition of Mach 2.7, 62,000 feet was chosen. Structures were computed using that (1962) atmospheric properties. Finite size cores, induced overpressures, and reduced shock pressure rise were among the signature improvements investigated.

Flow field alteration mechanisms considered included free combustion, boundary layer mass addition, force fields, and laser-generated heat fields.

Weight penalties of the order of the baseline aircraft gross weight were found for all attempts to modify the complete baseline aircraft-airframe. If this additional weight were borne by the baseline aircraft, an additional overpressure would result which would, in many cases, negate the effect of the alteration improvement.

Considerably smaller weight penalties for factors of 4-7 were found to be required to create a pressure signal that would warn of the impending sonic boom. However, the merit of such a scheme rest on actualized dynamic sensing of human endurance.

Finally, the concept of a separate "penalty aircraft" was put forth. This would be an artificial, pressure-only carrying no payload, that would fly in close proximity (as that the sonic boom lasting) to the baseline aircraft and reduce the necessity of increasing the baseline aircraft gross weight because of sonic boom alteration schemes. The additional weight would be borne by the commercial aircraft, and its air distribution would be tailored to provide, in part, the desired overhead signature.

17. Key Words Sonic boom theory Flow fields Free combustion Boundary layer mass addition Laser application		18. Distribution Statement Availability is unlimited. Document may be released to the National Tech. Information Service, Springfield, Virginia 22151. Available to the public.	
19. Security Classif. (of this report) Unclassified	20. Security Classif. (of this page) Unclassified	21. No. of Pages 120	22. Price $3.00 P.C. $1.25 M.F.

Form DOT F 1700.7 (8-69)

TABLE OF CONTENTS

SECTION	PAGE
INTRODUCTION	1
A. General	1
B. Background	1
C. Present Study Objectives	7
CALCULATION METHODS	8
A. Signature Calculation	8
B. Area and F-Function Calculations	16
C. Heat, Force and Mass Equivalency	18
DESIRED SIGNATURE MODIFICATION	23
A. Basic Signature Parameters	23
IDEALIZED SIGNATURE COMPUTATIONS	28
A. Finite Rise Time Requirements	28
B. Front Shock Elimination	32
C. Finite Rise Time - Rear Shock	39
D. Plateau Pressures	53
COMPOSITE SIGNATURE COMPUTATIONS	57
A. Finite Rise Time "Warnings"	58
B. Two-Step Signatures	62
C. Rear Shock Effects	67

LIST OF ILLUSTRATIONS (continued)

FIGURE		PAGE
22a	5/2 Body Area Requirements for Finite Rise Time - Front Shock	61
22b	5/2 Body Area Requirements for Finite Rise Time - Front Shock	61
23a	Interpolation Curve - Shock Pressure Rise vs Length	63
23b	Interpolation Curve - Rise Time vs Length	63
24	3/2 Power Body Signatures	64
25	Quadratic Body Signatures ($S = kx^2$)	65
26a	3/2 Quadratic Body Requirements - Front Shock Treatment	66
26b	3/2 Quadratic Body Requirements - Front Shock Treatment	66
27	Laser Energy Release Requirements for Thermal Pulse	74
28	Boundary Layer Blowing Effects on External Flow Deflection	80
29	Mass Flux Ratio Required for Flow Deflection Angle of 2°	82
30	Flow Deflection Resulting from Uniform Injection and Combustion of Hydrogen in Boundary Layer	83
31	Flow Deflection Angle Due to Boundary Layer with Zero Mass Injection	84
32	Schematic of Jet Flow with Combustion	86
33	Calculated Displacement Areas Due to Combustion	89
34a	Enthalpy Profile Comparison	91
34b	Velocity Profile Comparison	92
34c	Mass Flux Profile Comparison	93
35	Effect of Initial Length on Area Variation	
36	Breakdown Characteristics of Various Gases at $\lambda \cong .7\ \mu$ (Reference 36)	98
37	Optimum Thrust/Area Relationship for Turbojet Cycle	102
38	Variation of Thrust with Exit Area for Various Turbomachine Efficiencies	103

LIST OF ILLUSTRATIONS (continued)

FIGURE		PAGE
39	Variation of Specific Impulse with Exit Area for Various Turbomachine Efficiencies	104
40	Variation of Thrust with Exit Area for Various Exit Specific Heat Ratios	105
41	Variation of Specific Impulse with Exit Area for Various Exit Specific Heat Ratios	106
42	Thrust/Area Relationship for Ideal Turbomachine Efficiency	107
43	Variation of Baseline Front Shock ΔP with Gross Weight	116

Subscripts

A	volume
a	aircraft
c	compressor
g	ground
i	injectant
L	lift
m	maximum
o	initial or undisturbed value
p	penalty
ref	reference
t	turbine
v	volume
x	exit

INTRODUCTION

(A) General. The sonic boom is a persistent accomplice of supersonic flight, and may have varying non-negligible effects on people, structures and the ecology along the flight path. The complete sonic boom "problem" may be divided into three parts: source characteristics, effects of propagation through the atmosphere, and effects at the receptor. A great deal of effort has been devoted by researchers in the U.S. and abroad towards understanding and predicting the formation of pressure disturbances about supersonic vehicles, propagation of the resulting sonic boom and the effects of this boom on various receptors.

This study deals with modifications to be accomplished at or near the source in order to yield a more acceptable sonic boom signature at the receptor. Thus it is necessary to consider all portions of the problem, not only the source modifications themselves, but their effect on propagation phenomena, and of course, the types of ground signatures that are desirable for various receptors.

(B) Background. The idea of sonic boom alleviation or minimization is not new and has been the subject of many previous papers and approaches. An excellent summary is given by Seebass[1] beginning with Busemann and his famous biplane (which eliminates the boom due to aircraft volume), and

presenting some recent calculations which define various minima for propagation in an isothermal atmosphere. These minimization calculations all deal with idealized sources with prescribed Whitham F-functions(the fundamental descriptor of the pressure distribution near the airplane).

However, there is another class of minimization processes, to which the present study rightfully belongs, that deals with physical processes that could conceivably be included in a real flight system to modify the flow characteristics near the airplane in such a way to improve its ground signature. Table I summarizes some of the past efforts along these lines.

Cahn and Andrew[2] proposed, in a controversial paper in 1968, an electroaerodynamic scheme of creating a reduced shock wave strength by means of static charges. Their paper was then analyzed by Cheng and Goldburg[3], who assigned unit weight penalties for the electrical equipment required for the scheme. Unfortunately, their analysis did not include a realistic assessment of the effects of the electrical forces on the boom signature.

TABLE I

PREVIOUS INVESTIGATIONS

	Reference	Mechanism	Flow Effect	Modified Signature	Penalties
2	Cahn & Andrew AIAA 68-24	electroaerodynamics	"diffusive bow shock"	-	-
3	Cheng & Goldburg AIAA 69-38	electroaerodynamics	stream thrust (effective blunt body)	-	200-2000 lb wt lb force
4	R. L. Chuan U. S. Patent 3510095	mass removal	air condensation (cryopumping)	estimated to be plateau type	limited to flow in A/C boundary layer
5	Carlson & Miller NASA TN D-5582	heat fields force fields	{channel flow + and - power} {extra drag	finite rise time $0<t_r<0.4$ sec	$\ell > 1040$ ft $p \sim 550$ mw
6	Batdorf AIAA 70-1323	heat field	displacement due to density (small perturb.)	finite rise time-10 msec (no signature given)	reshaped A/C 200 mw 37% extrapol.
7	Resler AFOSR-UTIAS Symp. -'68	1 family waves or Buseman Biplane	streamtube contraction	reduced ΔP	increased drag redesigned engine
9	Rethorst AFFDL-TR-69-62				

Chuan's patent[4] deals with mass removal from the airstream through air condensation in the aircraft boundary layer. This would effect a fractional reduction of the portion of the sonic boom due to volume , while having no benefit to the portion due to lift.

The concept of tailored heat fields which create in effect a "phantom" aircraft extension has been put forth in References 5 and 6, and has the potential for substantial changes to the ground signature, in contrast to the preceding schemes. The basic idea is to create a flow displacement through combustion which, when superimposed on the basic aircraft shape and lift distribution, creates a specified ground signature. In this case, a signature having finite rise time instead of an initial shock was chosen; the merits of finite rise time signatures are discussed below on page 23.

Both heat and force fields were considered in the Carlson and Miller study.[5] However, in order to completely cancel the shocks, it was found necessary to both add heat in some regions and remove it in others. Large quantities of heat may readily be added through combustion, but no such potentially light-weight mechanism exists for cooling. In addition, the force fields considered were deployed in the axial direction, which has serious implications with regard to aircraft propulsion.

Batdorf[6] eliminated the cooling requirment very conveniently by postulating a reshaped airplane, such that the heat field is required mainly for creating a phantom nose of about 200 feet. The baseline aircraft lift and volume distribution are thus no longer free parameters, but must combine with the thermal nose in a prescribed way for that particular flight condition. As discussed below, this requires a variation of the total aircraft effective area (combined effects of lift, volume, and heating) as the 5/2 power of the distance from the phantom nose. The effect on the rear shock was not considered.

A useful concept presented by Batdorf and considered by others as well, is that of off-axis superposition of effects. According to linearized theory, observers on the ground cannot distinguish from which location in space disturbances along a given Mach line emanate; thus a lengthening effect may be accomplished by extending a phantom body downward from the aircraft or by deploying a parallel body below (Figure 1). This technique eliminates the problem of heating the baseline aircraft itself by the boom-alleviating heat field. Batdorf's concept employed a "thermal keel" extending downward and consisting of a series of ramburners in parallel. The propulsive and control implications of this scheme were not considered.

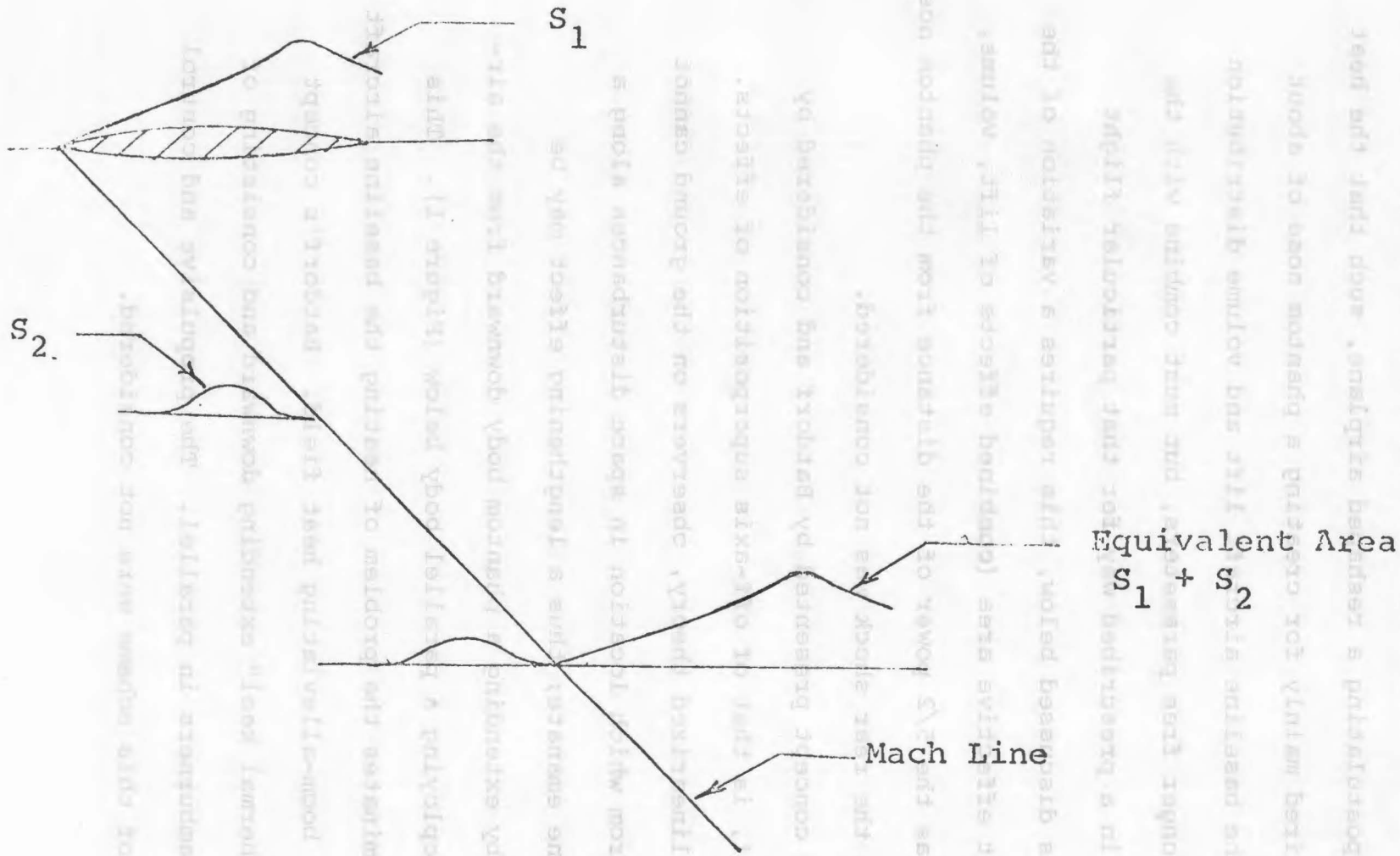

FIGURE 1 - SCHEMATIC OF OFF AXIS AREA RULE STACKING

The final class of sonic boom alleviation schemes considered in the past is concerned with streamtube contraction by the propulsion system. Resler[7] noted that a "negative" volume effect could be used to cancel a portion of the lift effect if an engine could be designed whose exit cross-sectional area was less than the inlet. Galanis[8] examined the concomitant engine requirements, concluding that a new cycle with airstream cooling was required using the fuel as a heat sink. The area reduction possibilities using conventional engines were examined in the present study, and are presented in pages 100-107. Rethorst's concept[9] was similar in that powerplant streamtube contraction was also required, albeit implicitly. Also both concepts involved wing configurations with lift from the top surface only (the bottom behaves as a flat plate); such wings provide only half the lift at the same wave drag and thus would involve a structural weight penalty when employed in a real aircraft.

(C) Present Study Objectives. The objective of the present study was to consider all identifiable means of altering the flow near the aircraft that could improve the ground signature, to examine the technical feasibility and practicality of achieving the desired flow field modifications, and to include a realistic assessment of the aircraft penalties incurred in the implementation of these various means.

Accordingly, a realistic SST configuration was desired for use as a baseline. The characteristics of the NASA SCAT-15F configuration were obtained through the courtesy of Mr. Harry Carlson of the Langley Research Center, and this baseline was retained throughout the study. A cruise condition was selected, with flight at Mach 2.7, 62,000 feet, and a gross weight of 600,000 lbs. The baseline aircraft length was 298 feet.

Although a wide range of flow field alteration schemes was considered, the study was limited to ideas for which the penalties to the aircraft could be defined and readily calculated. No changes to the volume or lift distributions of the baseline aircraft were allowed.

CALCULATION METHODS

(A) Signature Calculation. In order to provide maximum realism in the signature calculations, the computer program "Sonic Boom Propagation in a Stratified Atmosphere," by Hayes and his co-workers[10] was obtained. The program was operated using the ARDC 1962 Standard Atmosphere mode for an aircraft in straight and level flight during supersonic cruise (steady).

A comparison of the baseline aircraft signature front shock strength as estimated from various methods is given in Table II. The signature is shown in Figure 2, together with the F-function for lift and volume and the total effective area. The front shock overpressure is 1.84 psf., based on a ground reflection factor of 1.8 (which has been used throughout).

Based on Whitham's far field expression for the front shock strength

$$\Delta P/P_{ref} = k_r (2\beta)^{\frac{1}{4}} \frac{\gamma}{\sqrt{\gamma+1}} \frac{\left[\int_0^{y_m} F(x)\,dx\right]^{\frac{1}{2}}}{h^{3/4}} \qquad (1)$$

where y_m is the value of x which yields the maximum positive value of the integral, a value of $\Delta P/P_{ref} = .0031$ is obtained. Now P_{ref} is frequently taken as $\sqrt{P_a P_g}$, in which case the overpressure would be obtained as 1.65 psf. However, George and Plotkin[11] have given a more accurate estimate of $P_{ref}/\sqrt{P_a P_g}$, and using their results, the overpressure due to (1) is found to be 1.86 psf. Thus, although the baseline point selected is not truly far field, as has been pointed out by many investigators, the midfield effects are quite small. This is consistent with McLean's results,[12] which showed large midfield effects (lower overpressures) at M = 1.414, and practically none at M = 2.7, particularly for realistic aircraft shapes. For idealized pointed bodies, (no immediate shock formed), there was still some effect at Mach 2.7 in McLean's results.

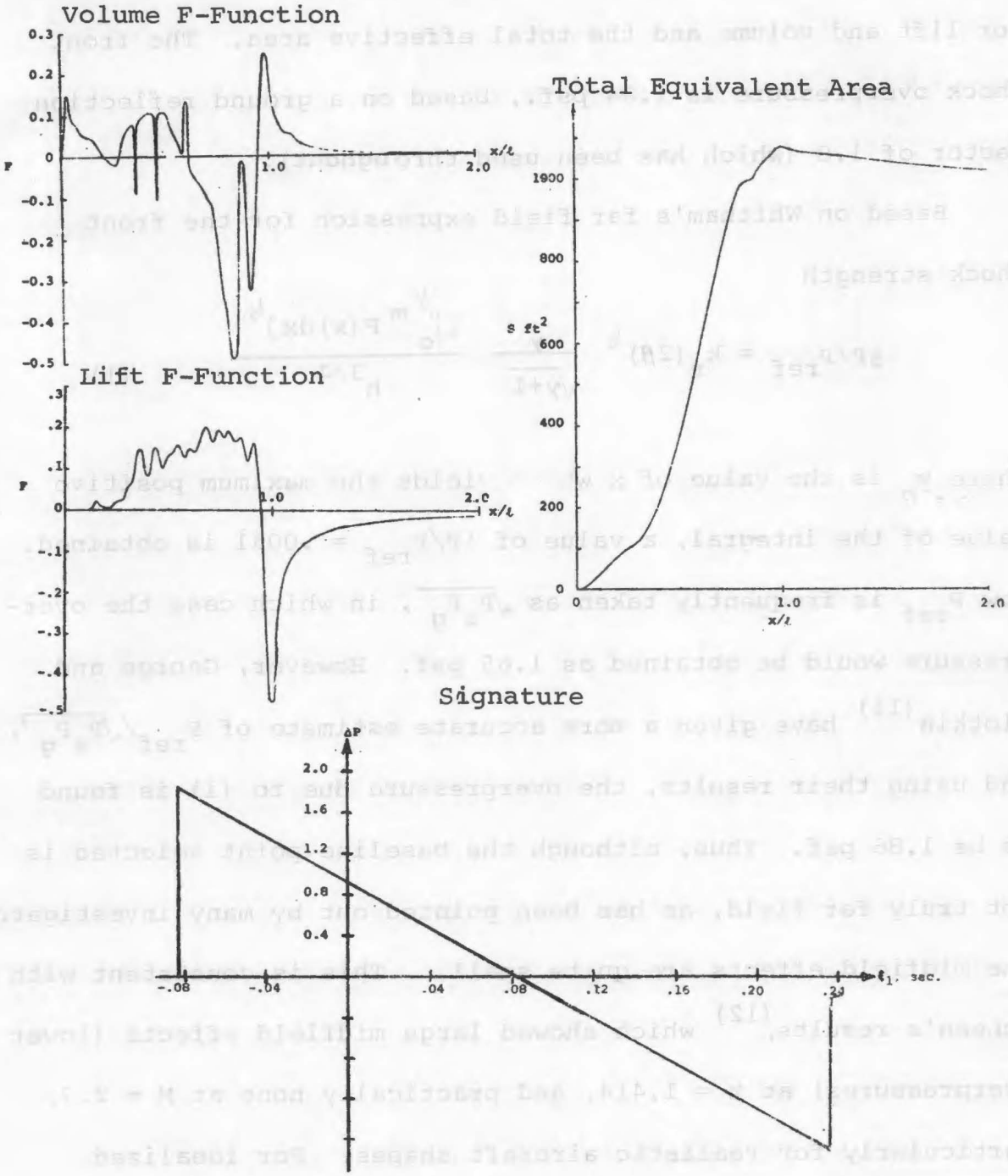

FIGURE 2 - Baseline Airplane Characteristics

For comparison purposes, the Jones' far field minimum overpressure values are listed in Table II, according to Jones[13] and Seebass,[1] for W = 600,000 lbs, M = 2.7, h = 62,000 feet, and K_r = 1.8. The Jones expression in (13) is

$$\frac{\Delta P}{P} = \frac{(2\beta)^{\frac{1}{4}}\gamma}{\sqrt{\gamma + 1}} \frac{1}{h^{3/4}} \left[\frac{1}{4\sqrt{\ell}} \frac{\beta W}{\rho v^2} \right]^{\frac{1}{2}} \qquad (2)$$

and is based on the use of a δ function in the effective area distribution.

Since additional effective aircraft lengths were to be considered in the signature modification, the "advance" used in the signature determination is of interest. The advance of a portion of the signal with respect to a base point is, of course, a result of the faster propagation of those portions of the signal with greater overpressure. This phenomenon gives rise to shocks even for bodies whose effective area distributions are perfectly smooth and have no local shocks attached. The Hayes program accounts for this by the use of a variable referred to as "age" defined as

$$\tau = \frac{\gamma+1}{2v} \int_{-z} \frac{d(-z)}{a \sin\theta \cos\theta \sqrt{\rho A \sin\theta \cos\theta}} \qquad (3)$$

TABLE II

BASELINE SIGNATURE FRONT SHOCK STRENGTH

(K_r = 1.8)

Method	Value - psf	$P_{ref.}$
Computer program (Ref. 10)	1.84	real atm.
Whitham far field	1.65	$\sqrt{P_a P_g}$
	1.86	real atm. correction (11)
Jones' Far Field Minimum Values		
Reference 13	1.476	real atm. correction (11)
Reference 1	1.586	H = 25,000 ft.

This integral is evaluated numerically in the program, and of course may be solved in closed form for either uniform or isothermal atmospheres. A comparison for h = 62,000 ft. is given in Figure 3; since the standard atmosphere is isothermal from 36,000 - 60,000 ft., the agreement between the real and isothermal atmosphere (when H = 20,700 ft.) is excellent, this demonstrates the "freezing" effect mentioned by Hayes and others; i.e., most of the age or distortion of the signal due to non-linear advance occurs in the first one or two scale heights away from the aircraft. However, as pointed out by George and Plotkin, it is necessary to take other values for H in order to obtain correct overpressure magnitudes; Seebass in (1) used H = 25,000 feet as a compromise, for example.

The difference in age between uniform and real atmospheres at 60,000 feet will be seen in the subsequent sections to have a substantial favorable effect on the aircraft length required for mid field effects to persist.

The effect of altitude on the propagation of the baseline signature may be seen from Figure 4 which shows the signature for various pseudo ground locations. A reflection factor of 1.0 is used for $h_g > 0$. The geometrical acoustic theory upon which the Hayes' program is based is not strictly

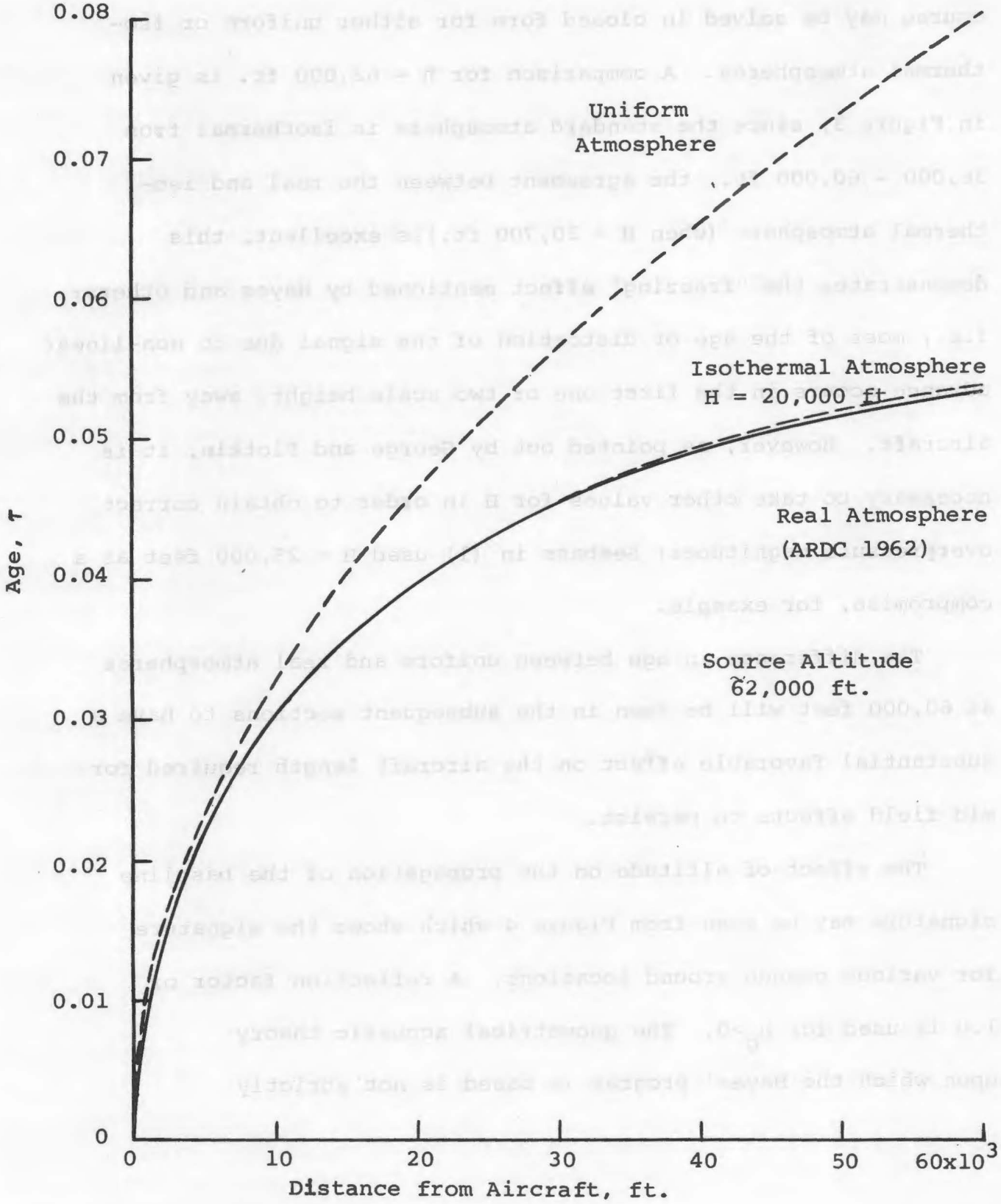

FIGURE 3 - Age Variable for Various Atmospheres

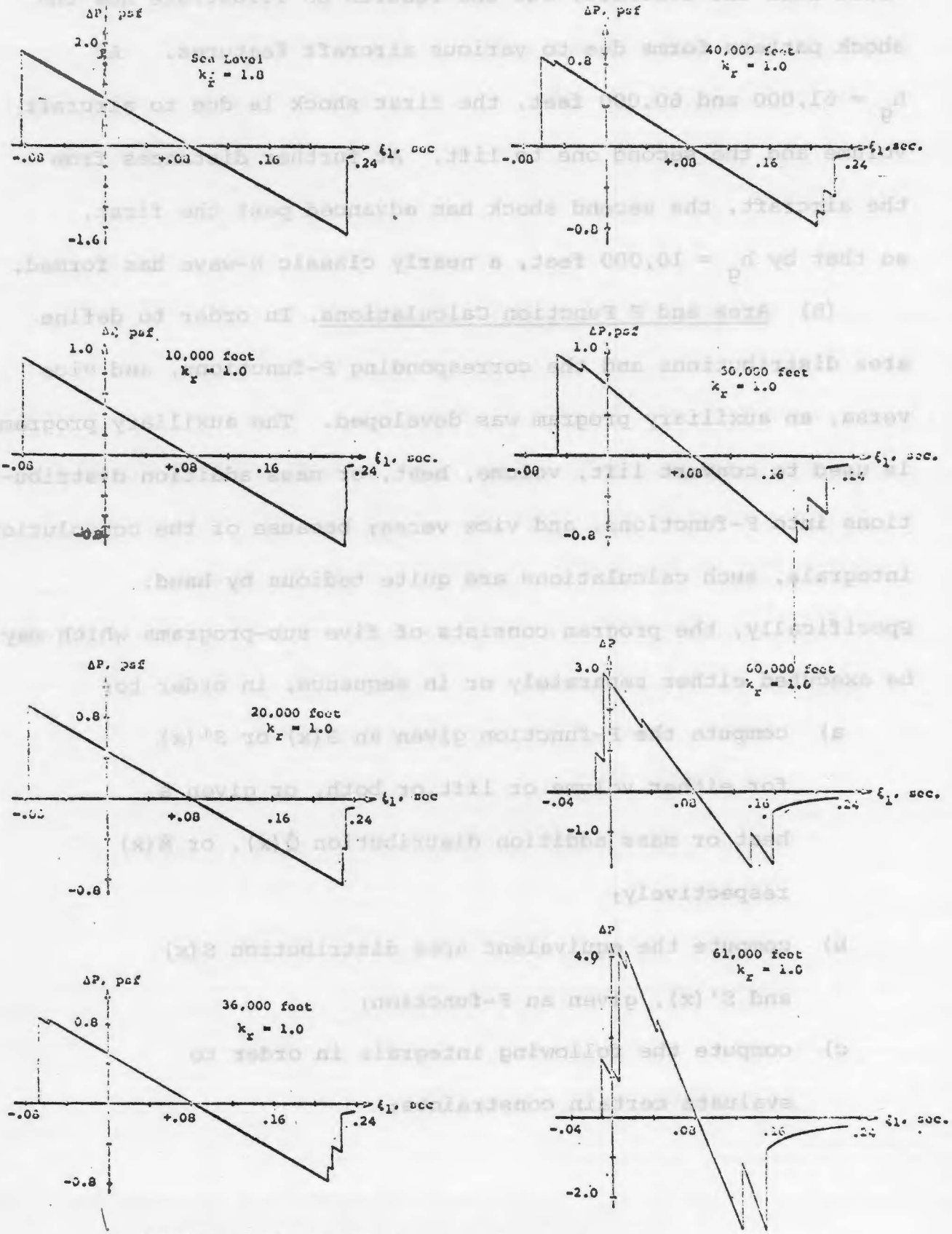

FIGURE 4 - Baseline Signature Development - Aircraft at 62,000 ft.

valid near the aircraft, but the results do illustrate how the shock pattern forms due to various aircraft features. At h_g = 61,000 and 60,000 feet, the first shock is due to aircraft volume and the second one to lift. At further distances from the aircraft, the second shock has advanced past the first, so that by h_g = 10,000 feet, a nearly classic N-wave has formed.

(B) Area and F Function Calculations. In order to define area distributions and the corresponding F-functions, and vice versa, an auxiliary program was developed. The auxiliary program is used to convert lift, volume, heat, or mass addition distributions into F-functions, and vice versa; because of the convolution integrals, such calculations are quite tedious by hand. Specifically, the program consists of five sub-programs which may be executed either separately or in sequence, in order to:

a) compute the F-function given an S(x) or S'(x) for either volume or lift,or both, or given a heat or mass addition distribution $\dot{Q}(x)$, or $\dot{M}(x)$ respectively;

b) compute the equivalent area distribution S(x) and S'(x), given an F-function;

c) compute the following integrals in order to evaluate certain constraints:

aircraft lift: $\int_0^{\ell} F(t)\sqrt{\ell-t}\,dt$

aircraft volume: $\int_0^{\ell} F(t)\,(\ell-t)^{3/2}\,dt$

F function closure: $\int_{-\infty}^{\infty} F(t)\,dt$;

d) calculate the wave drag coefficient from the F function;

e) convert the normalized F-functions for lift and volume to physical values associated with a given vehicle geometry and flight condition.

This program was used to compute the effective area distribution of the baseline aircraft, based on the F function, which had been supplied. This area distribution was then used for recomputing new F functions with flow field modification effects superposed. It was also used, as a check on numerical integration accuracy, to recompute the original baseline F function, which it did satisfactorily with the exception of exact reproduction of peak spike points.

(C) Heat, Force, and Mass Equivalency. The effects of heat, force and mass distribution on the flow field may be computed in several ways. Reference 5, for example, adopts a one-dimensional stream tube approach. Unfortunately, this approach requires the specification of a stream tube "capture area" over which the desired flow field alteration mechanism acts.

This limitation may be avoided through the use of the linearized equations following Chu.[14,15] This approach is limited to the basic linearization assumptions; for example, the rate of heat release should be

$$\frac{q}{a_o p_o} << 1$$

At Mach 2.7, 62,000 feet, this statement is equivalent to specifying that the heat release be much less than 340 BTU/lb of free stream air and implies very small global equivalence ratios (φ), since stoichiometric combustion (φ=1) of ordinary hydrocarbon fuel releases about 1200 BTU/lb of air.

While, in the case of free stream combustion this small perturbation limitation may seem restrictive, it is completely consistent with the use of the Whitham theory for the boom signature and with the generally quite slender pointed bodies contemplated for aircraft extensions. It is also consistent with boundary layer phenomena associated with mass injection.

The basic equations of motion are given as:

$$\frac{d\rho}{dt} + \rho \nabla\cdot\vec{V} = \dot{M}$$

$$\rho \frac{d\vec{V}}{dt} + \nabla p = \vec{F} + \nabla\cdot\bar{\bar{\tau}}$$

$$\frac{1}{\rho a^2}\frac{dp}{dt} - \frac{1}{\rho}\frac{d\rho}{dt} = \frac{\dot{Q}}{\rho C_p T} - \frac{\nabla\cdot\vec{q}}{\rho C_p T} + \frac{\Gamma}{\rho C_p T}$$

$$a^2 = \gamma \frac{p}{\rho}$$

where

$\dot{M}$ = injected mass per unit vol. per sec.

$\bar{\bar{\tau}}$ = viscous stress tensor

$\bar{F}$ = body forces

$\dot{Q}$ = heat release per unit vol. per sec. due to chemical release

$\nabla\cdot\vec{q}$ = heat release due to conduction

Γ = heat release due to viscous dissipation

Linearizing and neglecting transport terms $\bar{\bar{\tau}}$, $\vec{q}$, Γ

$$\frac{d\rho}{dt} + \rho_o \nabla\cdot\vec{V} = \dot{M} \tag{4}$$

$$\rho_o \frac{d\vec{V}}{dt} + \nabla p = \vec{F} \tag{5}$$

$$\frac{1}{\rho_o a_o^2}\frac{dp}{dt} - \frac{1}{\rho_o}\frac{d\rho}{dt} = \frac{\dot{Q}}{\rho_o C_p T_o} \tag{6}$$

$$\left[\frac{d}{dt} = \frac{\partial}{\partial t} + U_o \frac{\partial}{\partial x}\right]$$

When $\dot{M}$, $\vec{F}$, $\dot{Q}$ are all zero, we have the usual homogeneous system of pár-partial differential equations with lift and volume boundary conditions on the vehicle surface. For a slender body in steady supersonic flight, $\frac{d}{dt} = U_o \frac{\partial}{\partial x}$, and the linearized pressure field is easy to determine;

$$p \simeq \frac{1}{2\pi} \frac{\rho_o U_o^2}{\sqrt{2\beta r}} \int_o^{x-\beta r} \frac{S_v''(\xi) + \frac{\beta}{\rho_o U_o^2} \ell'(\xi)}{\sqrt{x-\beta r-\xi}} d\xi \qquad (7)$$

This expression is then corrected for far-field wave steepening in order to compute the ground signature.

Because of our linearizing assumptions we can find the effects of $\dot{M}$, $\dot{Q}$, and $\vec{F}$, independently of the lift and volume, ℓ and S_v, and of each other, and superpose.

From energy and mass conservation (6) and (4) we eliminate ρ;

$$\frac{1}{C_o^2} \frac{dp}{dt} + \rho_o \nabla \cdot \vec{V} = \dot{M} + \frac{\dot{Q}}{C_p T_o} \qquad (8)$$

From the momentum equations, (5), eliminate $\vec{V}$,

$$\frac{1}{C_o^2} \frac{d^2 p}{dt^2} - \nabla^2 p = \frac{d}{dt} [\dot{M} + \frac{\dot{Q}}{C_p T_o}] - \nabla \cdot \vec{F} \qquad (9)$$

Say $\dot{M}$, $\dot{Q}$, and $\vec{F}$ are concentrated along the axis. The effect of a concentrated region of body force is indistinguishable

from the usual line distribution of lift, ℓ, and can be absorbed into it. The $\dot{M}$ and $\dot{Q}$ effects are axisymmetric, so that

$$\nabla^2 = \frac{\partial^2}{\partial x^2} + \frac{1}{r}\frac{\partial}{\partial r} r \frac{\partial}{\partial r}$$

$$\dot{M} = M \quad (x)\ \delta(r)$$

$$\dot{Q} = \sigma(x)\ \delta(r)$$

$$\int_0^{2\pi}\int_0^{\epsilon} \delta(r)\ r dr d\theta \equiv 1$$

or

$$\beta^2 \frac{\partial^2 p}{\partial x^2} - \frac{1}{r}\frac{\partial}{\partial r}\left(r \frac{\partial p}{\partial r}\right) = U \frac{\partial}{\partial x}\left(m + \frac{\sigma}{C_p T}\right)\ \delta(r) = T_x \delta(r) \qquad (10)$$

This equation has the solution

$$p(x,r) = \frac{1}{2\pi}\int_0^{x-\beta r} \frac{T(\xi)}{\sqrt{(x-\xi)^2 - \beta^2 r^2}}\, d\xi \simeq \frac{1}{2\pi\sqrt{2\beta r}}\int_0^{x-\beta r} \frac{T(\xi)\, d\xi}{\sqrt{x-\beta r-\xi}} \qquad (11)$$

This is of the same form as (7), if we define a total area

$$S''(x) = S''_v(x) + \frac{\beta}{2q}\,\ell'(x) + \frac{M'(x)}{\rho_i U_o} + \frac{\sigma'(x)}{\rho_o U_o C_p T_o} \qquad (12)$$

These terms of Eq. (12) give us the desired equivalency of force fields (lift), mass injection, and heat release.

When viscosity, conduction, diffusion and chemical coupling effects are not negligible, then the corresponding real gas flow problem is solved to find the resulting position of the dividing streamline and S_m' and S_δ' .

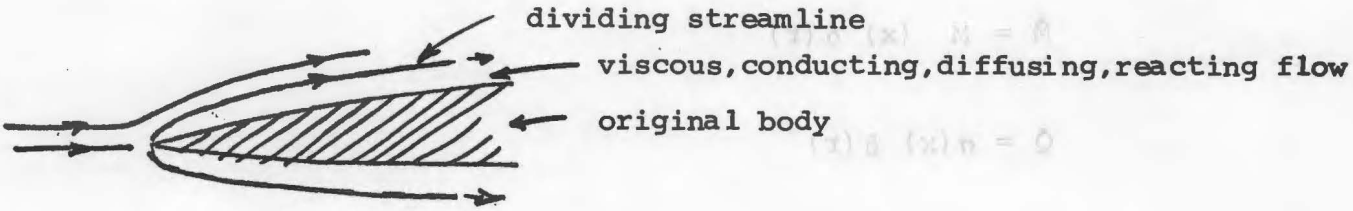

Note that the dividing streamline is unique and no anomolous behavior arises either in the inviscid or real gas formulation (such as seem to arise in the one-dimensional stream tube formulation).

DESIRED SIGNATURE MODIFICATIONS

(A) Basic Signature Parameters. A sonic boom may be characterized by several parameters. These include:

(1) rise time, Δt

(2) shock pressure rise, ΔP_s

(3) peak overpressure, ΔP_{max}

(4) total impulse, $\int_{t_{max}}^{t_1} (\Delta P)\,dt$

(5) wave length, t_{max} ,

and are illustrated in Figure 5 . Each contributes to the degree of annoyance or structural damage associated with the signature.

Rise time is related to the so-called startle effect, an important aspect of human response. Laboratory studies have shown that very small increases in rise time can lower the apparent loudness of the signal appreciably, as shown in Figure 6 , the data for which was taken from Reference 16. These effects apply only to outdoor observers, since the response indoors is appreciably altered by the structure. Figure 6 would imply that, considering only human annoyance effects, a substantial increase in overpressure could be tolerated from signature modifications that provide sufficient finite rise time. It should be noted that atmospheric effects can provide some thickening of the shock wave such that the "normal" rise time is frequently taken around 3 msec.

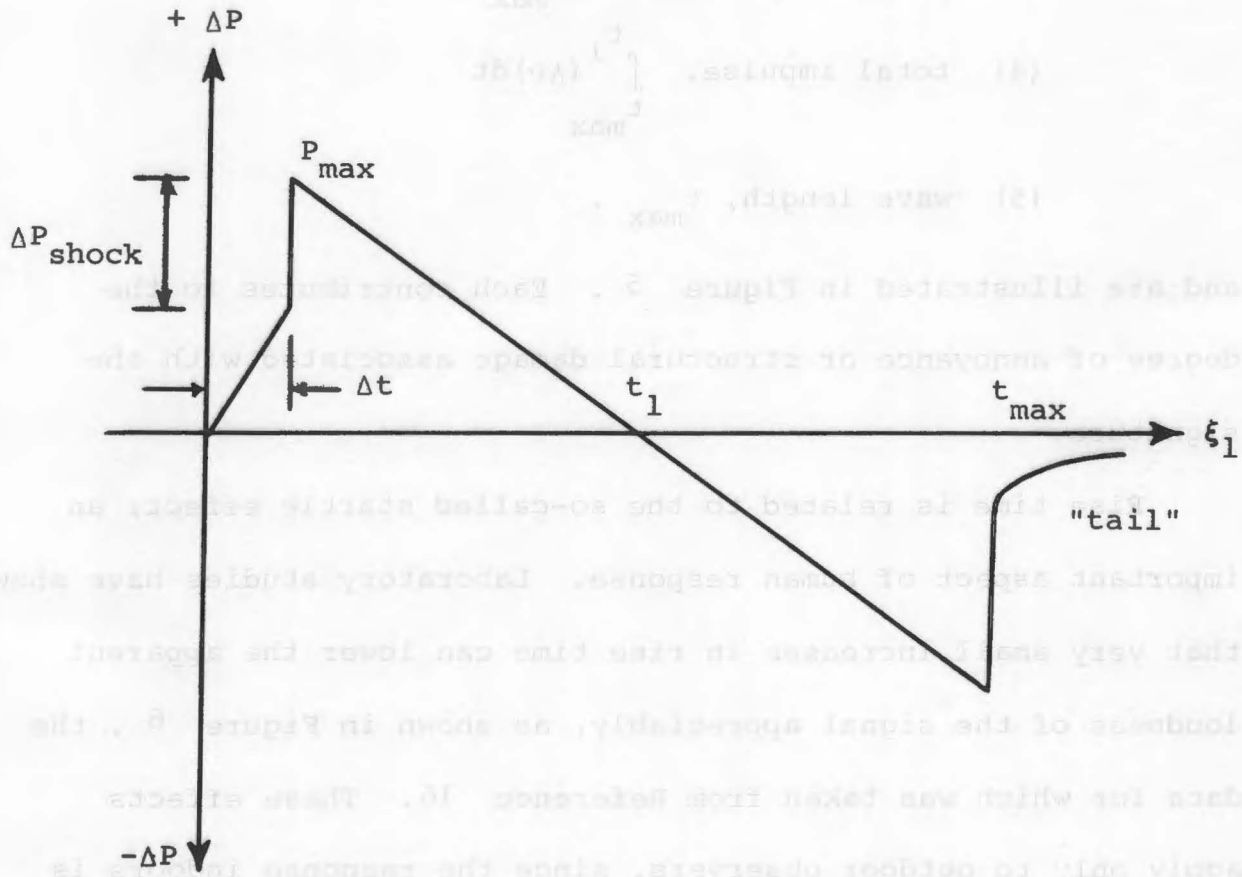

FIGURE 5 - Sonic Boom Signature Parameters

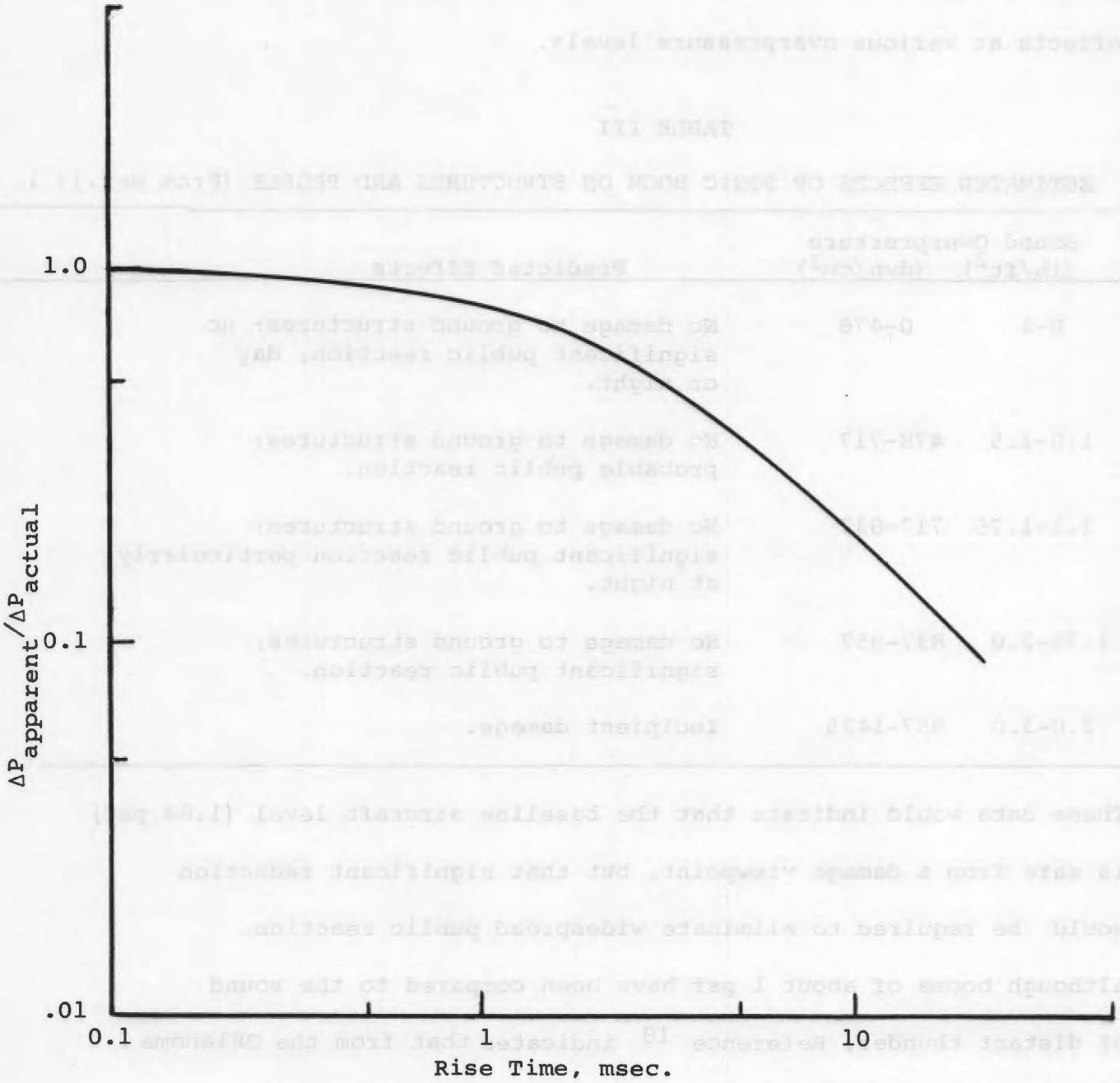

FIGURE 6 - Effect of Finite Rise Time on Perceived Sound Pressure (From Reference 16)

Shock pressure rise is another important parameter with regard to human annoyance, as well as structural damage. Table III presents some estimates from Reference [17] of the effects at various overpressure levels.

TABLE III

ESTIMATED EFFECTS OF SONIC BOOM ON STRUCTURES AND PEOPLE (From Ref.17)

Sound Overpressure (lb/ft^2)	(dyn/cm^2)	Predicted Effects
0-1	0-478	No damage to ground structures; no significant public reaction, day or night.
1.0-1.5	478-717	No damage to ground structures; probable public reaction.
1.5-1.75	717-837	No damage to ground structures; significant public reaction particularly at night.
1.75-2.0	837-957	No damage to ground structures; significant public reaction.
2.0-3.0	957-1435	Incipient damage.

These data would indicate that the baseline aircraft level (1.84 psf) is safe from a damage viewpoint, but that significant reduction would be required to eliminate widespread public reaction. Although booms of about 1 psf have been compared to the sound of distant thunder, Reference [18] indicates that from the Oklahoma City tests, a maximum tolerable shock pressure rise level is on the order of 0.4 psf.

The last three parameters, peak overpressure, total impulse, and signature wave length, are important in assessing structural damage. The impulse of a signature has meaning when its duration is small with respect to the fundamental vibratory period of the structure. This is the case for large buildings (~10 story)and small airplanes.

Reference 19 contains a great deal of data with regard to sonic boom structural damage. Some of the conclusions are repeated below:

(1) glass damage - Some damage at all overpressure levels can be expected, but probability levels less than 10^{-5} boom-sample* are predicted for large windows at overpressures below 3 psf.

(2) building damage - From tests at White Sands, a threshold value of about 16 psf was found for cumulative damage. At 2.0 psf, about 19 structures per million could be expected to suffer cumulative damage.

Thus the most common source of complaints, private dwellings, could not be significantly influenced by impulse changes associated with lengthened signatures at roughly constant overpressure level. This is also shown analytically in Reference 20, which considers sonic boom transmission through open windows, and shows the duration of the wave to have small effect if it is sufficiently large with respect to the room volume.

---

* 1 damage occurrence for every 10^5 (boom occurrence and sample window)

IDEALIZED SIGNATURE COMPUTATIONS

(A) Finite Rise Time Requirements. The requirement for a finite rise time signature to be felt on the ground is a single valued F-function or pressure signature after non-linear steepening has occurred. Although this is commonly translated into a requirement for a linearly varying F-function, which in turn results from a 5/2 power law area development, there are other possibilities as pointed out by Howell,[21] for example. The sketch below illustrates the steepening of signatures for bodies with various exponents of area development, $S = Kx^n$,

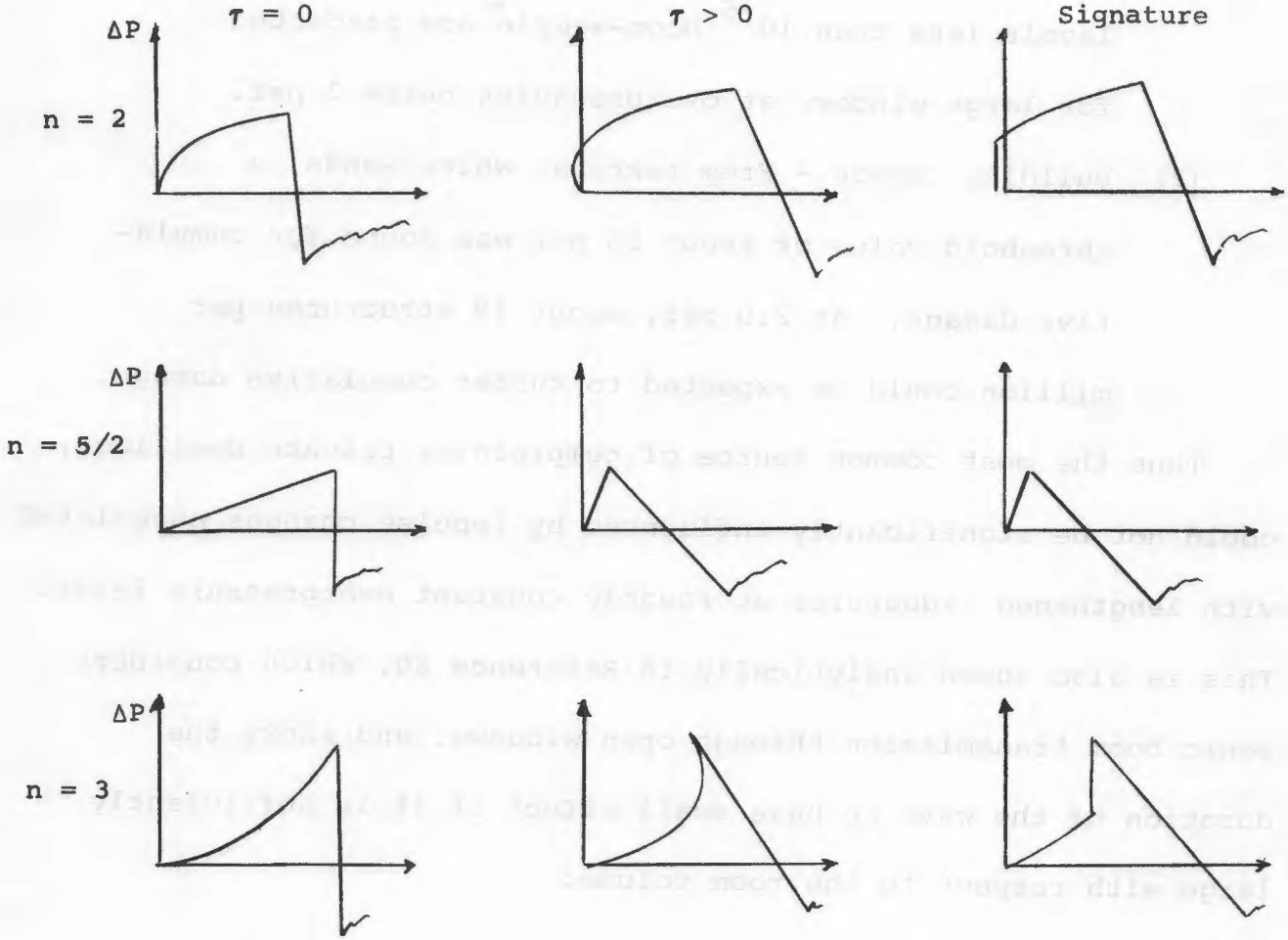

The critical point for shock formation is thus given by the slope of the distorted F-function, when it becomes either infinite or negative. Analytically, the following development illustrates the limitation:

$$F(x,\theta) = \frac{1}{2\pi}\int_0^x \frac{S''(t,\theta)}{\sqrt{x-t}}\,dt \tag{13}$$

For $S \alpha t^n$ then $F \alpha t^{n-3/2}$

After some advance in the signal τ, (age > 0,

$$\xi = \xi_o - \tau F,$$

therefore the slope of the distorted signal is given by

$$\mu = \frac{(n-3/2)\,K\,\xi^{(n-5/2)}}{1-(n-3/2)\;\tau K\;\xi^{(n-5/2)}}.$$

For $n = 5/2$, $\mu = \dfrac{K}{1-\tau K}$,

or the slope is positive (finite rise time) for $\tau K < 1$,

For $n = 3$, $\mu = \dfrac{3/2\;K\;\xi^{\frac{1}{2}}}{1-3/2\;\tau K\;\xi^{\frac{1}{2}}}$

μ is positive and finite for some values of ξ and τ.

For $n = 2$, $\mu = \dfrac{1/2K}{\xi^{\frac{1}{2}} - 1/2\ \tau K}$, and for $\xi = 0$, μ = negative, then a shock forms immediately, followed by finite rise times.

For $n = 3/2$, $\mu = 0$, but since F = constant, a shock is alwasy present.

This analysis shows that finite rise times are possible for $n > 5/2$, but that the permissible age will decrease (or required length will increase) for $n > 5/2$. Figure 7 gives the relative aircraft lengths and areas for various n values. Furthermore, in cases for which the area development of the "phantom" body must be matched to a given value of S' of the actual aircraft (discussed below), calculations showed that the minimum area for finite rise time also results at $n = 5/2$. For this reason, finite rise time computations were concentrated on 5/2 power law bodies.

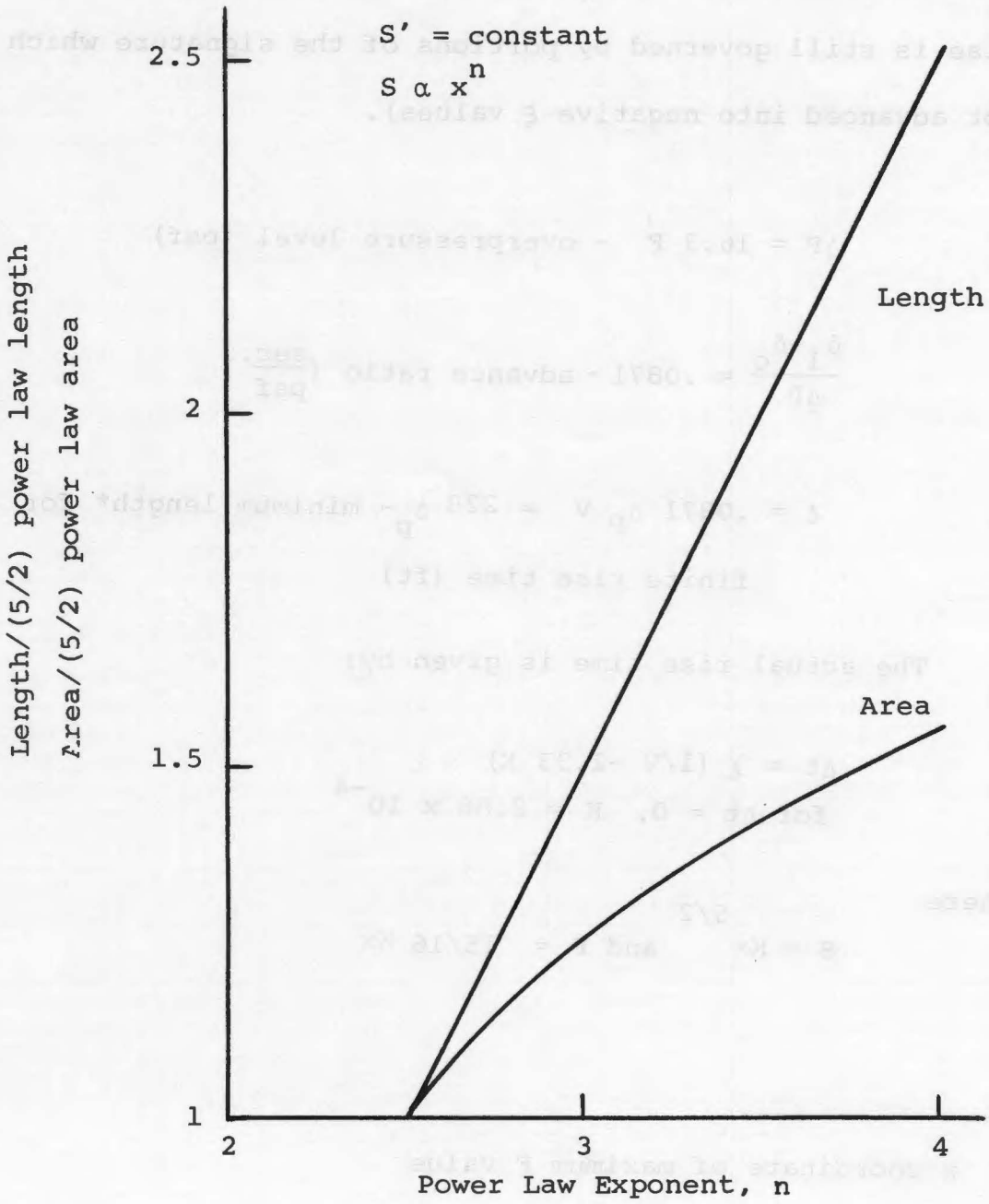

FIGURE 7 - Area and Length Ratios for Finite-Rise-Time Power Law Bodies

(B) Front Shock Elimination. The following formulas then apply for 5/2 power law bodies, for the age variable consistent with flight at Mach 2.7 and 62,000 feet (age = .05375), and provided mid field effects apply (i.e., the front shock pressure rise is still governed by portions of the signature which have not advanced into negative ξ values).

$$\Delta P = 16.3\ F \quad \text{- overpressure level (psf)}$$

$$\frac{\delta_1 - \delta_o}{\Delta P} = .0871 \text{ - advance ratio } \left(\frac{\text{sec.}}{\text{psf}}\right)$$

$$\ell = .0871\ \Delta_p\ V = 228\ \Delta_p \text{ - minimum length* for finite rise time (ft)}$$

The actual rise time is given by:

$$\Delta t = \ell\ (1/V - 1.33\ K)$$

$$\text{for } \Delta t = 0, \quad K = 2.86 \times 10^{-4}$$

where

$$S = Kx^{5/2} \quad \text{and } F = 15/16\ Kx$$

---

* x coordinate of maximum F value

Thus the aircraft length required for finite rise depends not only on the proper shaping ($S = Kx^{5/2}$) but also on the overpressure level, i.e., the value of K. There are several constraints that may be applied in considering this problem:

(1) gross weight of an ideally shaped airplane

$$W \propto \int_0^{\ell} F(t)\, dt \quad , \quad S(\ell) = \frac{\beta W}{\rho V_\infty^2}$$

or for $$S = Kx^{5/2}, \quad K = \frac{\beta W}{\rho V_\infty^2}\, \ell^{-5/2}$$

Considering a finite rise time positive signature only (no rear shock treatment) the length required for various rise times as a function of gross weight is given in Figure 8. This is about 10% greater than predicted by Seebass[1] for an isothermal atmosphere, 10% less than McLean for a uniform atmosphere[12] and about 40% shorter than that given by Batdorf[6]. Altitude variations are given in Figure 9. for constant Mach number and gross weight, assuming no volume contribution to the signature.

Figure 8 also presents curves of maximum overpressure and impulse for the same conditions. It is seen that the increased slenderness required for increasing (finite) rise time leads to lower overpressures and very slightly lower impulse. The degree of slenderness required for this family of

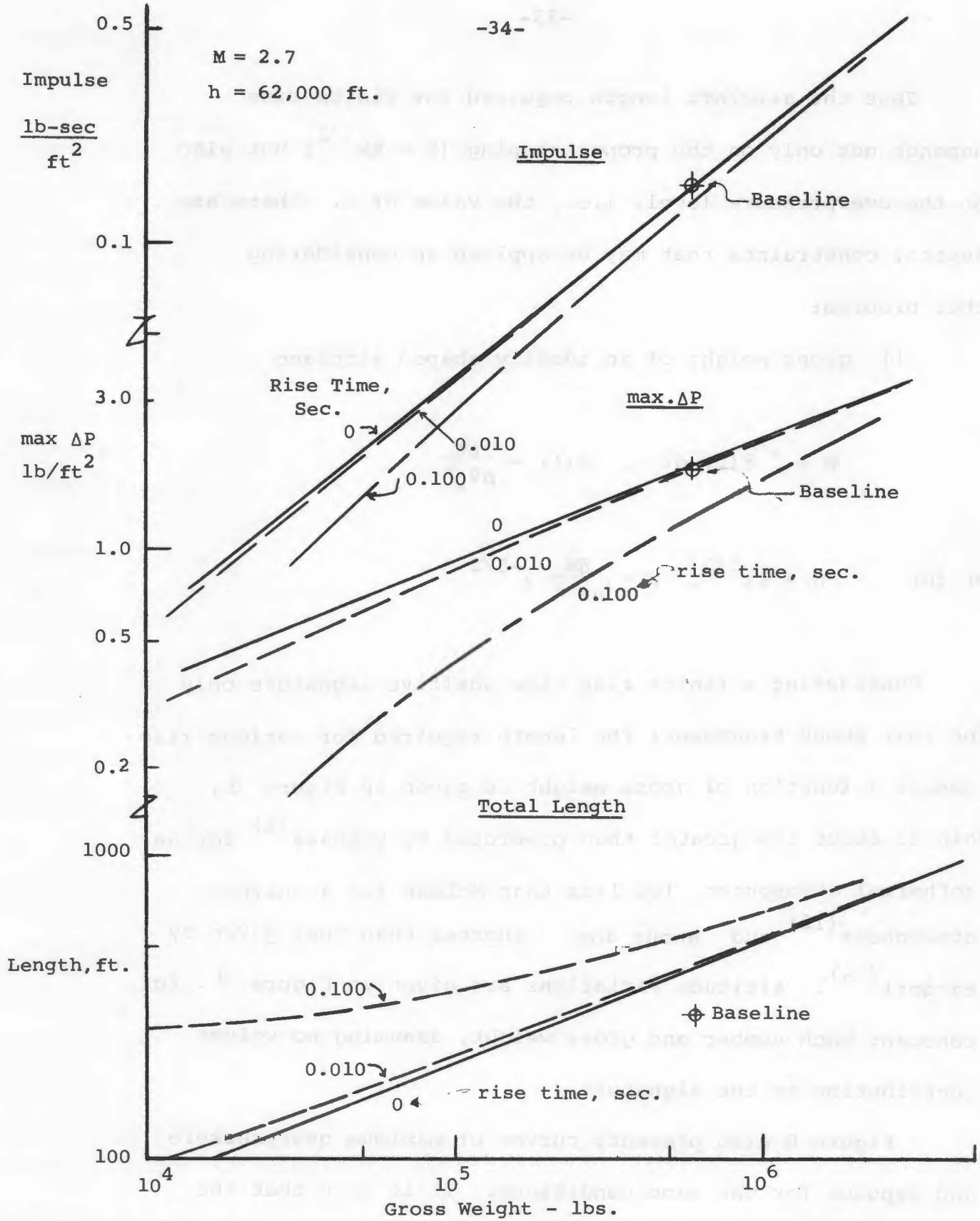

FIGURE 8 - Finite Rise Time Requirements
(Ideally Shaped Airplanes) Front Shock Only

ideally shaped aircraft may be seen by comparing the length-weight relationships with the baseline SST configuration. The agreement of the impulse and overpressure values is of course fortuitous, and illustrates that configurations with shocks need not have higher overpressures than those with finite rise times. Altitude effects are given in Figure 9 which shows the benefit of lower cruising altitude.

(2) thermal spike (heat addition only)

Another alternative to the ideally-shaped airplane is of course superposition of a distribution of heat or mass injection sources to create the required effective area distribution. The practical constraint then becomes one of specifying only heat or mass addition (i.e., no cooling or mass removal). This means, from Eq. (12) above, that $\Delta S'$ is always positive, decreasing to zero at the maximum value of S' of the baseline area distribution. This value is 8.09 ft^2/ft at $x = 178.8$ ft. (Figure 2). The complete specification of the thermal spike plus baseline aircraft is thus

$$S' = 2.5\,K(x_o+x)^{3/2} \qquad 0 < x < x_o+178.8$$

$$S'(x_o+178.8) = 8.09$$

$$S = S_{\text{baseline aircraft}} + S(x_o+178.8) - 593 \qquad (x > x_o+178.8)$$

$$[S_{\text{baseline aircraft}}(178.8) = 593]$$

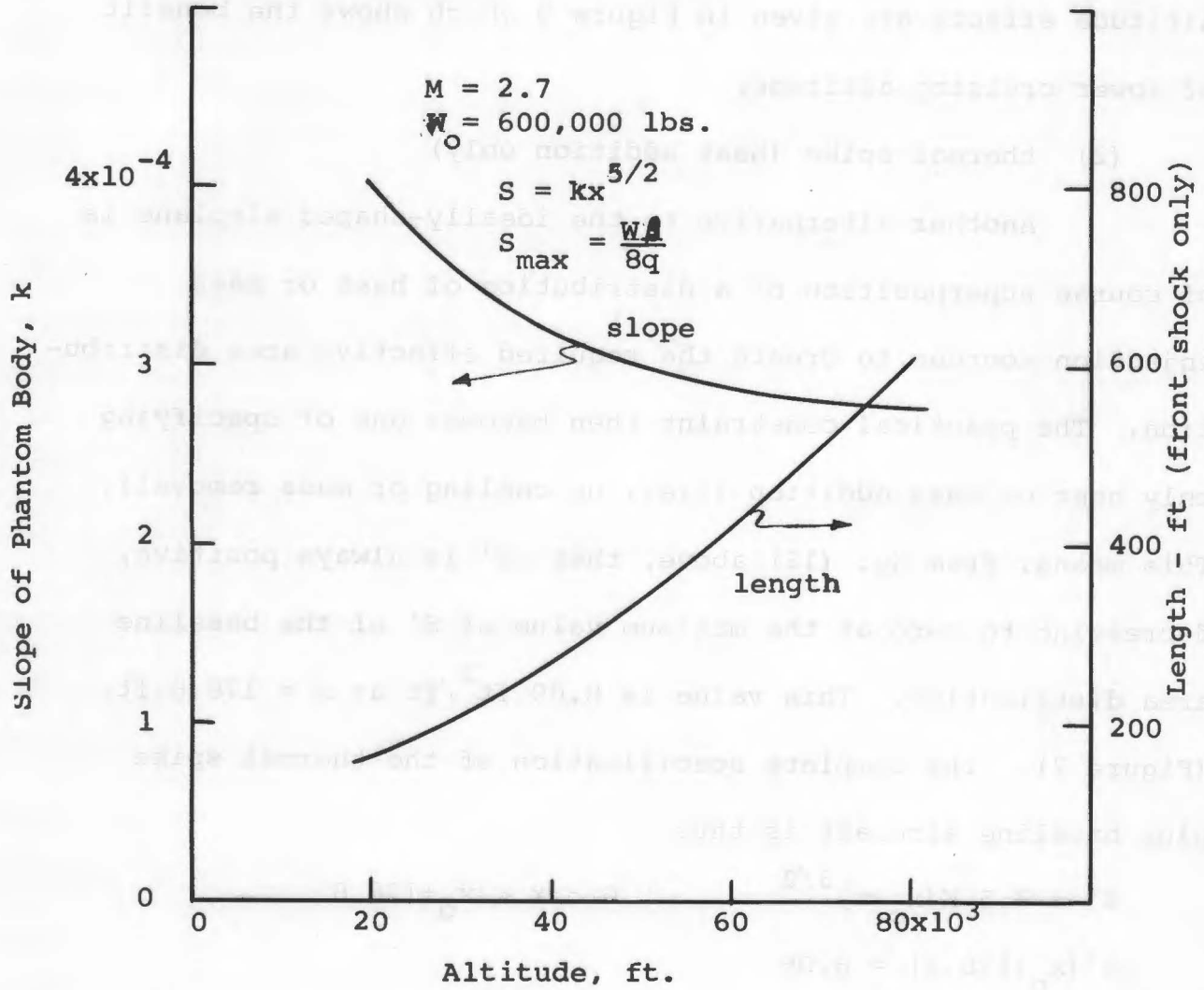

FIGURE 9 - Altitude Effects on Finite Rise Time Requirements

Again, for finite rise time, K must not exceed 2.86×10^{-4}, thus the minimum value of x_o is 325 ft., which gives a total aircraft length of 623 ft. Figure 10 presents data computed for various values of $K < 2.86 \times 10^{-4}$. We see that the overpressures are higher than the baseline for values of $x_o < 550$ ft; i.e., it is necessary to practically triple the aircraft length in order to achieve a finite rise time without increasing the overpressure. Large penalties in terms of effective area and impulse increase are incurred. Detailed consideration of the effective area penalties is given below on pages 108-118.

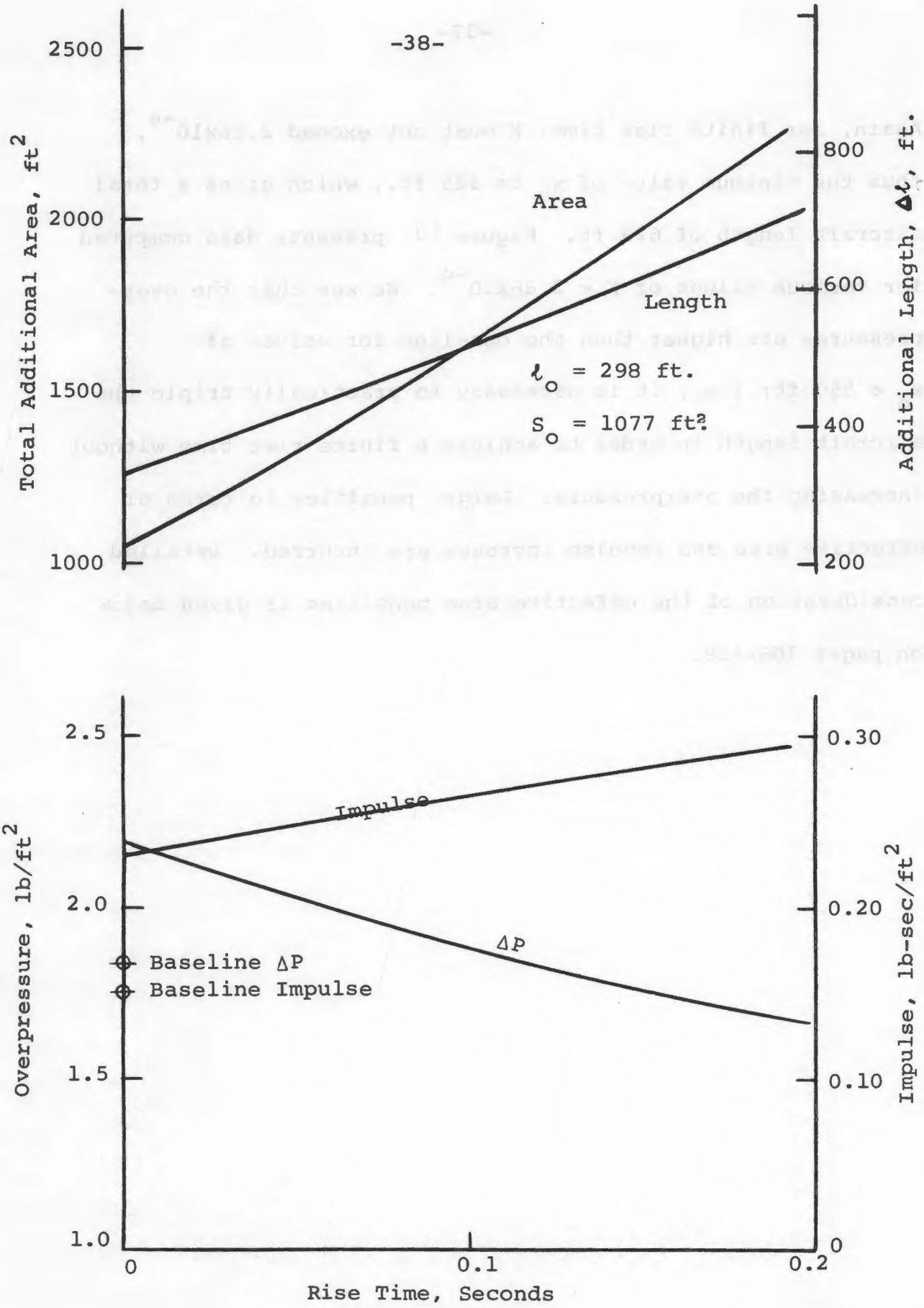

FIGURE 10- Front Shock Elimination Requirements

(C) Finite Rise Time - Rear Shock. Elimination of the rear shock in favor of a finite rise time to the maximum negative ΔP is, of course, as desirable as for the front shock, although the "startle" effect of the rear shock should be somewhat less.

The rear shock is formed from negative ΔP's (resulting from negative F's) advancing rearward until a double-valued F-distribution is formed, just as in the case of the front shock. Therefore, the optimum F-function has the same slope, K, in the rear as in the front (see sketch on Page 28). However, the resulting area distributions front and rear are considerably different since the area is given by the convolution integral

$$S(x) = 4\int_0^x F(t)\sqrt{x-t}\,dt \tag{14}$$

In addition, the complete F function cannot be symmetric because $F(t) \neq 0$ for $t > \ell$.

A general formulation for the desired F function is thus given by

$$\left.\begin{aligned} F(x) &= F_1\, x/\lambda \qquad 0 < x < \lambda \\ F(x) &= F_1\, x/\lambda - (F_1 - F_2) \qquad \lambda < x < \ell \end{aligned}\right\} \tag{15}$$

This defines an area distribution, S, and an S' distribution from 0 to ℓ. In the wake region, $x > \ell$, the lift portion of the total effective area remains constant, as do the heat and mass injection terms, (within the context of this study, which ignores viscous mixing and dissipation). However, the volume effects for real airplanes are not constant, due to wake mixing and engine exhaust effects. These effects are noticeably present in the baseline area distribution, for example. The actual area distribution for $x > \ell$ should thus be used to define F in this region and is determined from

$$F(x) = \frac{1}{2\pi} \int_0^x \frac{S''(t)}{\sqrt{x-t}} \, dt \, .$$

A further property must be satisfied, namely the F function closure condition

$$\int_0^\infty F(t) \, dt = 0 \qquad (16)$$

This is discussed by Whitham,[26] for example, within the context of the total mass flow perturbed by the passage of the wave, which must return to the undisturbed condition after passage of the wave. Several aircraft lengths may be required to essentially satisfy (16); for the baseline aircraft a

residual of 25% of the maximum positive phase integral remained at $x = 2\ell$, for example. The region $x > \ell$ is frequently referred to as the "tail" of the signature.

Some of the properties of bodies having F-functions given by (15) are shown in Figures 11 and 12 . Depending upon the value of F_2/F_1, the body may exhibit a maximum area, decreasing to a minimum, and then increasing again ($-F_2/F_1 > (\sqrt{3}-1)$); it may show a point of inflection with horizontal tangent, ($-F_2/F_1 = (\sqrt{3}-1)$); or it may continuously increase ($-F_2/F_1 < (\sqrt{3}-1)$).

Several particular cases have been studied before. McLean (12) chose a distribution with $F_2 \cong - F_1$ and $\ell \cong 2\lambda$. This gives an inordinate length for finite rise time and fixed lift, since the value of S at $x = \ell$ is substantially <u>less</u> than the maximum, and F_2/λ has a fixed value for finite rise time. The solution found by both Hayes [23] Seebass [1] involve $\ell = 3/2\ \lambda$ and $F_2/F_1 = - (\sqrt{3}-1)$, which has the following additional properties:

- $S'(\ell) = 0$
- $S''(\ell) = 0$
- Of the group of solutions with $S'(\ell) = 0$, $S(\ell)$ is a maximum.

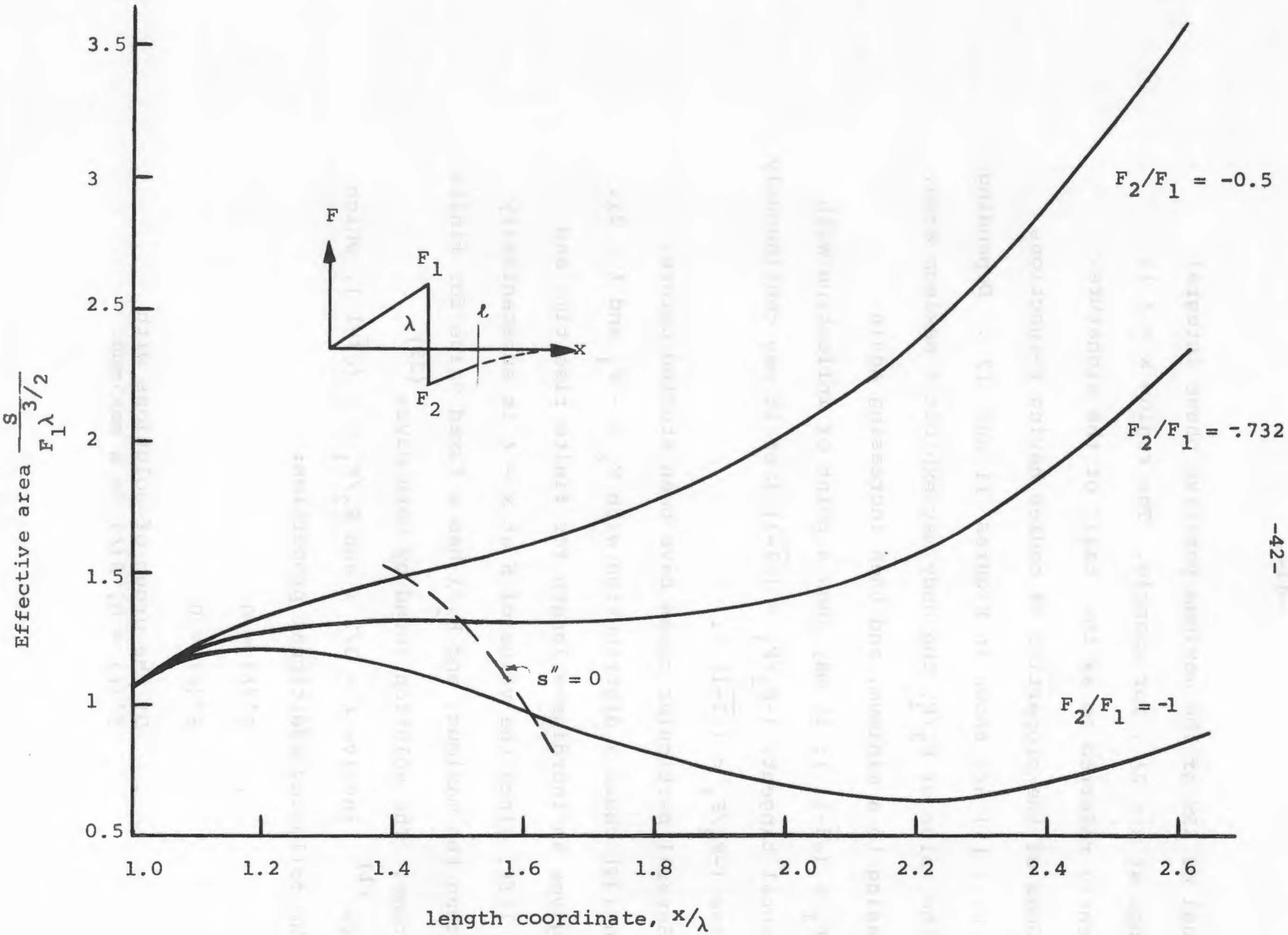

FIGURE 11 - Body Shapes For Finite Rise Time - Front and Rear

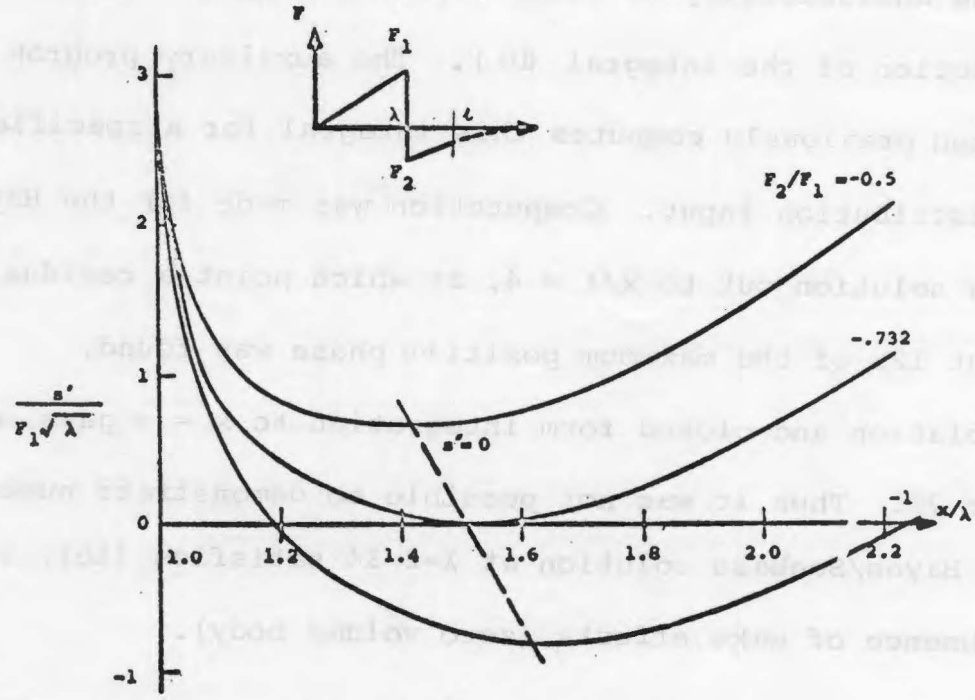

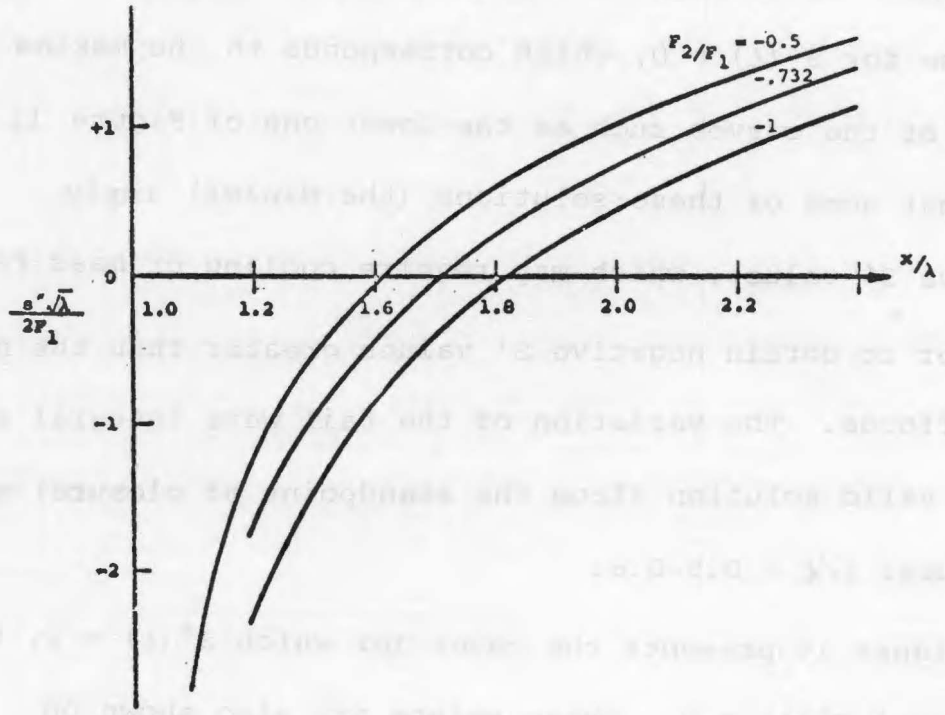

FIGURE 12 - Body Shape Derivatives for Finite Rise Time - Front and Rear

The admissibility of these solutions depends upon satisfaction of the integral (16). The auxiliary program described previously computes this integral for a specified area distribution input. Computation was made for the Hayes/Seebass solution out to $x/\ell = 4$, at which point a residual of about 12% of the maximum positive phase was found. Extrapolation and closed form integration to $x = \infty$ gave only another 7%. Thus it was not possible to demonstrate numerically that the Hayes/Seebass solution at $\lambda=2/3\ell$ satisfies (16), at least in the absence of wake effects (zero volume body).

Figures 13 and 14 present additional computations of the properties of unsymmetrical F-function bodies. Figure 13 was done for $S'(\ell) = 0$, which corresponds to the maxima and minima of the curves such as the lower one of Figure 11. Note that some of these solutions (the minima) imply negative S' values, which may require cooling or mass removal in order to obtain negative S' values greater than the natural wake affords. The variation of the tail wave integral shows that a valid solution (from the standpoint of closure) may be found near $\lambda/\ell = 0.5$-0.6.

Figure 14 presents the cases for which $S''(\ell) = 0$, but in general $S'(\ell) \neq 0$. These points are also shown on Figure 12 and are logical terminations in order to make a smooth transition to $S' = 0$ or to the wake values.

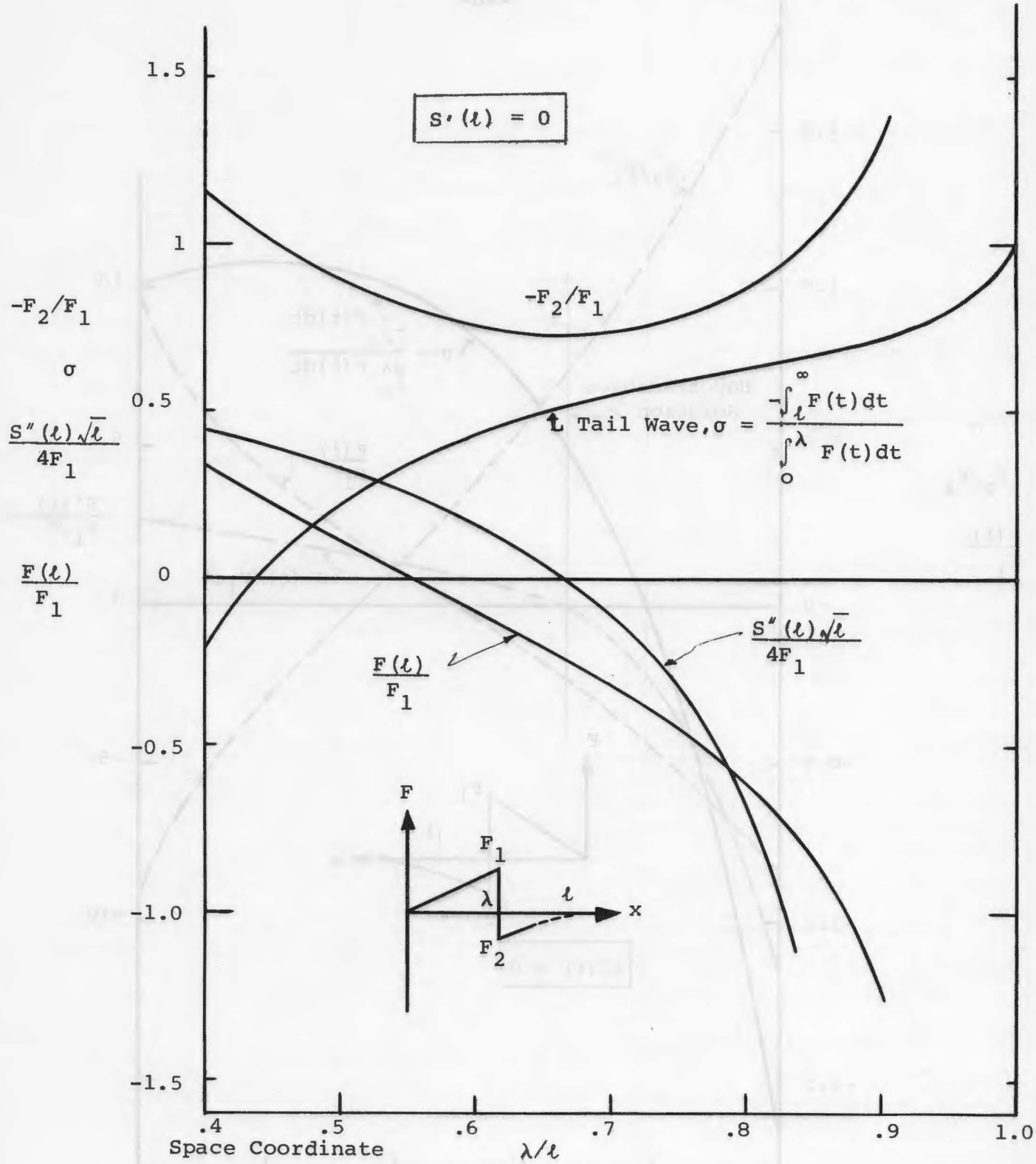

FIGURE 13 - Finite Rise Time Body Characteristics for $S'(\ell)=0$

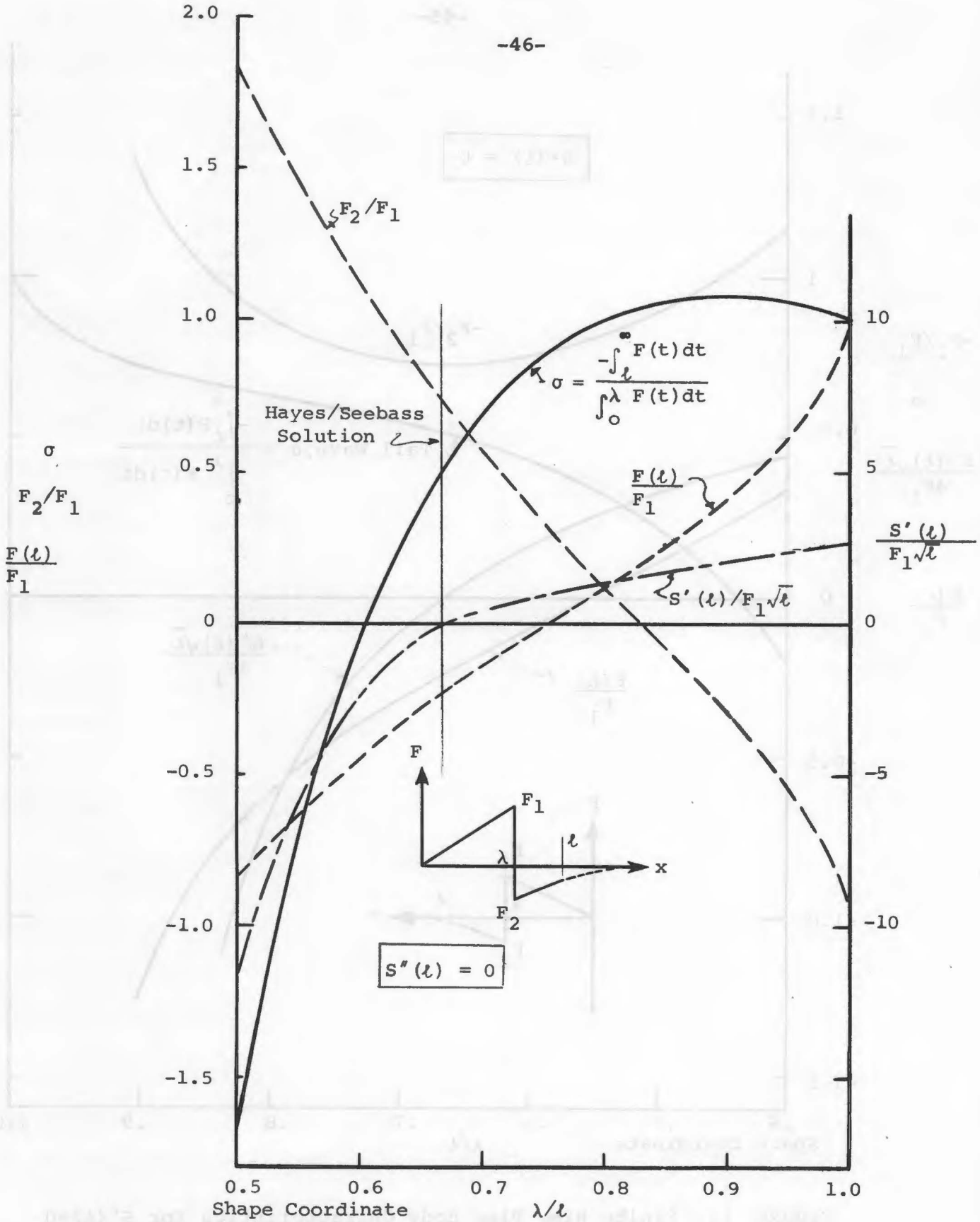

FIGURE 14 - Finite Rise Time Body Characteristics for $S''(\ell)=0$

Figures 15 to 17 present the results of some calculations made for arbitrary F functions and area distributions with $S''(\ell) \neq 0$. Three different fairings of the effective area distribution were tried in the test region, including a sharp discontinuity. The discontinuous case of course gives rise to an F function spike at $x/\ell = 1.0$, the magnitude of which is governed (in this case) by the numerical grid spacing for the S values used to compute F. Two values of this peak were used, and the results show that the maximum rear shock pressure rise is affected less than linearly by the minimum F value.

The results of these calculations imply that the Hayes-Seebass solution requiring $\lambda = 2/3\ \ell$ may be relaxed considerably without significant rear shock penalty.

In general, these S' functions are not too different from the envelope of the baseline aircraft, as shown in Figure 18, for the Hayes/Seebass case where $S'(\ell) = S''(\ell) = 0$. Computations were made of the requirements for complete shock elimination, front and rear, with no negative $\Delta S'$ contribution. The results are given below, together with the calculation for an "ideal" body where $S(\ell)$ is sufficient for the lift only, all for just finite rise time ($\Delta t \rightarrow 0$). The results are seen to be only slightly different from the front shock requirements shown previously.

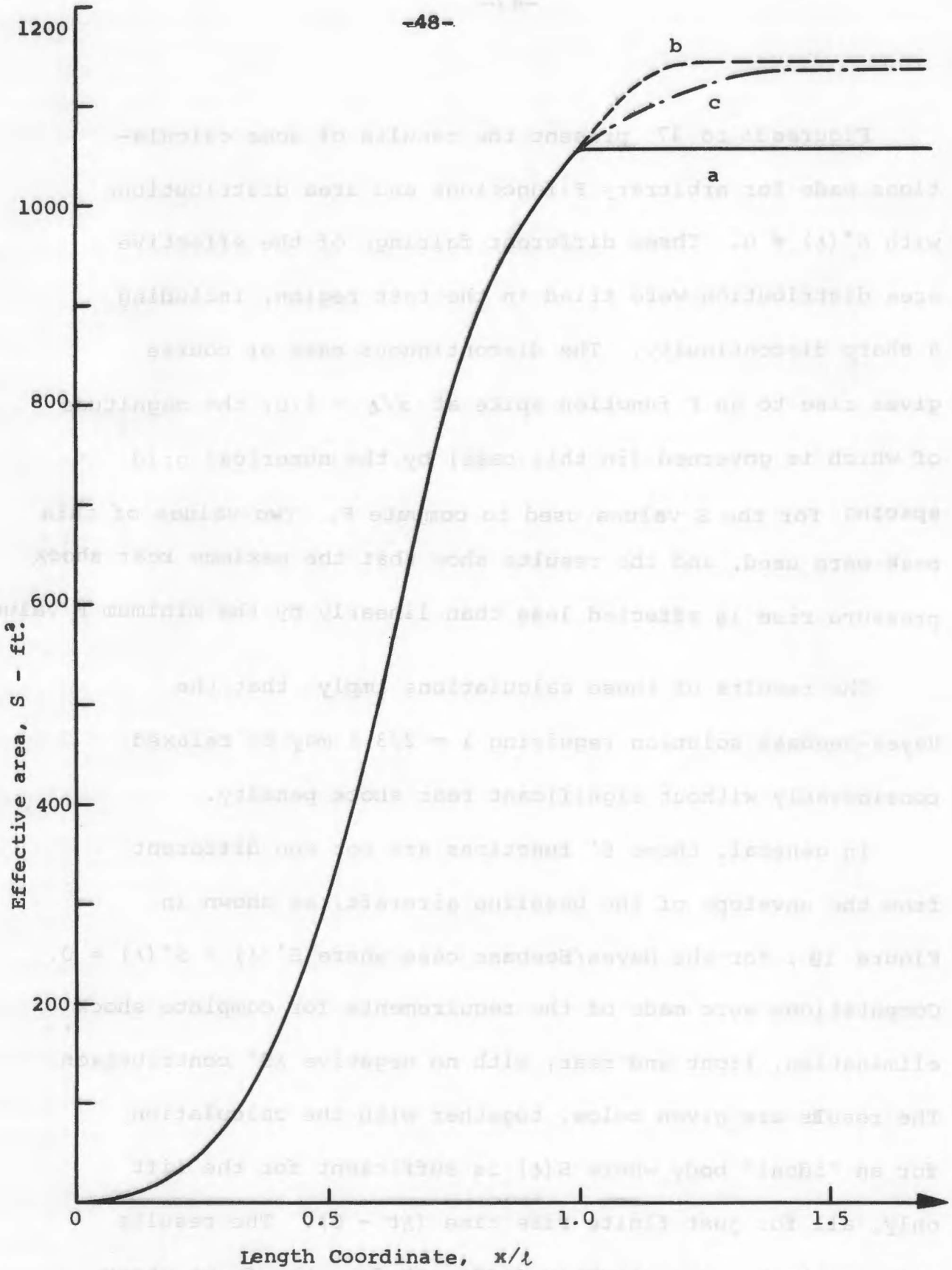

FIGURE 15 - Effective Area Distribution for Ideal Shapes With Rear Discontinuities

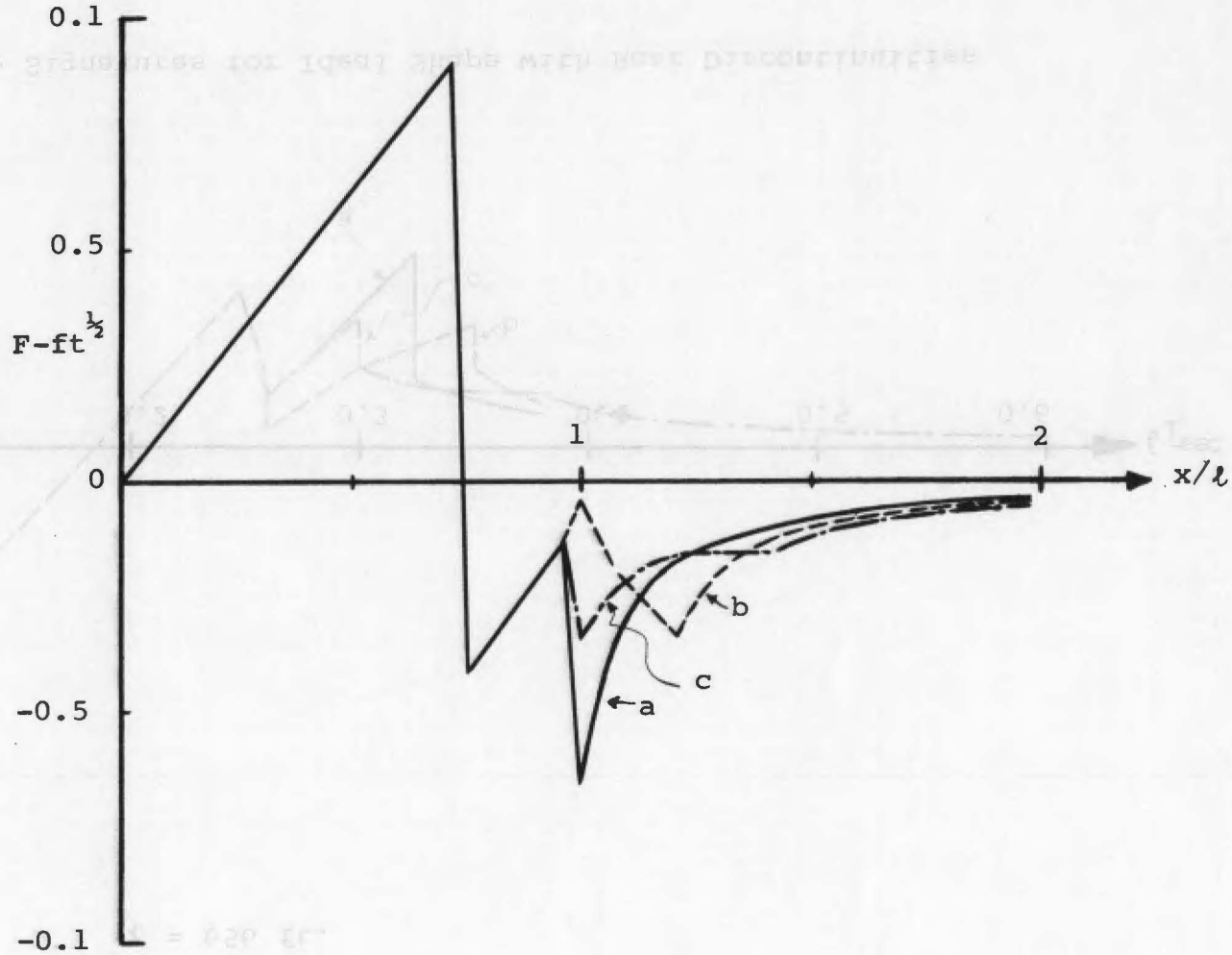

FIGURE 16 - F Function for Ideal Shape with Rear Discontinuities

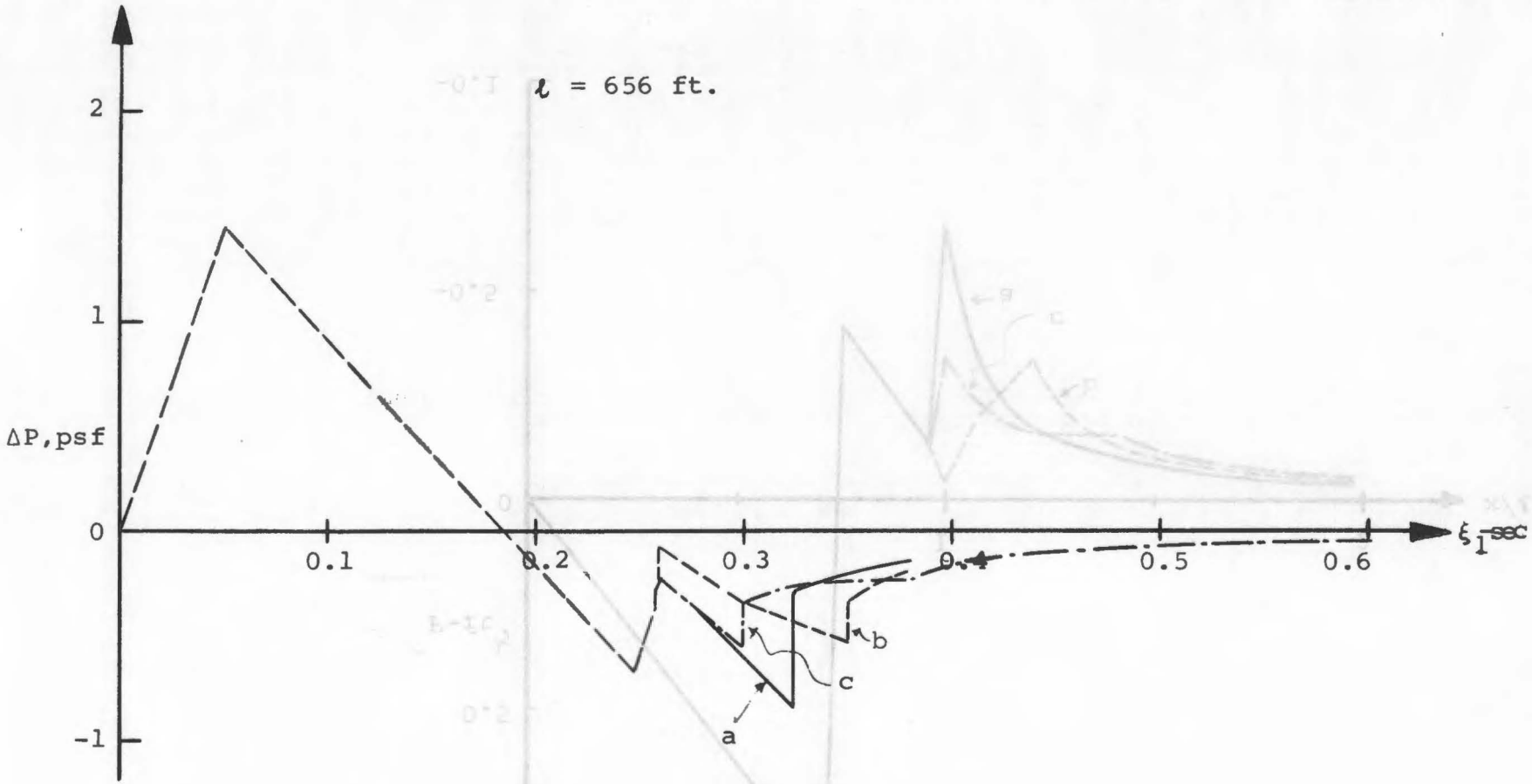

FIGURE 17(a) - Signatures for Ideal Shape with Rear Discontinuities

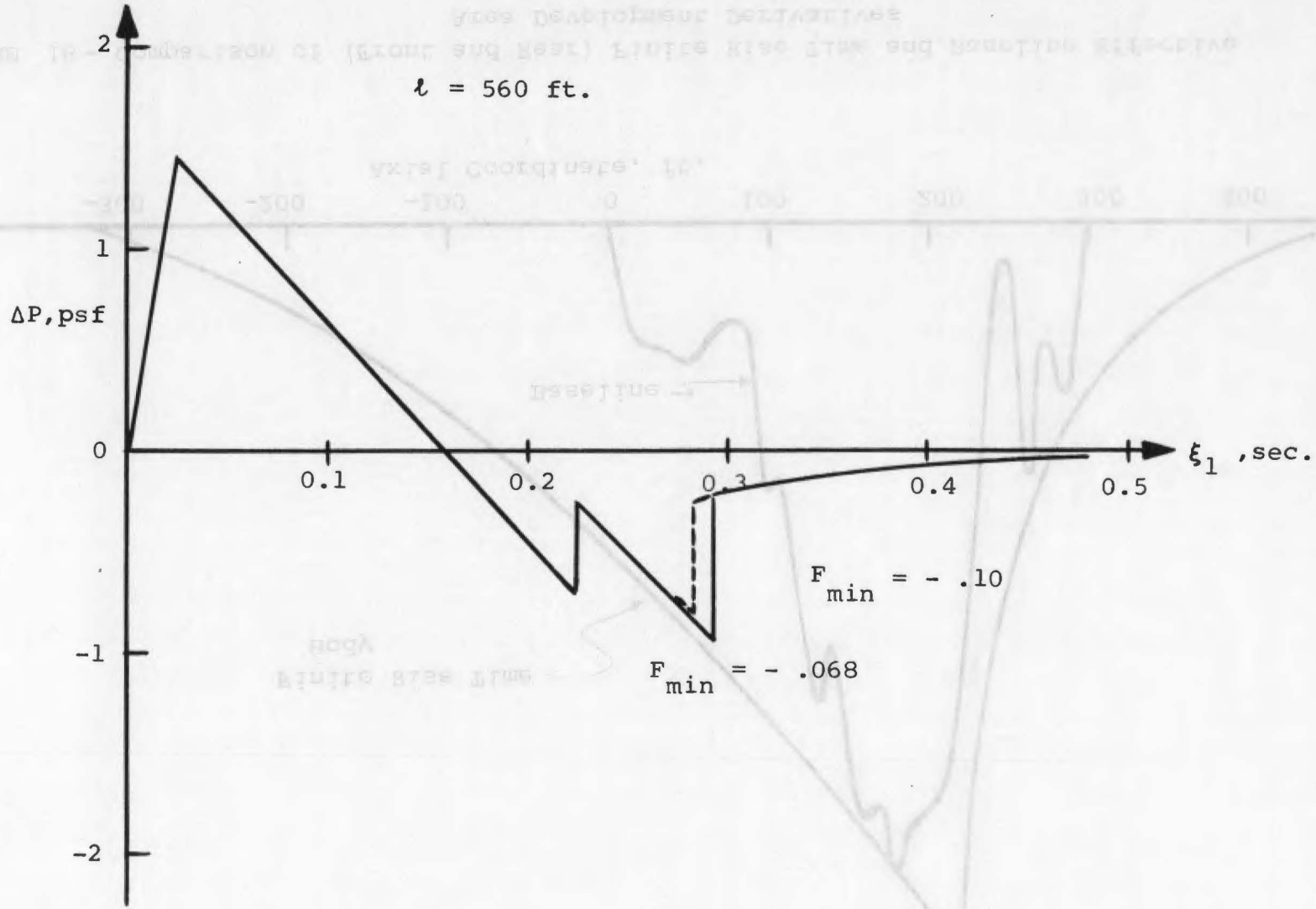

FIGURE 17(b) - Signatures for Ideal Shape with Rear Discontinuities

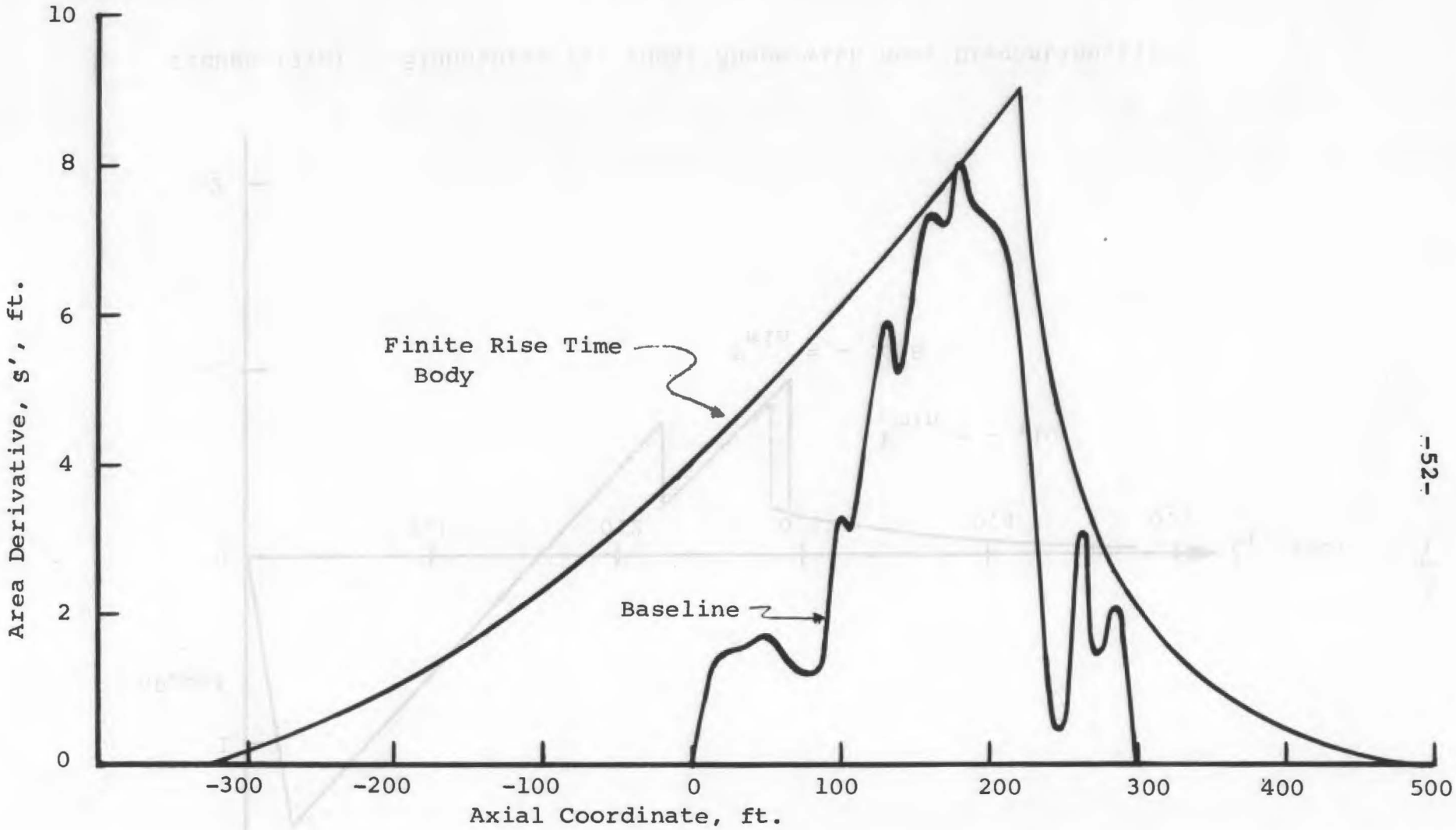

FIGURE 18 - Comparison of (Front and Rear) Finite Rise Time and Baseline Effective Area Development Derivatives

Finite Rise Time
(front and rear)

	Ideal	Heating Only	Front Shock Only	Baseline
Total Length	600	817	623	298 ft.
Total Eff. Area	1077	2430	2120	1077 $ft.^2$
Max. Positive ΔP	1.68	2.36	2.2	1.84 psf
Max. Negative ΔP	1.24	1.73	~1.4	1.71 psf
Positive Impulse	.129	.246	.215	.153 lb sec/ft^2

(D) Plateau Pressures. The next class of signature improvements considered is the minimum overpressure, or plateau pressure signature. This results from an area development of the type

$$S = Kx^{3/2}$$

which results in a constant F function. However, George[22] and Seebass[1] have pointed out that a superposition of a δ function or spike will not contribute a higher shock pressure if the proper area balance is maintained, as shown in the sketch.

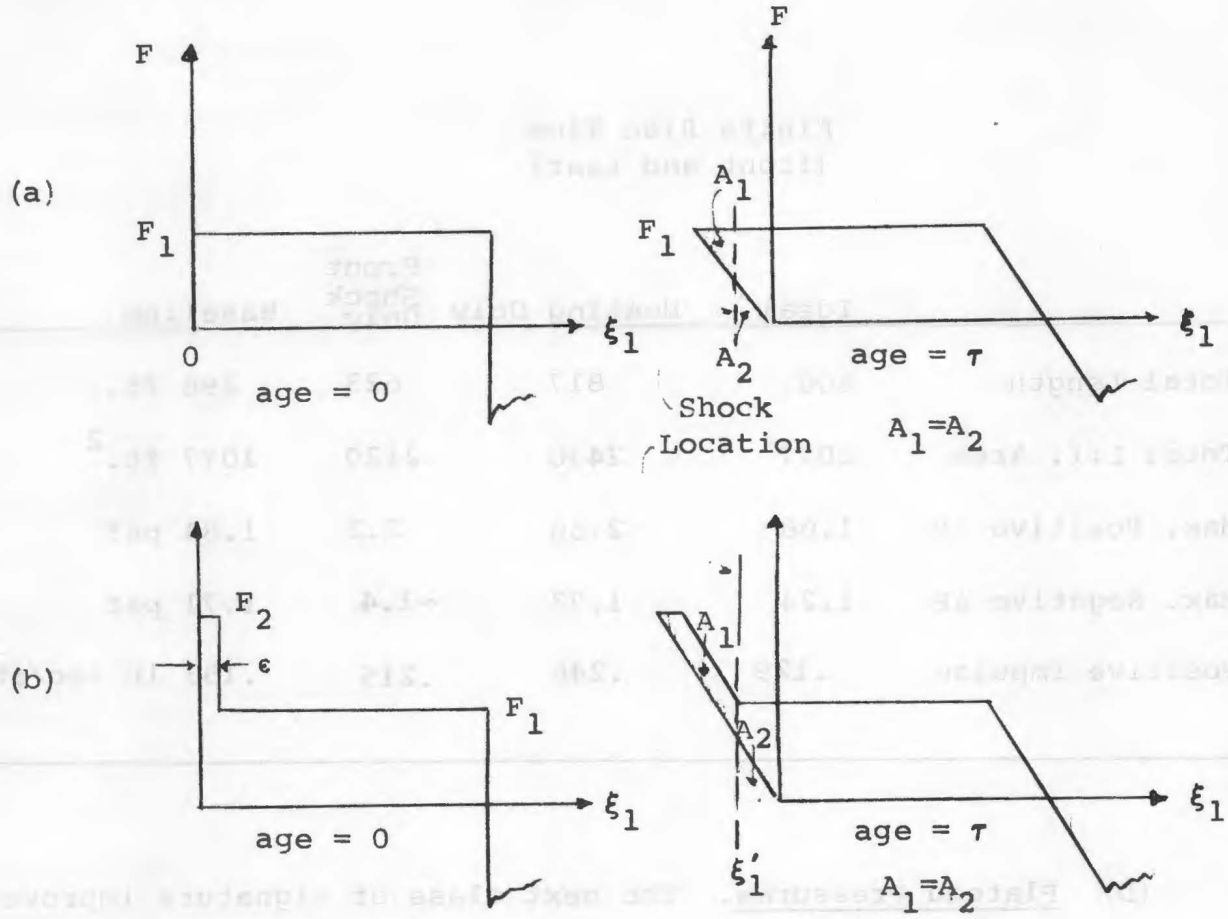

Thus, in sketch (b) the shock has advanced further to the left in order to balance the areas A_1 and A_2, but as long as it has not passed the point ξ_1', no increase in overpressure results. This technique is seen to be a combination of the Jones far field minimum (δ function) and the plateau pressure (3/2 power law) prescription, and offers a net improvement with respect to either one alone, in terms of the overpressure - gross weight characteristics, providing the age is sufficiently small (mid field).

The advantage in terms of effective area (or gross weight) may be computed in terms of a two-level F-function as shown in the sketch. As $\epsilon \to o$, the product $(F_2 - F_1)\epsilon$ remains finite (simulating a δ function), and is given by the area balancing requirement for locating the shock wave at ξ_1' :

$$\frac{\epsilon}{V} \cdot \frac{F_2}{F_1} = \frac{\alpha}{2} \Delta P_1$$

where α = the advance, $\frac{d\xi_1}{dP_1}$

The incremental area gained as $\epsilon \to o$ is given by $\Delta S/S = 3/2 \frac{\epsilon}{\ell} \frac{F_2}{F_1}$

Substituting for ϵF_2, we get $\frac{\Delta S}{S} = \frac{3}{2} \frac{V}{\ell} \frac{\alpha}{2} \Delta P_1$.

Using these same formulas, with $\epsilon \to 0$, it can be shown that the changes in S' are of second order. Thus, the δ function does not provide any relief in the area requirements when the phantom body must match a given value of S' for the baseline aircraft.

Figure 19 presents some numerical results for the overpressure and effective areas. The ideal shape provides greatly reduced overpressures, even at the same length as the baseline aircraft. However, when matching of the baseline aircraft maximum S' value (8.09 ft^2/ft) is imposed, this advantage disappears, and substantial lengths and additional effective areas are required.

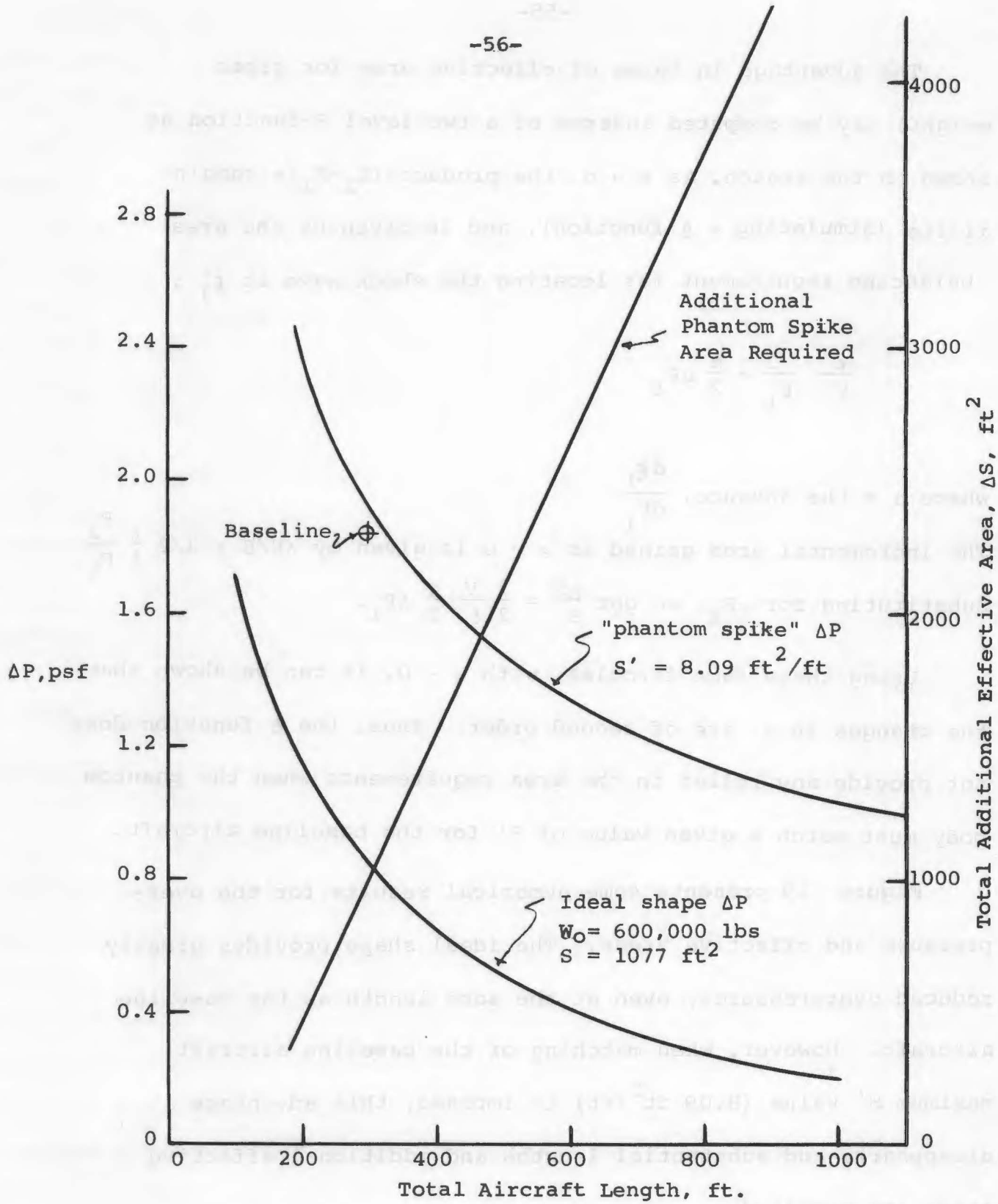

FIGURE 19 - Plateau Pressure Signature Requirements

COMPOSITE SIGNATURE COMPUTATIONS

The preceding work showed that very large effective area increments are required to effect improvements to the baseline aircraft signature when restricted to positive value of $\Delta S'(x)$ (i.e., mass and heat addition). As a more practical matter, an investigation was made of two-level signatures. Rather than mask the entire aircraft signature with the airstream alteration effects, such a scheme seeks to add a phantom nose in front of the aircraft that will either warn of an impending shock wave, or break the total shock pressure rise up into two or more tolerable jumps.

The question of minimum time separation between these two events must then be answered. Although apparently the human ear can discriminate two pulses from one pulse for separations as small as 10 μsec (Reference 25), a more realistic value for the separation would be 50-100 msec, the upper limit of which is the threshhold value quoted for detection of an N-wave as one shock rather than two (References 16 and 20). Because of this lack of precise definition,the time separation was a parameter in this study.

The baseline area distribution is shown in Figure (20) in terms of $S'(x)$. There are several prominent peaks present, each of which was chosen as an "anchor point" for the superposition of a phantom body. A value of $S_1'(x)$ and x_1 was selected, together with the extended body length x_o. Coordinates were then computed to give the specified value of $S_1'(x)$ with a given power law variation up to $x = x_o + x$. From that point on back, the original baseline area distribution was followed, with an increment added corresponding to the phantom body contribution (see p.35). A computer code was used for these area computations, which were then transformed to F-functions through the auxiliary program described previously.

This procedure was followed for several values of x_o.

(A) Finite Rise Time "Warnings". Figure (21) presents signatures for the four anchor points and $\ell = 656$ ft. We see that the rise time of the 5/2 spike decreases as the anchor point moves back on the body (from (1) to (4)), and higher overpressures are experienced. Both of these results are due to the greater advance experienced as the fineness ratio of the spike increases.

These data and some more limited data at other lengths are given in Figure 22 as a function of the total

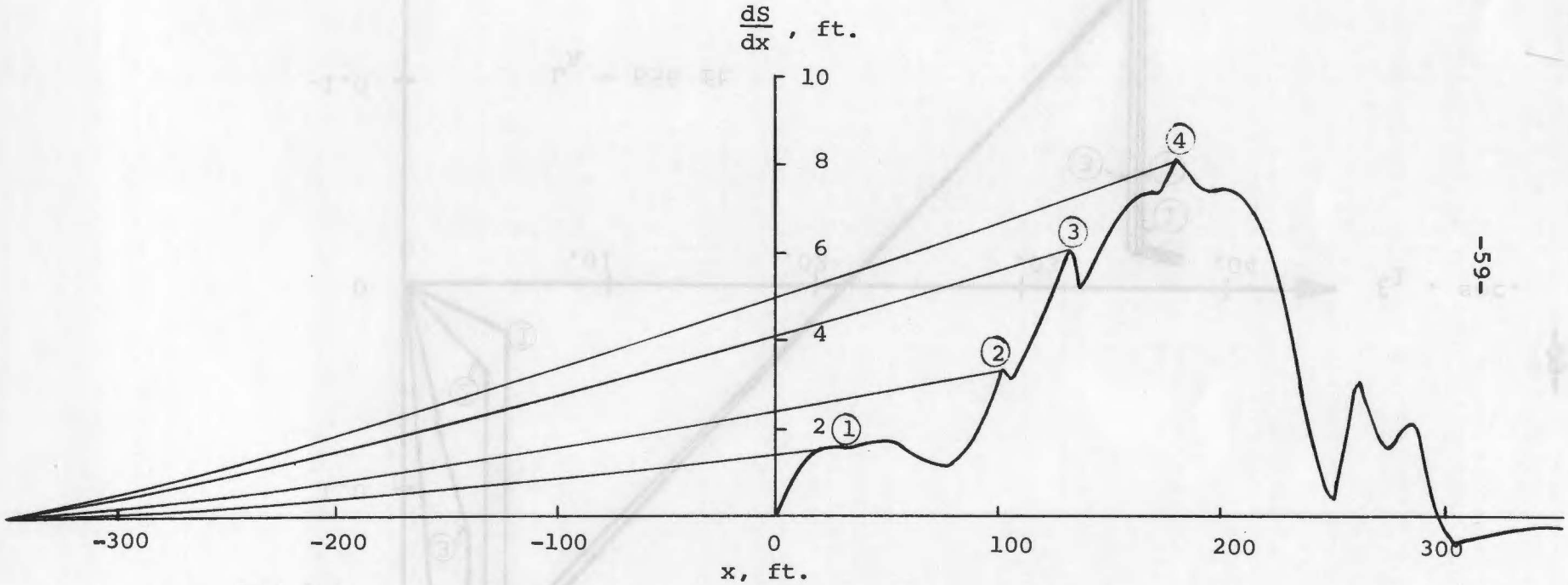

FIGURE 20 - S' Distribution Used to Generate Signatures

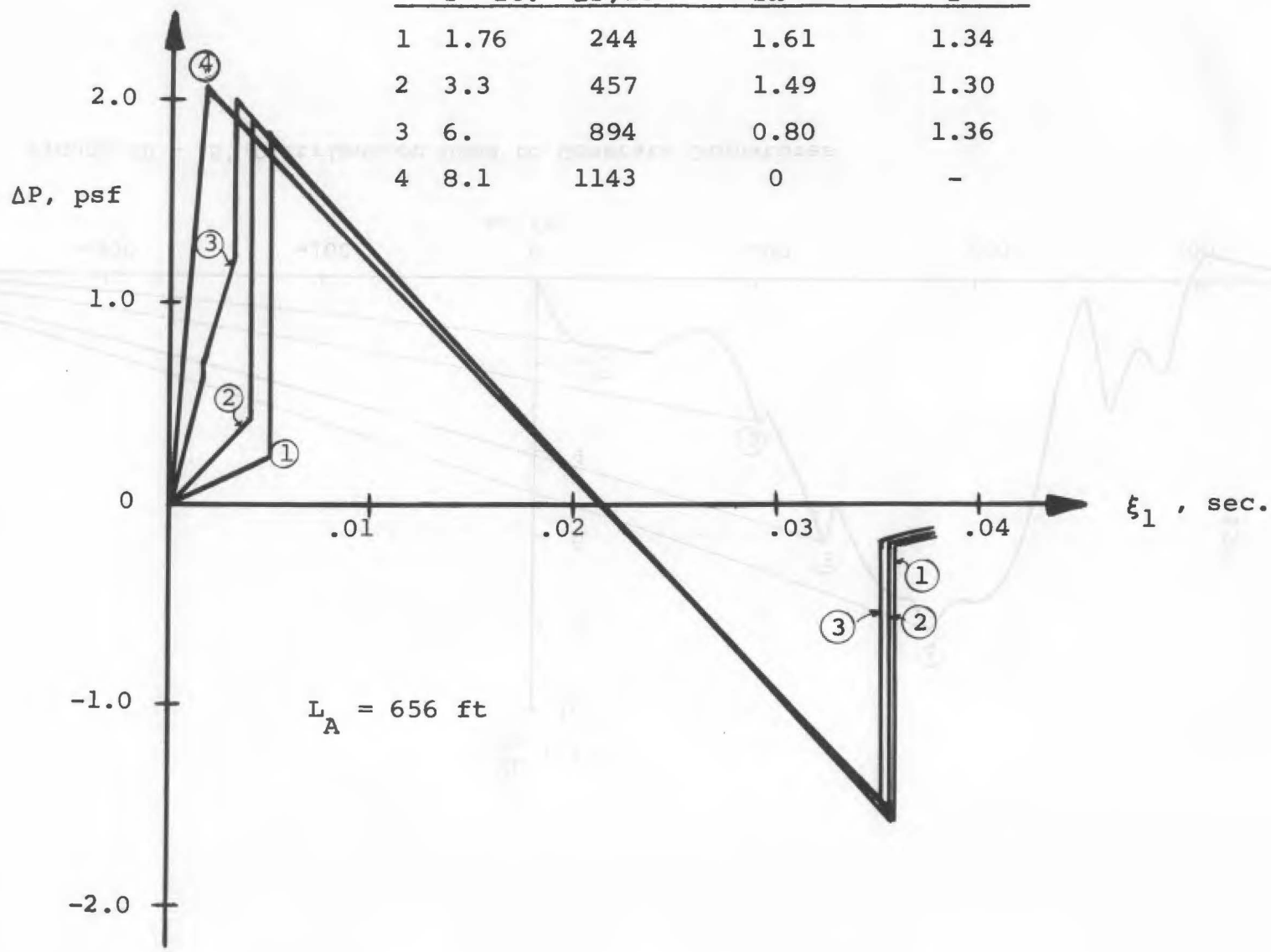

	S'-ft.	$\Delta S, ft^2$	ΔP_{sh}-psf	ΔP_r-psf
1	1.76	244	1.61	1.34
2	3.3	457	1.49	1.30
3	6.	894	0.80	1.36
4	8.1	1143	0	-

FIGURE 21 - 5/2 Power Body Signatures

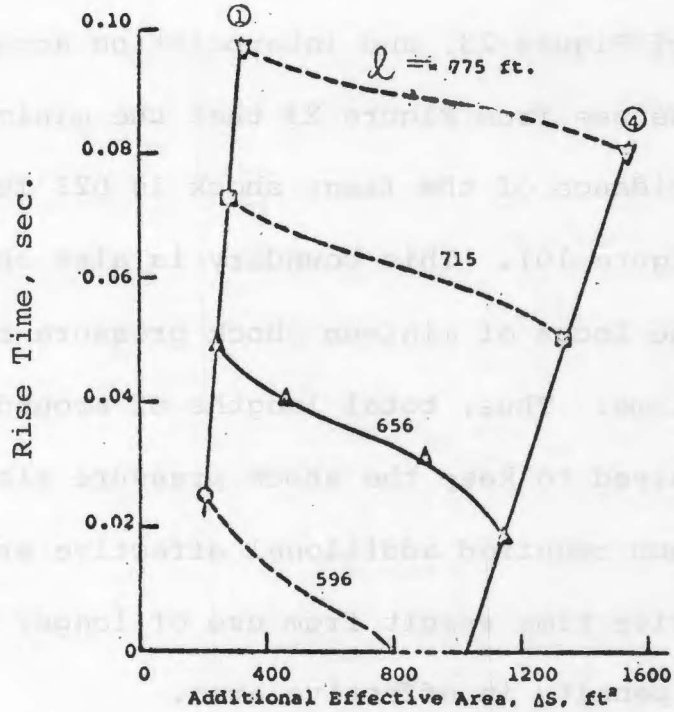

FIGURE 22(a) - 5/2 Body Area Requirements for Finite Rise Time - Front Shock

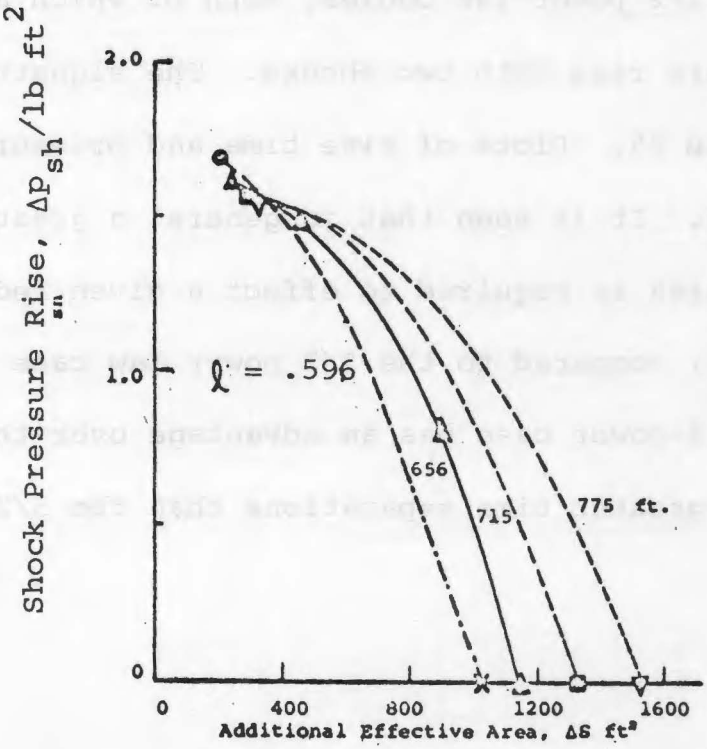

FIGURE 22(b) - 5/2 Body Area Requirements for Finite Rise Time - Front Shock

dditional effective area required for the spike. A "map" presentation was created from these limited data by the use of the linear rise time plot of Figure 23, and interpolation according to the ℓ = 656 data. We see from Figure 23 that the minimum length for complete avoidance of the front shock is 623 feet (corresponds also to Figure 10). This boundary is also shown on Figure 22, and forms the locus of minimum shock pressure rise at essentially zero rise time. Thus, total lengths of around 600 feet are generally required to keep the shock pressure rise below about 0.6 psf, at minimum required additional effective area. Substantial increases in rise time result from use of longer spikes, but at some additional penalty in effective area.

(B) Two-Step Signatures. A more limited investigation was made of n = 2 and n = 3/2 power law bodies, both of which affect the total front pressure rise with two shocks. The signatures are shown in Figures 24 and 25. Plots of rise time and pressure rise are given in Figure 26. It is seen that in general a greater additional effective area is required to effect a given reduction in shock pressure rise, compared to the 5/2 power law case (Figure 22), and that the 2-power case has an advantage over the 3/2. Both achieve somewhat greater time separations than the 5/2 case, however.

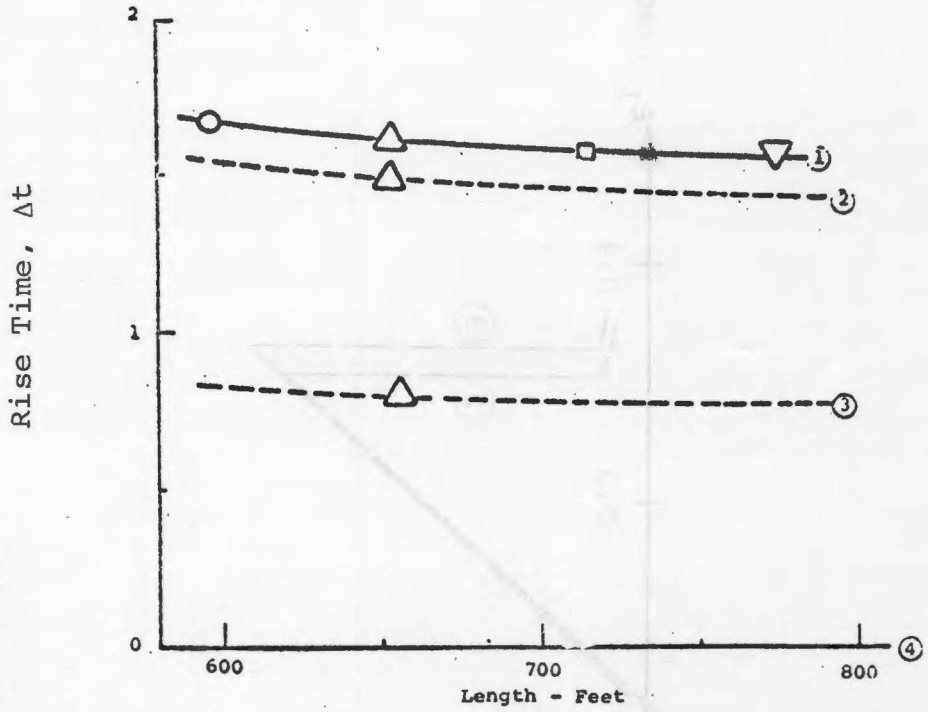

FIGURE 23(b) - Interpolation Curve - Shock Pressure Rise vs Length

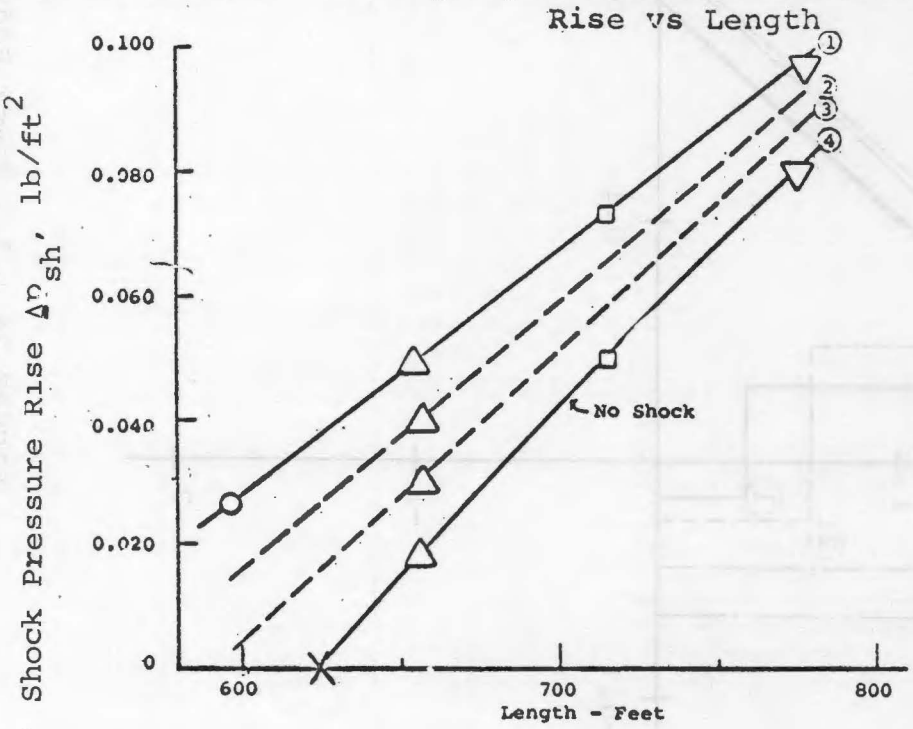

FIGURE 23(a) - Interpolation Curve - Rise Time vs Length

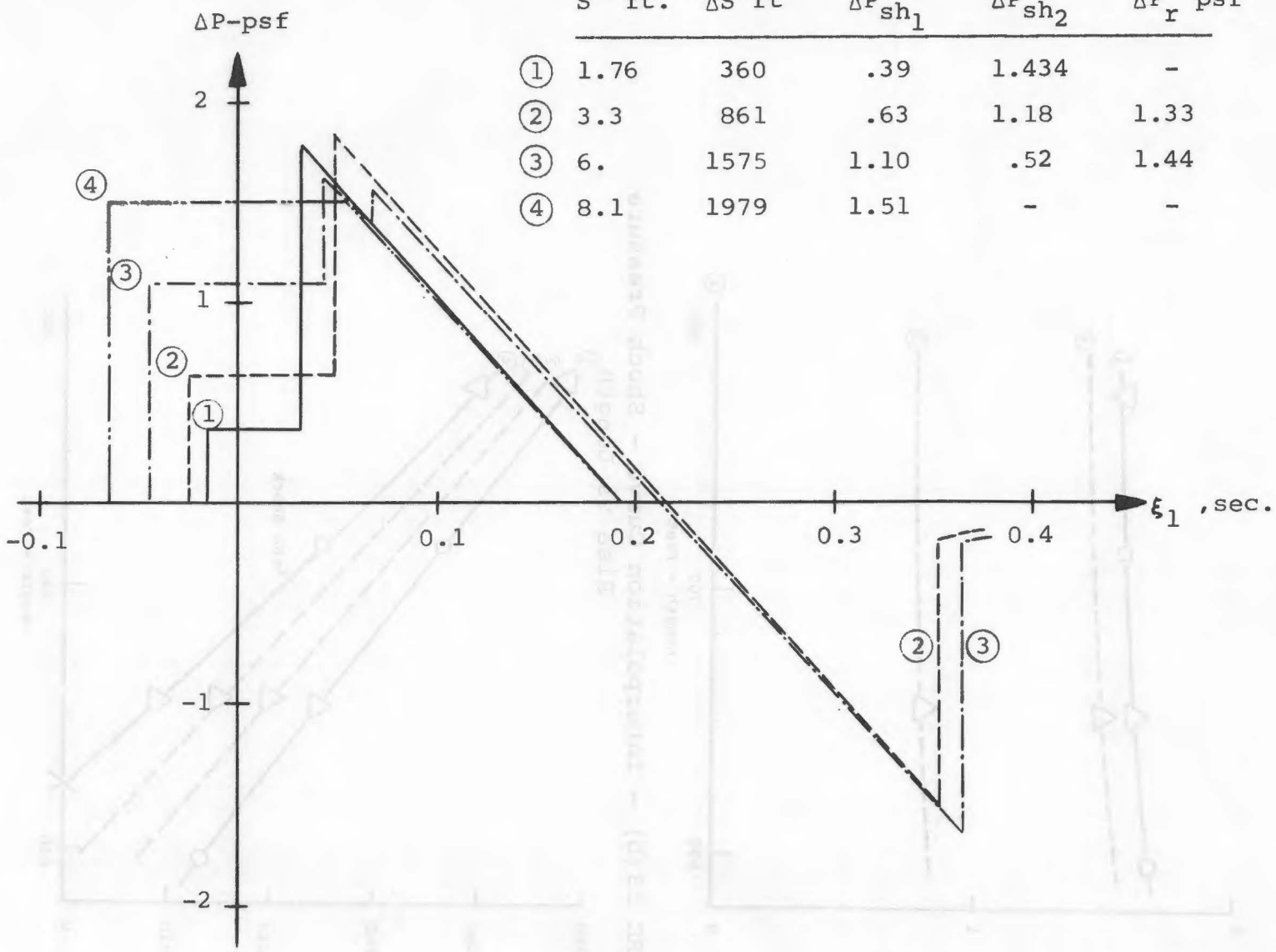

	S' ft.	ΔS ft^2	ΔP_{sh_1}	ΔP_{sh_2}	ΔP_r psf
1	1.76	360	.39	1.434	-
2	3.3	861	.63	1.18	1.33
3	6.	1575	1.10	.52	1.44
4	8.1	1979	1.51	-	-

FIGURE 24 - 3/2 Power Body Signatures

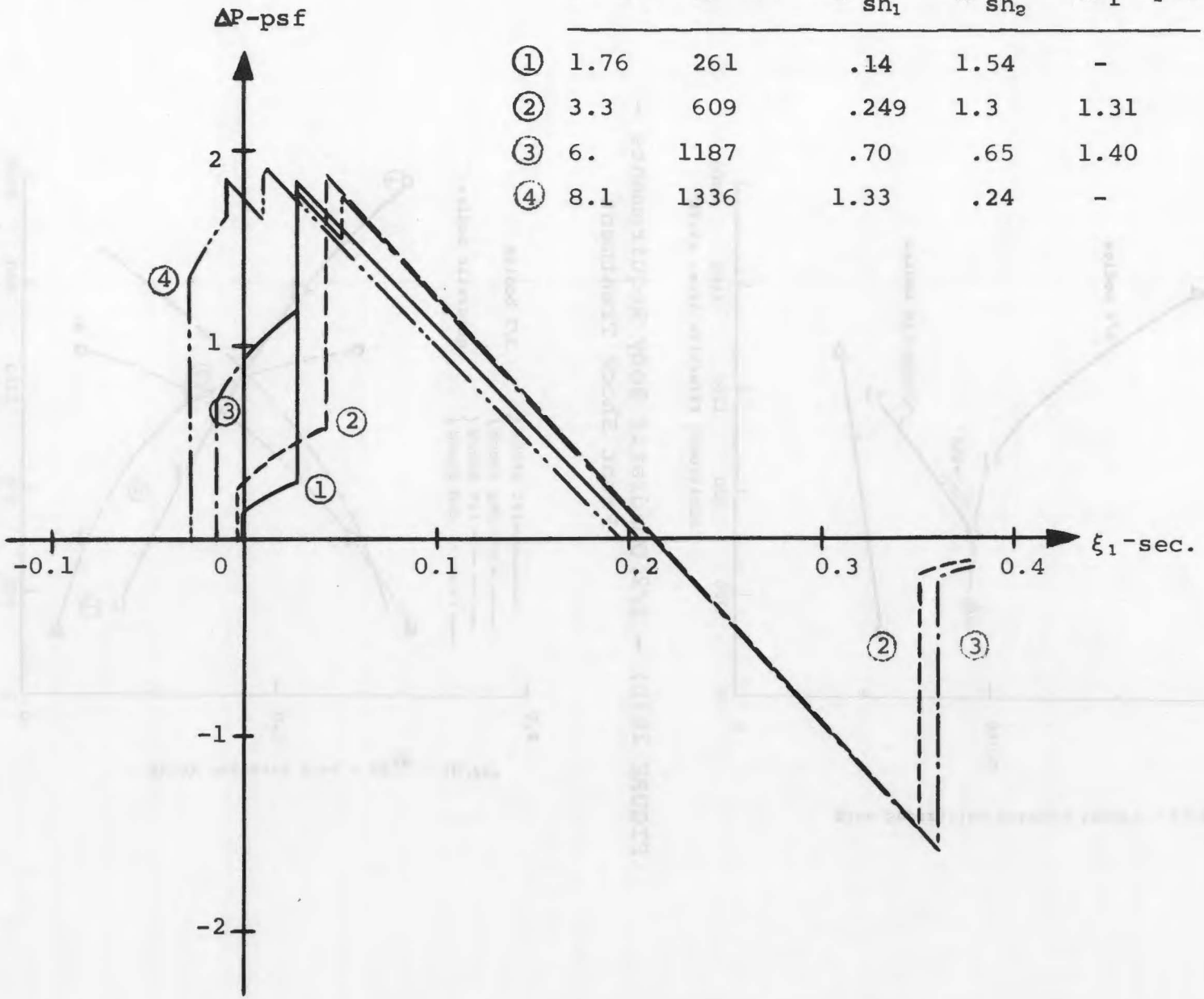

	S′ ft.	ΔS ft.²	ΔP_{sh_1}	ΔP_{sh_2}	ΔP_r psf
①	1.76	261	.14	1.54	-
②	3.3	609	.249	1.3	1.31
③	6.	1187	.70	.65	1.40
④	8.1	1336	1.33	.24	-

FIGURE 25 - Quadratic Body Signatures ($S = kx^2$)

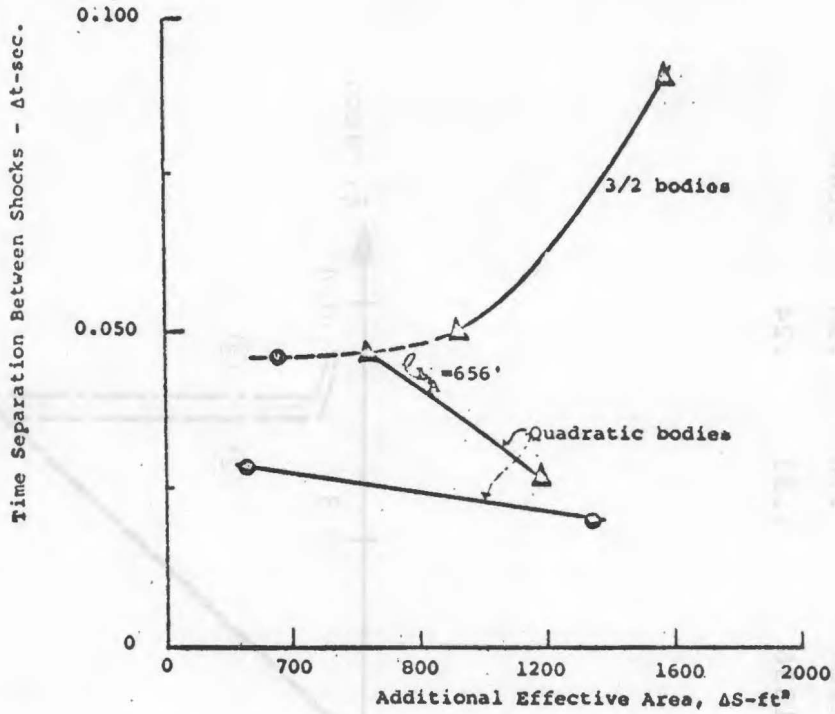

FIGURE 26(b) - 3/2, Quadratic Body Requirements - Front Shock Treatment

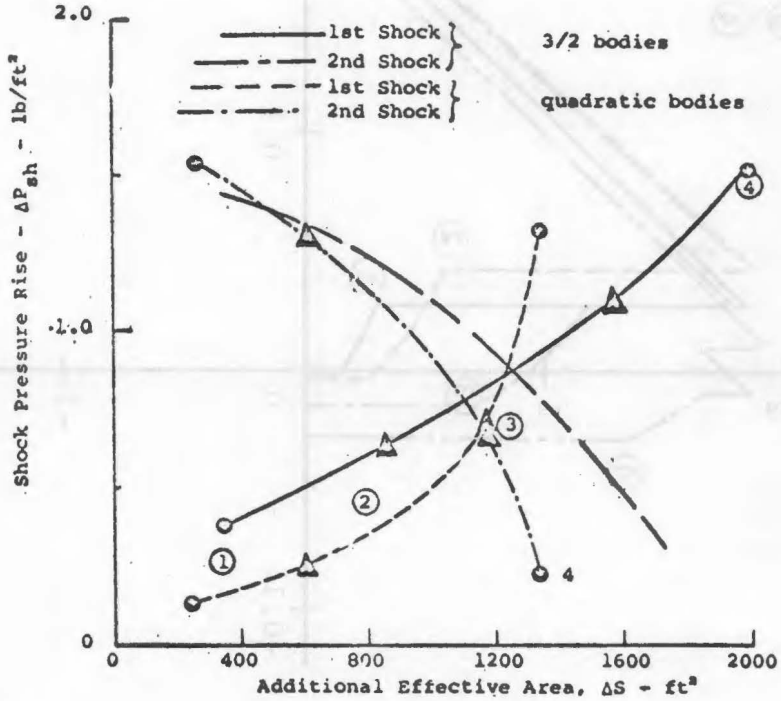

FIGURE 26(a) - 3/2, Quadratic Body Requirements - Front Shock Treatment

(C) Rear Shock Effects. Some of the signatures of Figures 21 to 25 show positive phases only. The rear shocks were not computed properly in these cases (because of lack of effective area definition for $x > \ell$ at that point in the study). The complete signatures shown were computer properly by using the derived baseline area distribution for all x greater than the point where the S' of the phantom nose matched the S' of the baseline. As a result, the calculations were carried out to fewer body lengths with the phantom nose added (since the tail length remains constant as the body length increases).

A comparison was made of the signature resulting from the F function for all x as described above, and that obtained by using the baseline F function for $x/\ell > 1$. It was determined that the rear shock results from an F discontinuity at x = 238 feet on the original body, rather than from the discontinuity at $x/\ell = 1$. However, the pressure rise associated with this shock depends on the area under the "tail" F curve, in accordance with the Whitham area balance rule. Thus the correct area distribution gave larger (negative) F values in the region $x/\ell > 1$; the shock is located further downstream and slightly higher overpressures result.

In general the rear shocks computed for the modified area distributions were slightly stronger than the base-line, but with lower overpressures than the front portion of the signature. As discussed above, use of additional effective area fairing in this region can further reduce the rear shock strengths by inclusion of finite rise time portions.

REMOTE ACTING WARNING SIGNAL

The foregoing results indicate that very large penalties are required to completely modify the baseline aircraft signature, i.e., create a finite rise time for the entire front pressure jump or break it up into two nearly equal parts. The additional effective area required is of the same order as the complete baseline aircraft. However, a precursor signal or warning of the arrival of the main shock can be created with much more modest penalties. Such a warning would do much to reduce the startle effect.

There is another way to create such a warning, rather than to provide a continuous disturbance distribution extending from the aircraft forward (or downward); that is to create a remote disturbance originating at the same upstream location but terminating shortly thereafter. Such a device could be a small drone aircraft. An alternative scheme would be remote addition of radiant energy, for example, through the use of a laser focussed to a remote spot.

Recent development of continuous high power lasers provide credence to this idea, which was suggested by A. R. Seebass. These developments include the gas dynamic laser (References 27 and 28) and the chemical laser (Reference 29), both of which utilize flowing gases to carry away the waste heat, which had been a limiting factor in non-flowing systems.

An excellent review of gas dynamic CO_2 lasers is given in References 27 and 30. Reference 27 discusses demonstrated performance up to 60 kw continuous output power. Reference 30 discusses use of the device to transmit electrical power over long distances without the use of wires, and discusses the attainment of high closed system efficiencies, the theoretical limit of which is unity. Note that for the gas dynamic laser, the input power must be supplied as shaft (pumping) power rather than electrical, which has a favorable effect on the total weight required for an airborne system.

However, attention must be given to the means by which the laser's radiant energy may be converted into a thermal pulse capable of creating a miniature sonic boom. There are at least two modes: continuous absorption of the radiation over the entire length of the beam, and a focused "breakdown" of the air at a localized spot.

The F-functions for these two modes are quite different. The wavelength of the radiation will determine the absorption characteristics of the beam at a given altitude; unfortunately, air is very nearly transparent to radiation in the 9-11 micron band at which most high power experimentation has been done. However, chemical lasers are capable of a wider range of frequencies.

As a result, the literature contains references to laser-generated spark breakdown, but not the continuous absorption type of heating, since the continuous high power devices have been at non-absorbing frequencies for the most part, and of course this is desirable for communication or transmission systems.

(A) Signature and F-Function Desired - The Thermal Pulse. The signature desired to provide a warning of an impending boom must have both the proper amplitude and timing with respect to the boom. The warning must be clearly audible but not so loud that it has appreciable startle effect of its own. A logical choice would be a level 20-30 db below the boom signal. In accordance with previous considerations of two-step signatures, the time interval should probably be around 50 msec. Obviously these choices should be the study of a psycho-acoustic response study for a precise definition.

Based on our baseline signature of 1.84 psf maximum overpressure, which would correspond to about 132 db peak, our warning signal should be at the 102-112 db level (peak),or .06 - .18 psf.

Typically, a thermal pulse gives an F-function shaped as in the sketch below

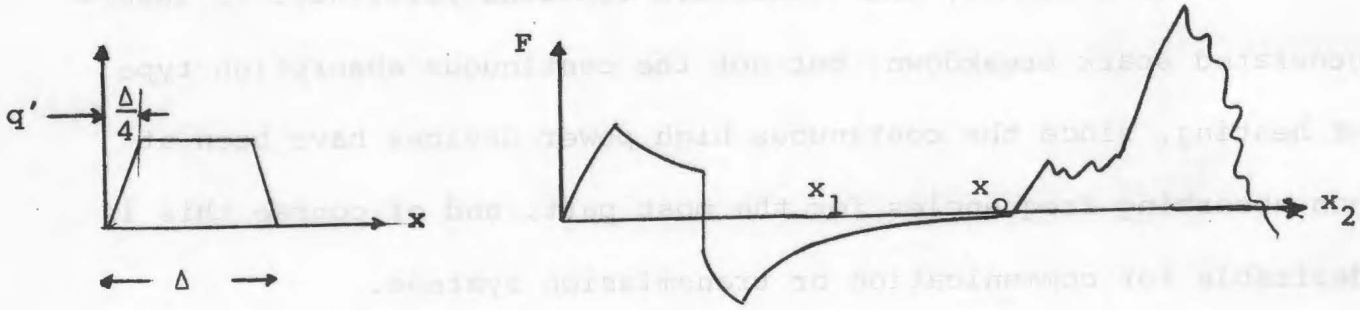

The assumption is made that the presence of the warning pulse does not change the baseline aircraft F function; i.e.

$$\int_{o}^{x_1} \frac{S''\,dt}{\sqrt{x-t}} << \int_{o}^{x_2} \frac{S''\,dt}{\sqrt{x-t}}$$

where x_2 has a value between x_o and x_L.

The resulting signature overpressures for the thermal pulse were found to be proportional to the square root of the F-function impulse, in accordance with (1):

$$\Delta P = 3.75 \left(\int_{o}^{y_o} F(y)\,dy\right)^{\frac{1}{2}} = 2.37 (F_{max} \cdot \Delta)^{\frac{1}{2}}$$

In terms of heat content of the thermal pulse

$$F_{max} = \left(\frac{2\ \sigma_o/\Delta}{\pi \rho u C_p T} \right) ft^{\frac{1}{2}}$$

$$Q = \frac{3}{4}\ \sigma_o \cdot \Delta \qquad \text{BTU/sec}$$

$$\Delta P = .0544\sqrt{Q/\Delta}$$

These relationships are shown in Figure 27 and it is seen that the required energy release is between 10 - 100 - kw.

(B) Continuous Absorption . The heat released per foot by means of continuous absorption of laser radiant energy may be expressed as

$$\sigma \ \alpha \ P_o \ e^{-kx} \qquad (17)$$

where P_o is the initial power level. Since our F function is given by

$$F = \frac{1}{2\pi} \int_o^x \sigma'(t) \ \frac{dt}{\sqrt{x-t}}$$

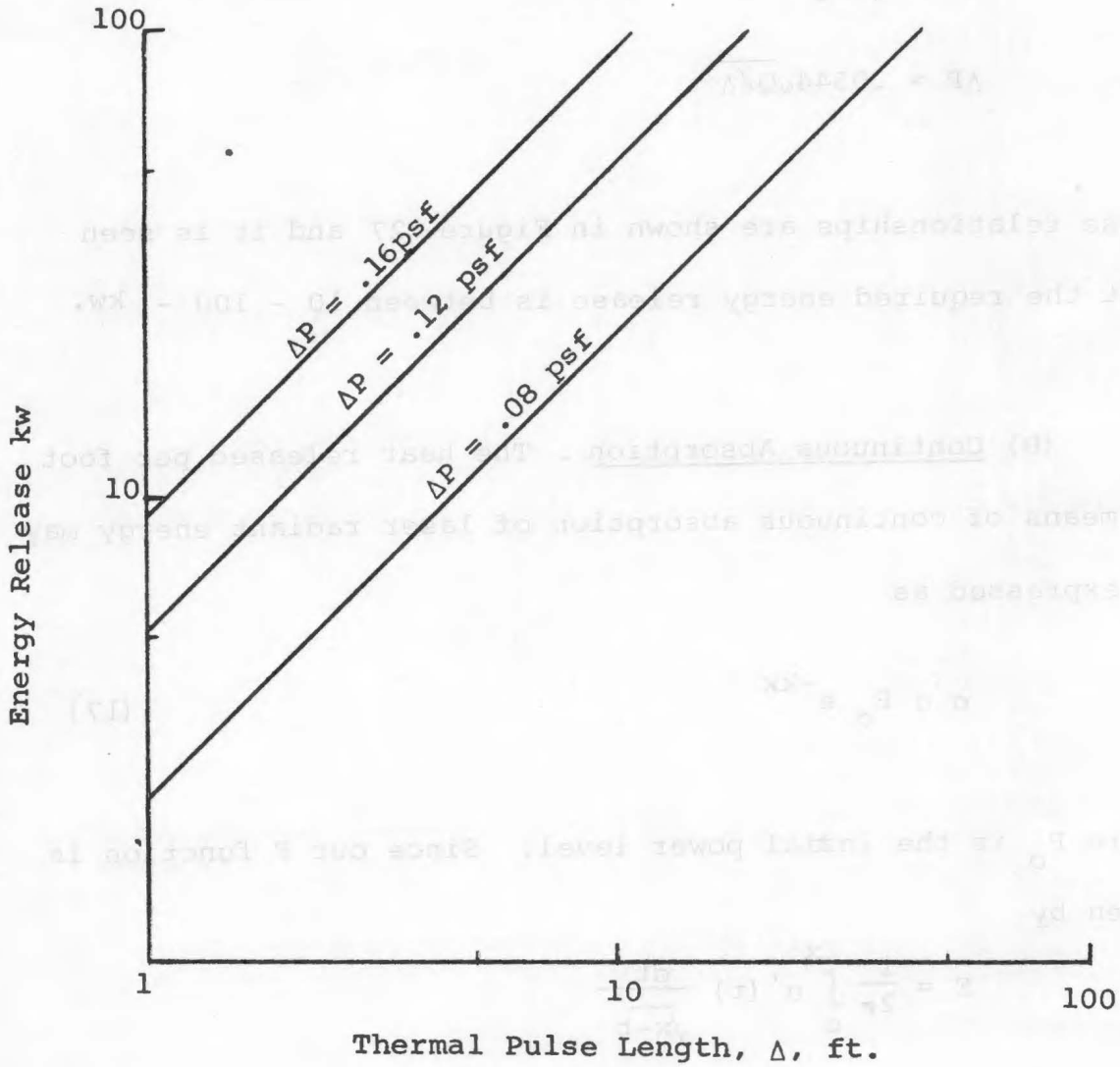

FIGURE 27 - Laser Energy Release Requirements for Thermal Pulse

This gives an expression for F of the form

$$F \alpha \ell^{kx} \operatorname{erf}\sqrt{kx}$$

which has its maximum value at large x; (x is measured from the aircraft nose upstream, in this case).

A strong absorption band is present at 4.3 μ due to resonance with the CO_2 normally present in atmospheric air. Using typical data from Reference 31, a maximum value of F of 1.3×10^{-5} is obtained at a laser output power of 1 mw. This is clearly too weak to provide a practical warning signal, being 80 db below the main signal. No further consideration was given to this mechanism of energy release.

IMPLEMENTATION STUDIES

An important part of this study of sonic boom alleviation through air stream alteration is the assessment of means of implementing the various alteration schemes and their effects on the baseline aircraft performance. Two types of methods were used for these assessments: the linearized theory described above, and actual calculations of pertinent physical processes.

(A) Linearised Theory Calculations. According to linearized theory,[14] force, heat and mass injection terms may each be related to an effective area distribution.

(1) force fields - Forces may be either axial (drag) or lateral (lift). An increase in effective area with no energy added corresponds to a drag, which would have an effect on the aircraft propulsion. A thrust force would, of course, be beneficial from both the standpoint of propulsion and local overpressure relief, but could not be used to create a phantom body, for example. Furthermore, it is physically difficult at Mach 2.7 to create a thrusting force aerodynamically without adding heat. Furthermore, considering typical airplane performance parameters, each additional pound of drag requires 2.2 pounds in extra fuel weight for 2,500 mile range.

However, lift forces are the simplest of all to implement, consisting only of dead weight and a surface to support it. In the case of a composite means of implementation this might be the weight associated with the equipment required for the other mechanisms (heat, mass addition).

From Eq. (12) the effective area and weight (lift) are related by

$$\Delta S_L = \frac{\beta \Delta W}{\rho u^2} \tag{18}$$

which for 62,000 feet, Mach 2.7 gives $\Delta S = \Delta W/554$.

From Reference 3 , considering electroaerodynamic force generation, a weight penalty of 200-2000 lbs. is incurred for each pound of force.

Thus, it is clear that the most practical method of providing a force distribution is through the use of lifting surfaces.

(2) Mass injection -

Referring again to Eq. (12),

$$\Delta S_m = \frac{\Delta \dot{M}}{\rho_i u_o}$$

which defines the effective area contribution due to mass injection. Note that this is an isentropic mass injection, from the linearized theory approach, and that the density of the injectant ρ_i must be considered.

For flight at 62,000 feet, Mach 2.7,

$$\Delta S_m = \frac{\Delta m}{17.1(\rho/\rho_o)} \quad , \quad \dot{m} \text{ in lb/sec} \tag{19}$$

(3) Heat addition -

From Eq. (12),

$$\Delta S'_Q = \frac{\Delta\sigma}{\rho_o u_o C_p T_o}$$ where σ is the heat release per unit length. At Mach 2.7, 62,000 feet, the relationship is $\Delta S_Q = Q/1600$; Q in BTU/sec. (20)

For combustion of hydrocarbon fuel, for example, with 18,000 BTU/lb. heating value,

$$\Delta S_Q = 1.1\ \Delta\dot{m}f \tag{21}$$

indicating the much larger theoretical effect of combustion with respect to pure mass addition.

(B) Physical Process Calculations.

(1) Mass addition - The process of mass addition was considered as boundary layer "blowing" or transpiration, for which

both experimental and theoretical results are available. The results are summarized in Figure 28, which shows data from the experiments of Referance [32] and two theoretical calculations made at GASL, using the methods of of Reference [33]. These results are for two-dimensional (flat plate) flow, which of course would only apply on a cylindrical body when the radius is large in comparison to the perturbed boundary layer thickness.

For both theoretical and experimental cases, a substnatially larger effedt is shown than predicted by linearized theory. This amplification factor, denoted k, varies from about 6 to 10, and is apparently due to the entrainment of a portion of the free stream and the thickening effect caused by the resulting deceleration.

Based on Figure 28, then Eq. (19) would be modified to read

$$\Delta S_m = \frac{\Delta \dot{m}}{1.7-3.0(\rho/\rho_o)} \tag{22}$$

a result that could be competitive with combustion for light gas injection $(\rho/\rho_o \cong 0.1)$.

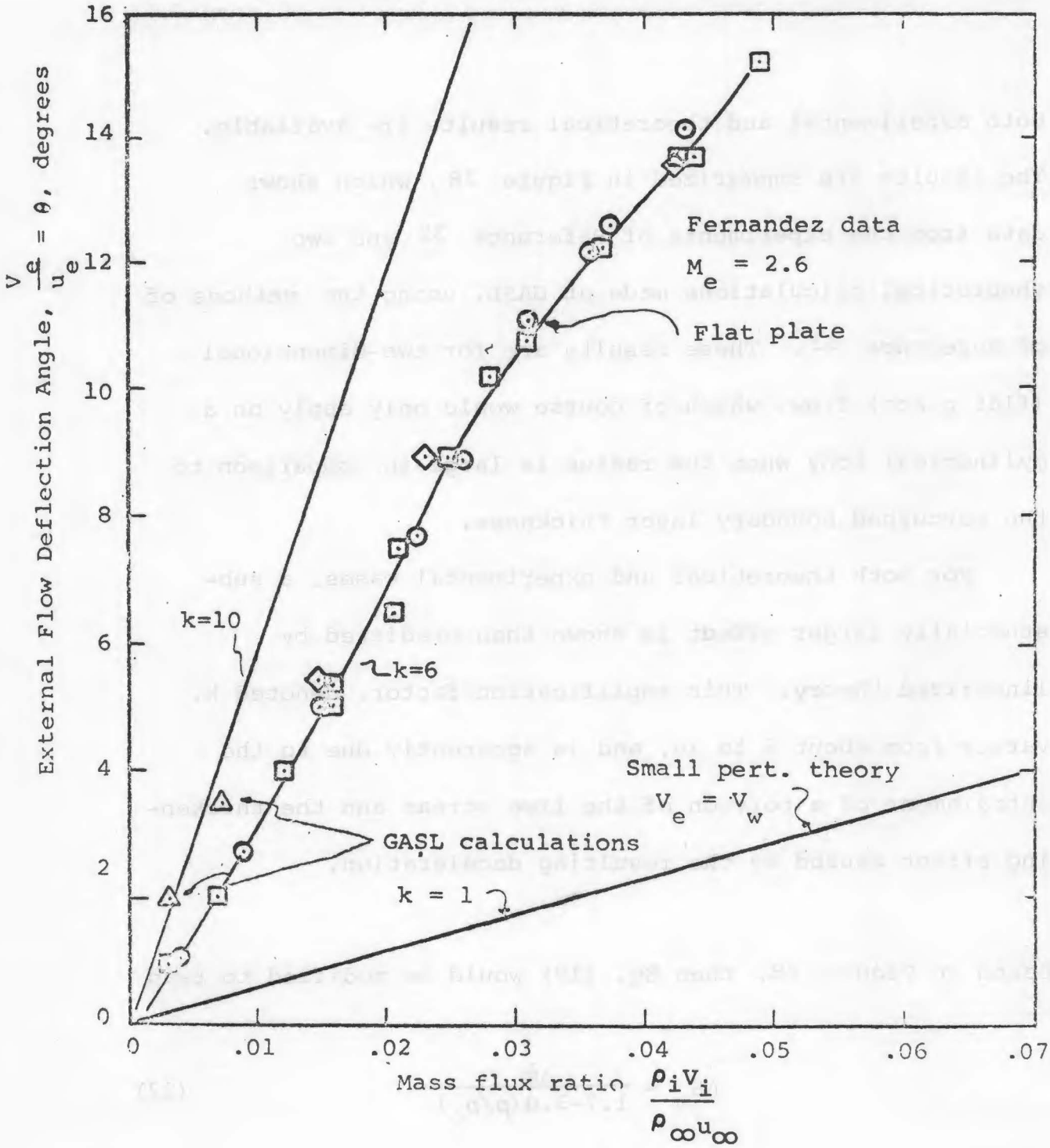

Figure 28 - Boundary Layer Blowing Effects on External Flow Deflection

Examples of the details of the theoretical boundary layer calculation are given in Figures 29 and 30, showing the effect of temperature and Reynolds number. The asymptotic portions of the curves were used on Figure 29. In Figure 30, the fact that combustion is taking place in the boundary layer decreases the density there and adds to the flow displacement effect.

Of course there is a displacement effect with zero blowing as well, just due to free stream entrainment. This is given in Figure 31, and is seen to correspond to about 0.5 degrees at high Reynolds numbers.

Although the detailed calculations of the present study were limited to cylindrical bodies (flat plate theory), the following expression was derived to convert the flat plate data for use on a conical surface of semi vertex angle α_c

$$dS/dx = \pi \sin \alpha_c [x(\tan^{-1}\theta)_{FP} + (\delta^* + \int_0^x \frac{\rho_i V_i}{\rho_\infty u_\infty} dx)_{FP}] \tag{23}$$

(2) Heat Addition - Combustion - Computation of heat addition processes was limited to cases involving free combustion, i.e., a combustion process in which the major portion of the air is supplied from the ambient. This is thus a mixing dominated process.

At the ambient conditions in question the ignition delay for hydrocarbon fuels is quite long (on the order of seconds) and

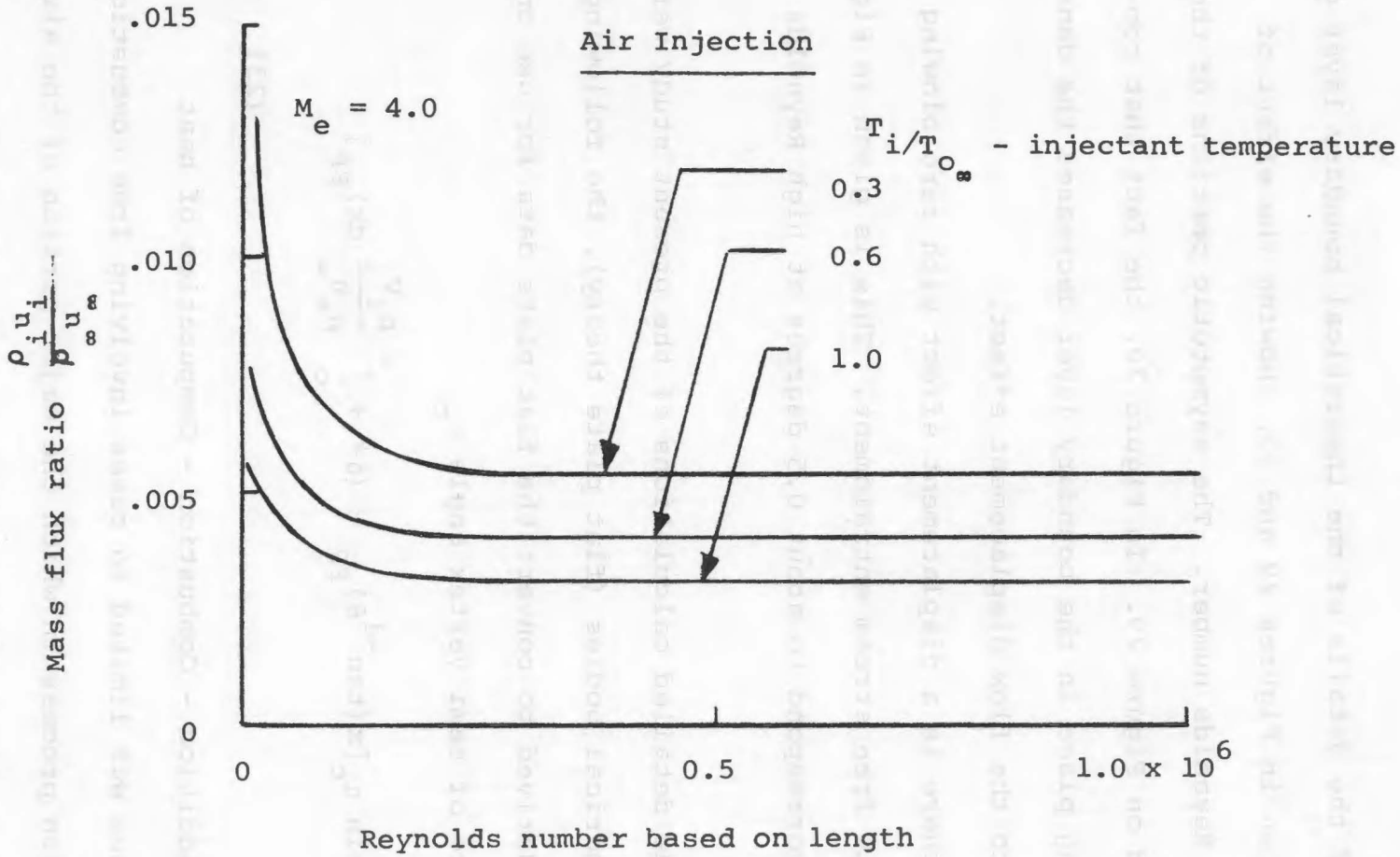

FIGURE 29 - Mass Flux Ratio Required for Flow Deflection Angle of 2°

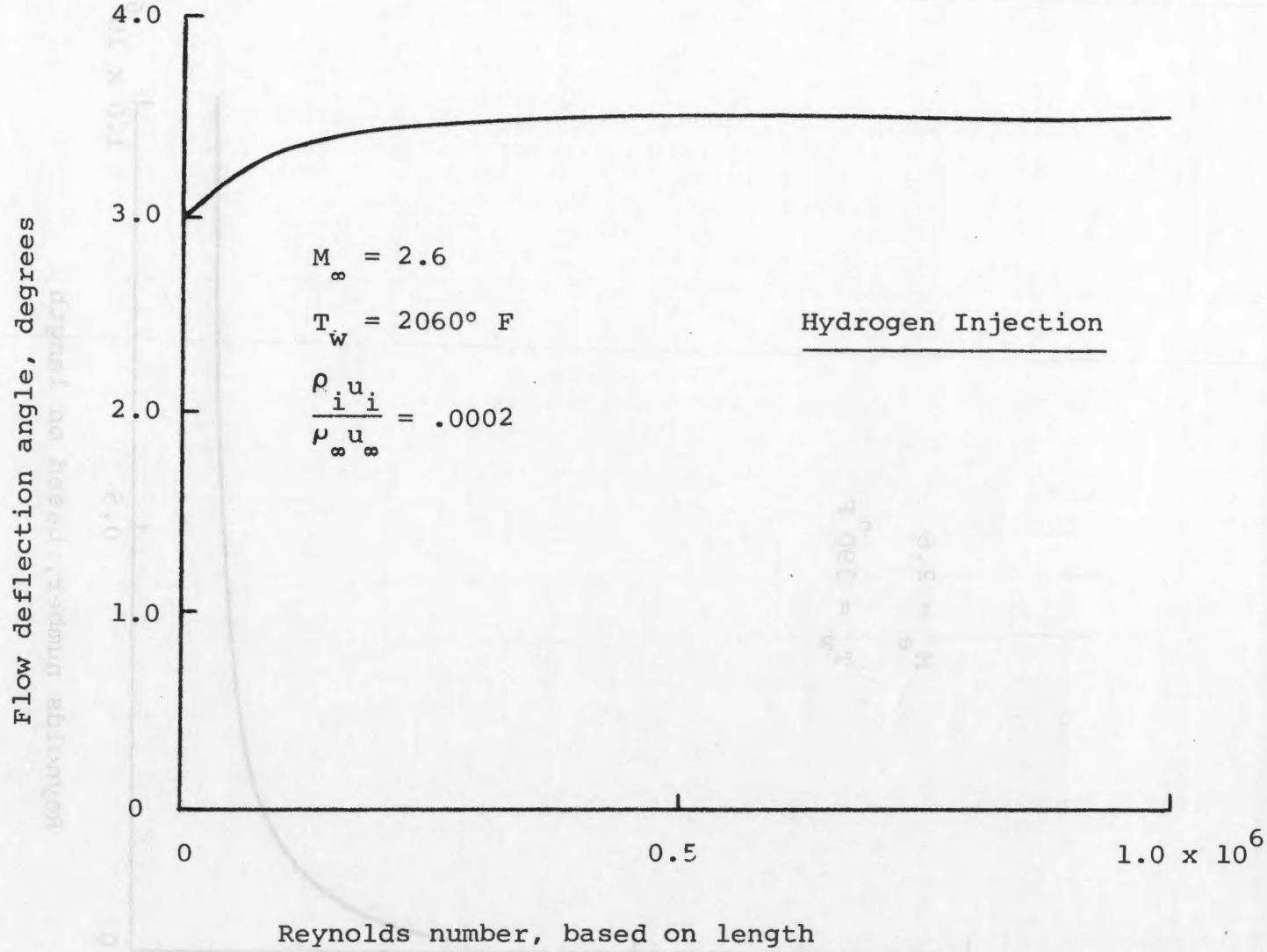

FIGURE 30 - Flow Deflection Resulting from Uniform Injection and Combustion of Hydrogen in Boundary Layer

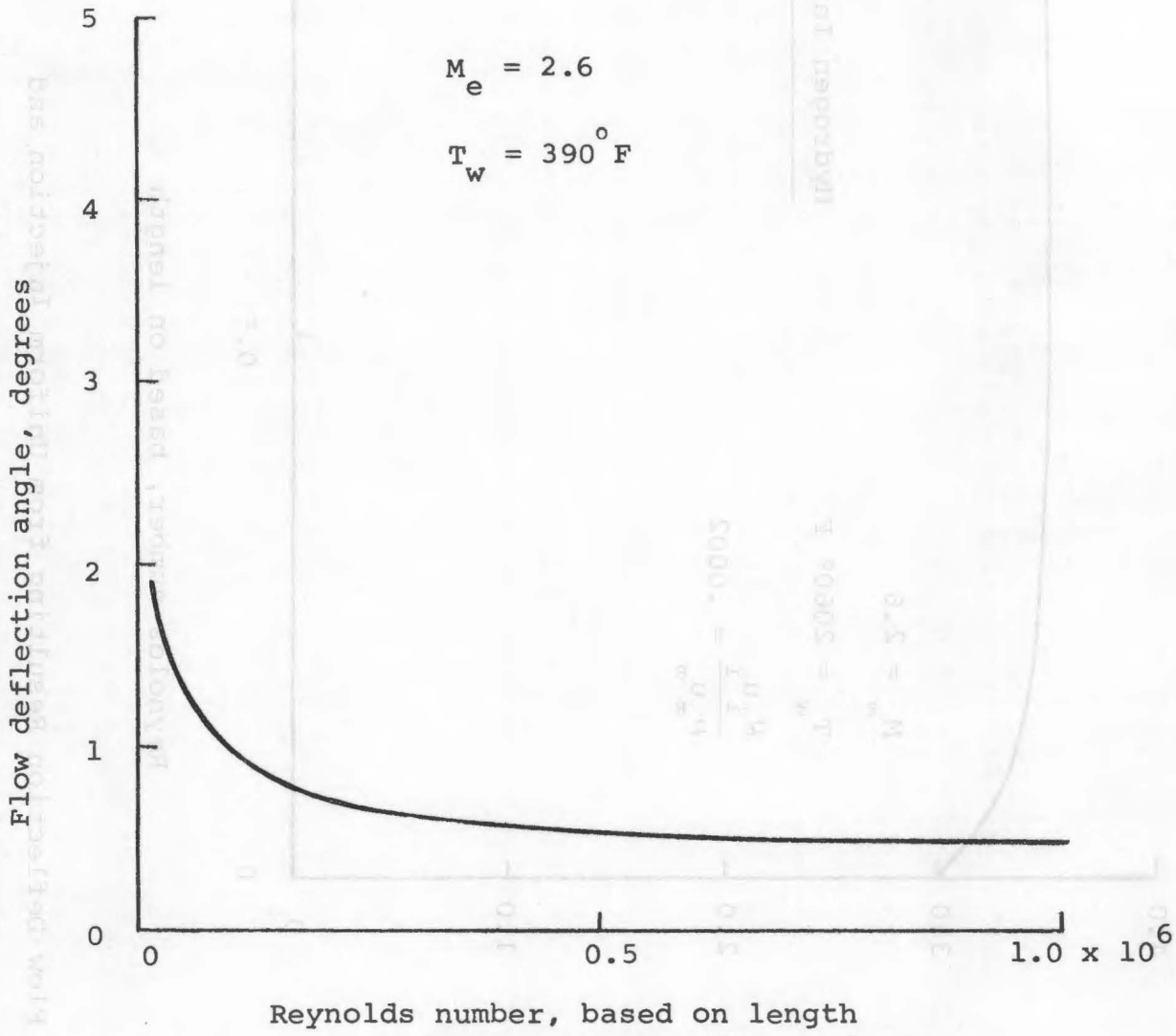

FIGURE 31 - Flow Deflection Angle Due To Boundary Layer With Zero Mass Injection

clearly an auxiliary means must be used to initiate the flame. Furthermore, care must be taken that this hot core be sufficiently large to prevent quenching by the cold ambient air. Such quenching is not only undesirable from an efficiency point of view, but unacceptable from an environmental point of view.

It was felt that the initial computation of combustion/mixing phenomena should be simple, and thus chemical kinetic limitations were not considered. Furthermore, the assumption of "complete combustion" was made, i.e., the only combustion products considered are H_2O and CO_2. The computational methods of Reference 34 were used. A schematic of the flow field is shown in Figure 32.

Within the limitations of the turbulent mixing model, these results may then be scaled to other jet diameters. This model is described more fullin in Reference 35, and consists of the following specification of the turbulent viscosity:

$$\mu_t = (4\ \rho_S\ x\ (u_{\mathfrak{L}} - u_S) + 1) \cdot 10^{-4} \qquad (24)$$

for x distances less than the potential core length

(where $u_{\mathfrak{L}} = u_{\mathfrak{L}\ x=o}$)

for greater x distances

$$\mu_t = 0.018\ r\ \frac{1}{2}\ (\rho u)_{\mathfrak{L}} \qquad (25)$$

where r ½ is the location of the mean mass flux at the axial station in question. These viscosity models have been correlated successfully with experimental results (References 34 and 35).

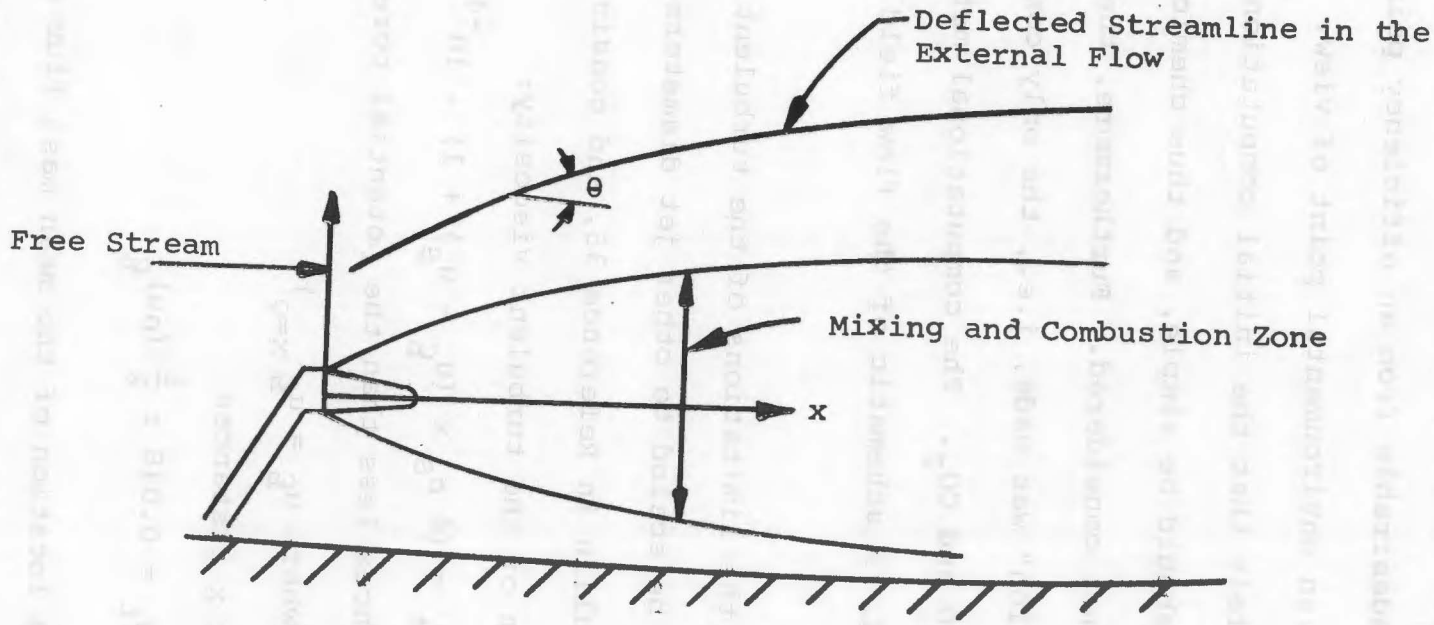

FIGURE 32 - Schematic of Jet Flow with Combustion

Three cases were computed under these ground rules:

Case 1 - hot fuel pilot jet

$T_j = 1500^\circ R$

$u_j = 950$ ft./sec.

$r_j = 0.5$ ft.

laminar mixing

Case 2 - same, with turbulent mixing

Case 3 - Supersonic, fuel rich burner exhaust pilot jet

$M_j = 2.0$

$T_j = 3600^\circ R$

$u_j = 6000$ ft./sec.

$r_j = 1.8$ ft.

turbulent mixing

In all cases, the fuel considered was C_9H_{20}, which gives a reasonable representation of common jet fuels (kerosene, JP, propane, etc.) with the limitations of the quasiglobal chemistry model (Ref. 34). However, with the assumption of complete combustion, these details are not important.

The laminar mixing case was included for completeness, but was found to have insignificant mixing at x distances for which transition to turbulent flow was quite certain. No results for this are discussed.

The turbulent cases are shown in Figure 33, in terms of the displacement area vs axial length. Case (3) is representative of a fuel-rich plume exhaust of a turbojet-type engine. The discontinuity at x = 10 feet results from the changeover in turbulent viscosity models at the end of the potential core, described above.

Case (2) was intended to represent truly free combustion; i.e., a central fuel jet with the entire air supply coming from the ambient. This is an impractical situation from a chemical kinetics point of view, and a strong pilot of some sort would be needed to sustain combustion. For this reason, the fuel injection temperature was chosen higher than is physically possible for most hydrocarbon fuels without excessive pyrolysis. The fuel injection conditions thus represent the combined effects of fuel and pilot. In contrast to case (3), case (2) displays a maximum displacement area at $x \cong 42$ feet. Beyond that point, a negative S′ would be felt, which could be an advantage at certain locations in the composite signature. The discontinuity at x = 4 ft. is again the end of the potential core. The difference in location of this discontinuity between case (a) and (b) reflects not only the differences in the initial radii (1.8 vs .5 ft) but in the initial conditions as well. It is interesting to note, however, the similarity between the two cases at $10 < x < 40$ feet, which follows from the similarity in the total heat added to the free stream.

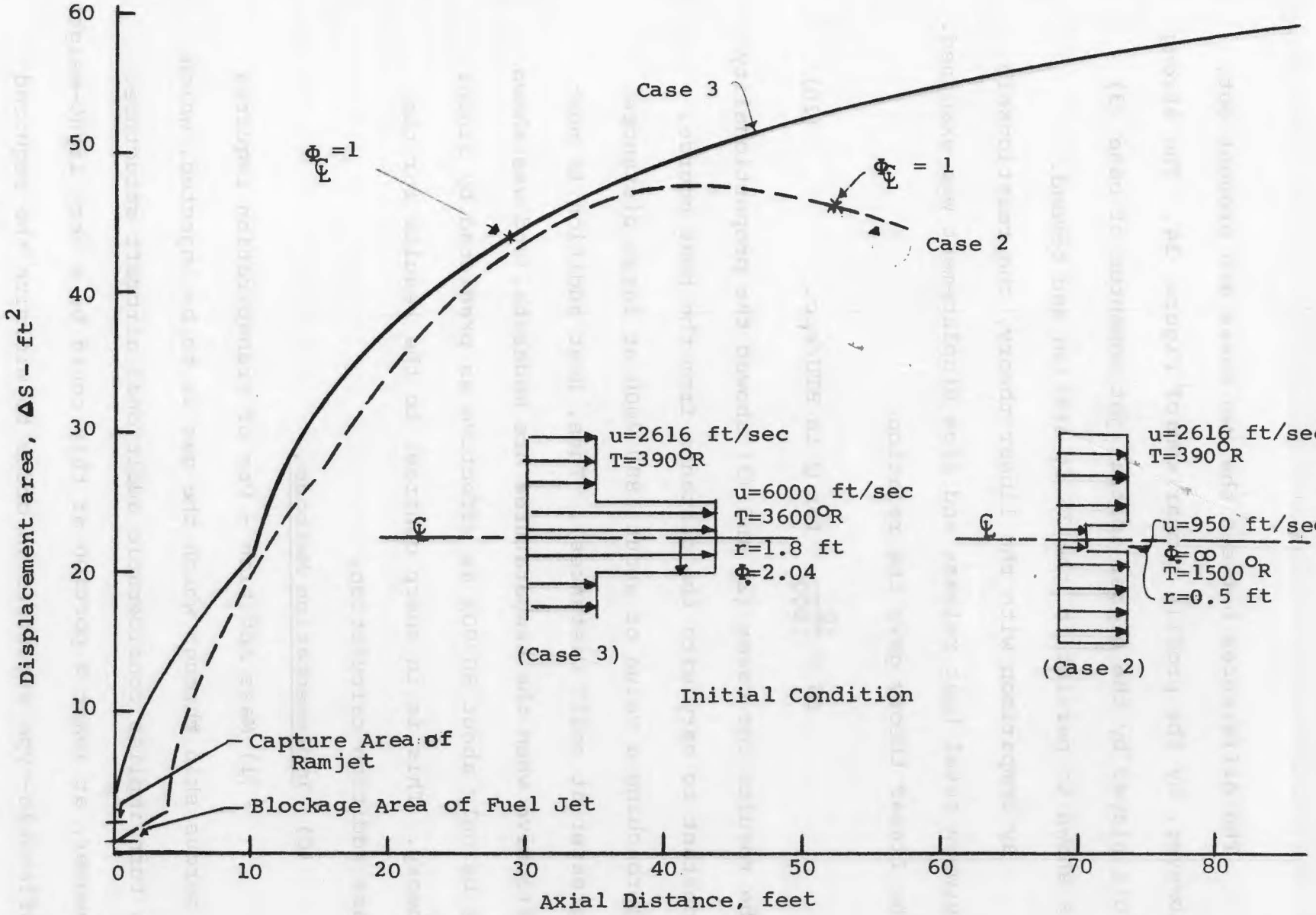

FIGURE 33 - Calculated Displacement Areas Due to Combustion

The differences between the two cases are brought out, however, by the profile comparisons of Figure 34. The strong role played by the higher initial jet momentum of case (3) is shown to persist to the 35 ft station and beyond.

By comparison with the linear theory, the relationship between total heat release and area displacement was examined. The linear theory gave the relation

$$\Delta S = \frac{\Delta Q}{1600} \quad \text{for } Q \text{ in BTU/sec.} \qquad (20)$$

The results for cases (2) and (3) showed the proportionality constant to vary with the distance from the heat source, approaching a value of about 1800-2000 at large distances (greater at small distances). Thus, heat addition is most effective when the temperatures are moderate, and was shown to be only about 80-90% as effective as predicted by linear theory. This is in sharp contrast to the results for the mass addition calculation.

(C) Implementation Methods.

(1) Mass Addition - Use of transpiration requires a porous skin through which the gas is to be injected, which in turn implies considerable additional aircraft structure. However, at least a portion of this could be a very light-weight inflatable-type structure in order to minimize the required lifting surfaces.

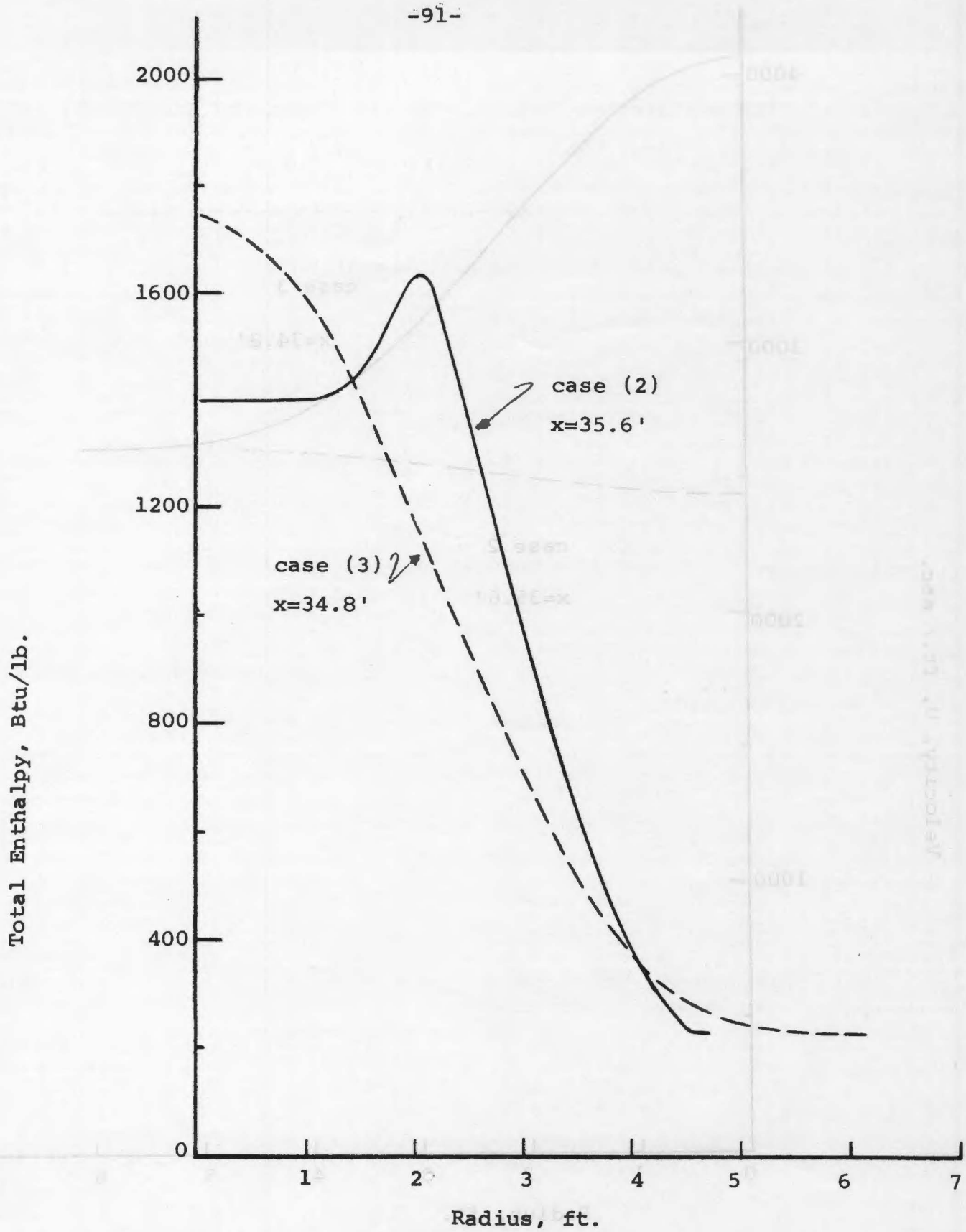

FIGURE 34(a) - Enthalpy Profile Comparison

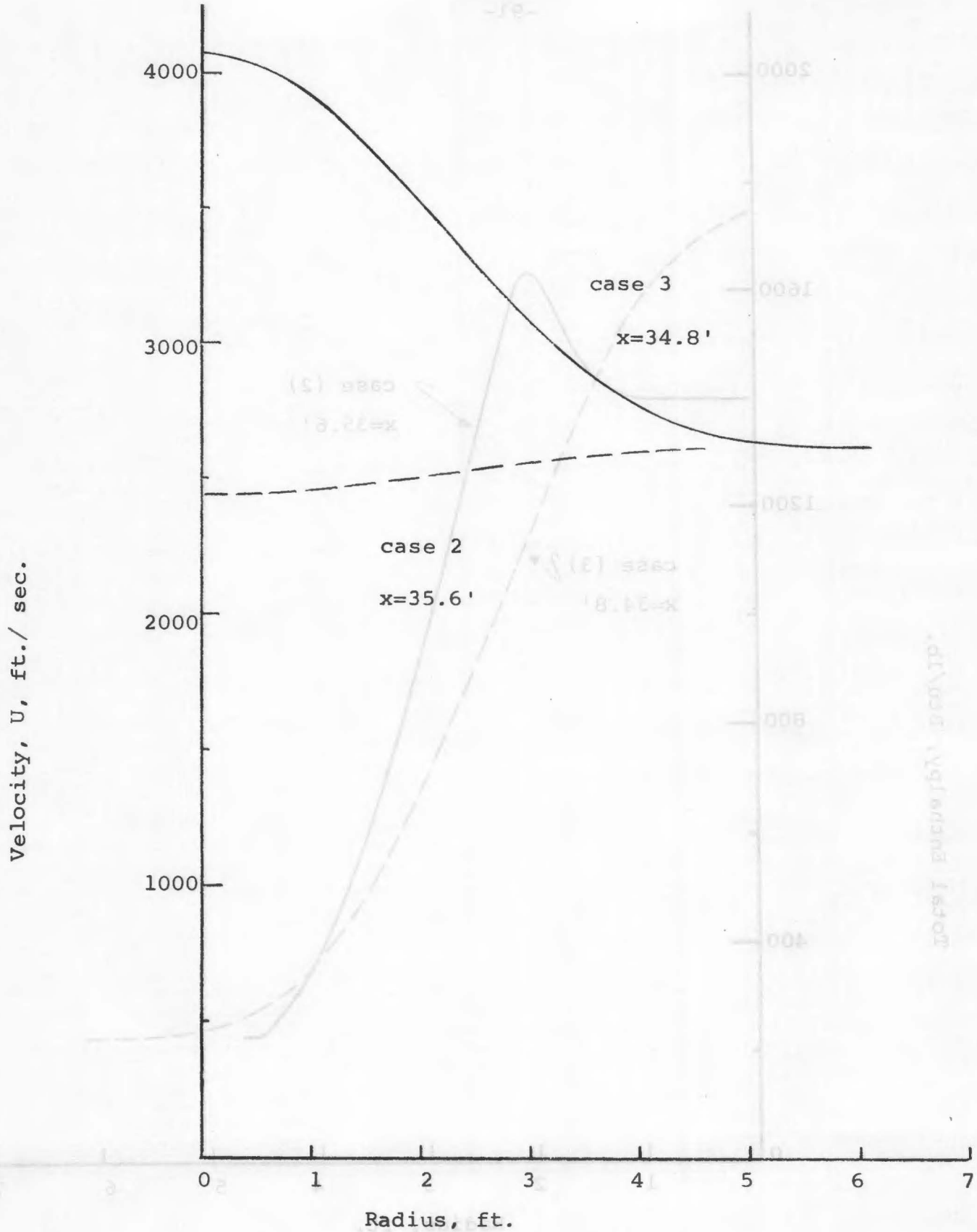

FIGURE 34(b) - Velocity Profile Comparison

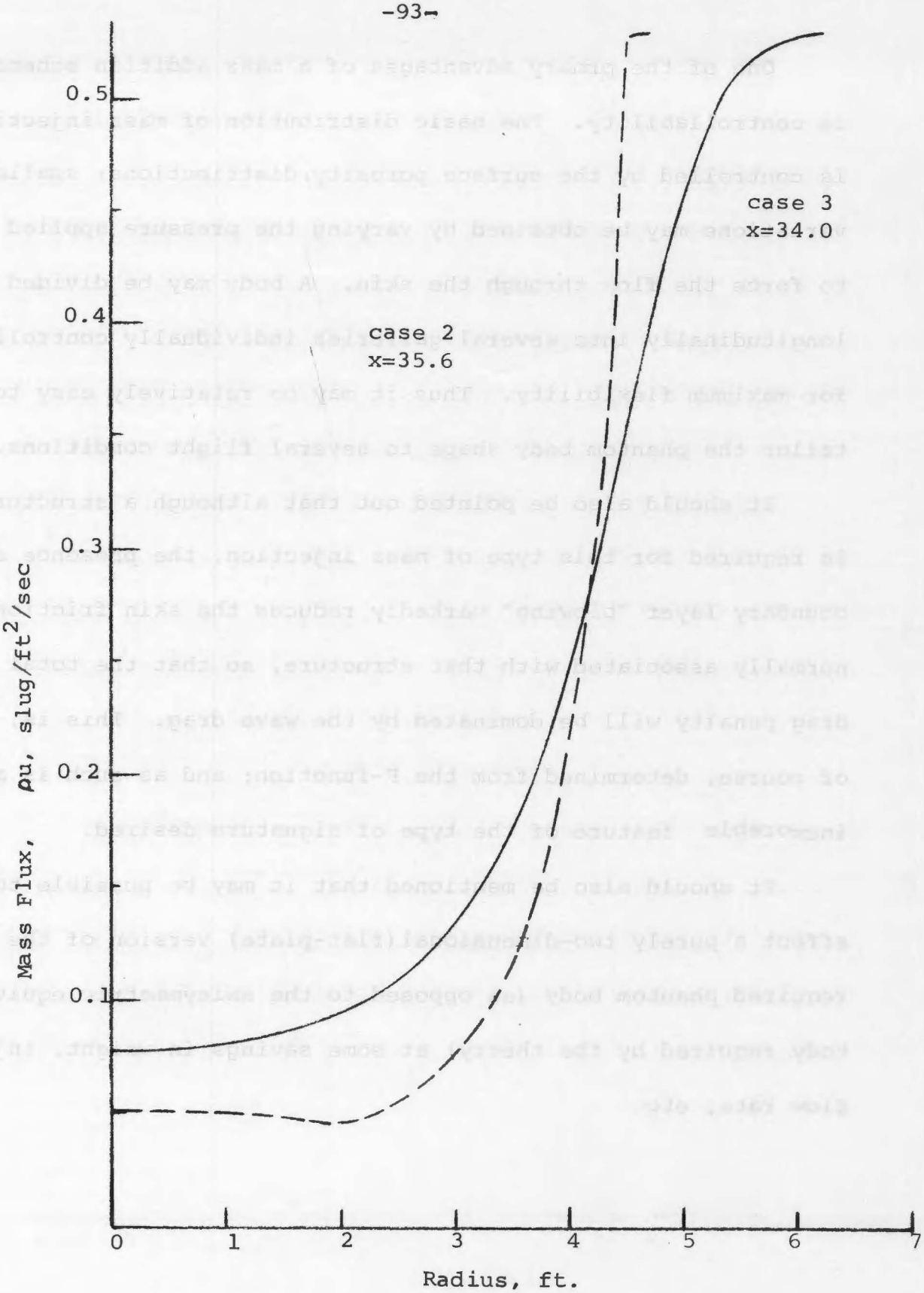

FIGURE 34(c) - Mass Flux Profile Comparison

One of the primary advantages of a mass addition scheme is controllability. The basic distribution of mass injection is controlled by the surface porosity distributions; smaller variations may be obtained by varying the pressure applied to force the flow through the skin. A body may be divided longitudinally into several galleries individually controlled for maximum flexibility. Thus it may be relatively easy to tailor the phantom body shape to several flight conditions.

It should also be pointed out that although a structure is required for this type of mass injection, the presence of boundary layer "blowing" markedly reduces the skin friction normally associated with that structure, so that the total drag penalty will be dominated by the wave drag. This is, of course, determined from the F-function; and as such is an inexorable feature of the type of signature desired.

It should also be mentioned that it may be possible to effect a purely two-dimensional (flat-plate) version of the required phantom body (as opposed to the axisymmetric equivalent body required by the theory) at some savings in weight, injection flow rate, etc.

(2) Heat Addition - Combustion - The combustion processes analyzed give equivalent area distributions of a particular shape, defined by the mixing rate. These shapes may presumably be expanded or contracted somewhat by varying the fuel flow rate, but the basic shape will tend to remain. Special steps must thus be taken in order to create a specified phantom body of different shape through combustion.

First of all, a tailored upstream nose could be used. Depending upon the length, portions of the equivalent body due to combustion can be made to assume a desired power law variation in this way. Figure 35 presents the data of case (3), in log coordinates, with various nose lengths. The ΔS values have been adjusted to account for the streamtube area required to capture the air needed for the initial combustion process. Use of a 20 ft nose will allow a 5/2 power law shape to be approximated for 10-15 feet additional length. Beyond that, an additional tailored heat source would be required to maintain the desired slope.

In the case of real, kinetically limited combustion processes, changes in altitude, wind speed, free stream turbulence,etc., would all affect the combustion processes and thus the superposition of sources.

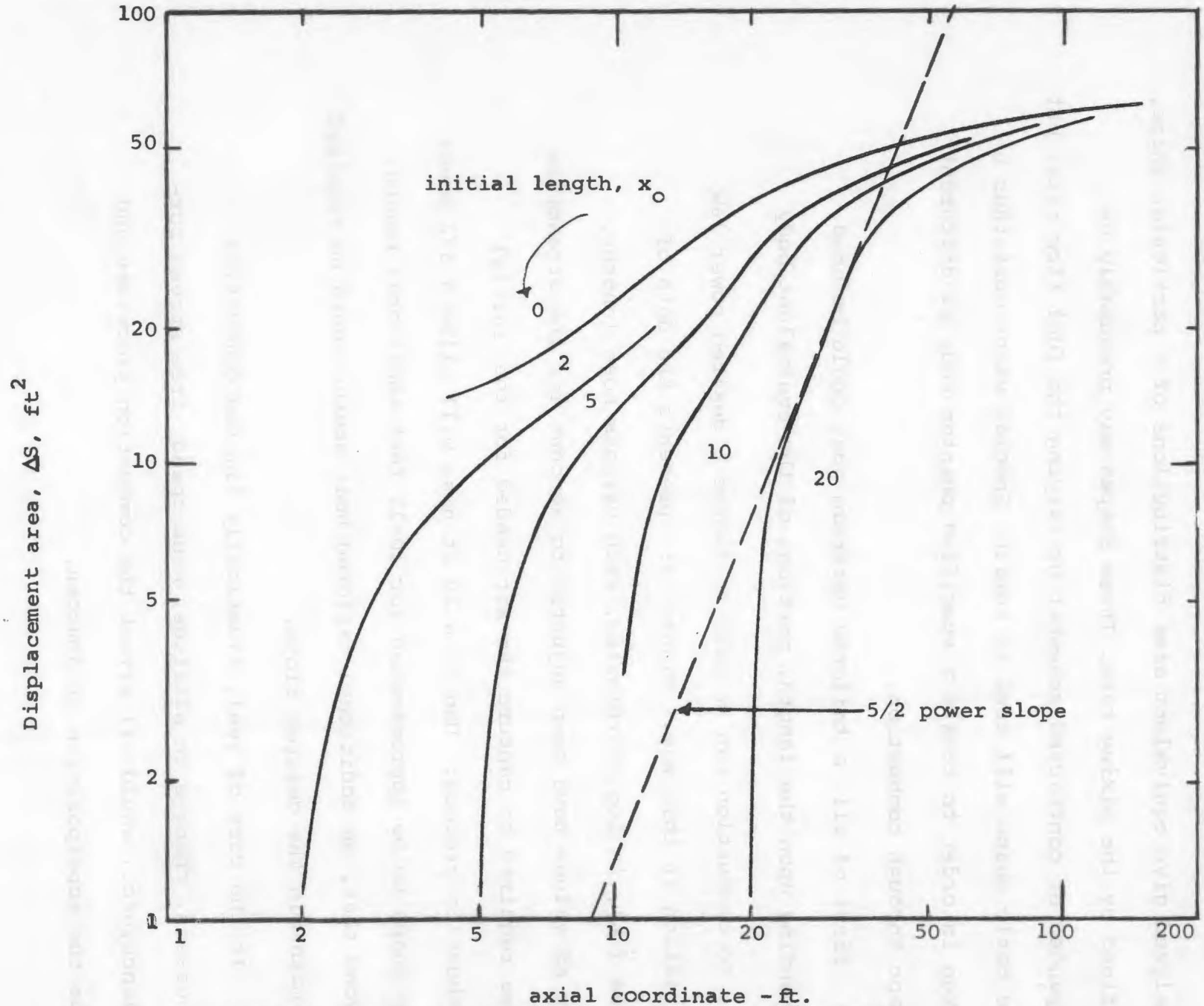

FIGURE 35 - Effect of Initial Length on Area Variation

(D) Implementation of Laser Heat Impulse. The requirements for an audible warning signal preceding the boom have been examined from the pressure perturbation point of view, using the linearized theory approach. In this section, actual laser operating characteristics are reviewed, based on available literature, in order to estimate feasibility and weight penalties.

(1) Breakdown characteristics - The literature consists of many examples of the breakdown of gases exposed to "giant" laser pulses. Figure 36, taken from Reference 36, presents the breakdown characteristics in terms of power required. At 1 atm in air, approximately 1 mw is required, based on Figure 36, while other investigators have reported values as high as 5-10 mw, apparently due to differences in focusing lenses. Extrapolating Figure 36 to P = 137 psf (62,000 ft.) would give an estimated power requirement of 5 mw under the best conditions.

The literature shows that about 60% of the incident energy is absorbed in the plasma that occurs at breakdown. The literature, which is based solely on pulsed operation, also contains references to various unsteady phenomena associated with the breakdown. These include the observation that the plasma tends to persist after the laser pulse has terminated, and that the breakdown behaves as a detonation wave, moving at a speed around 10^7 cm/sec.

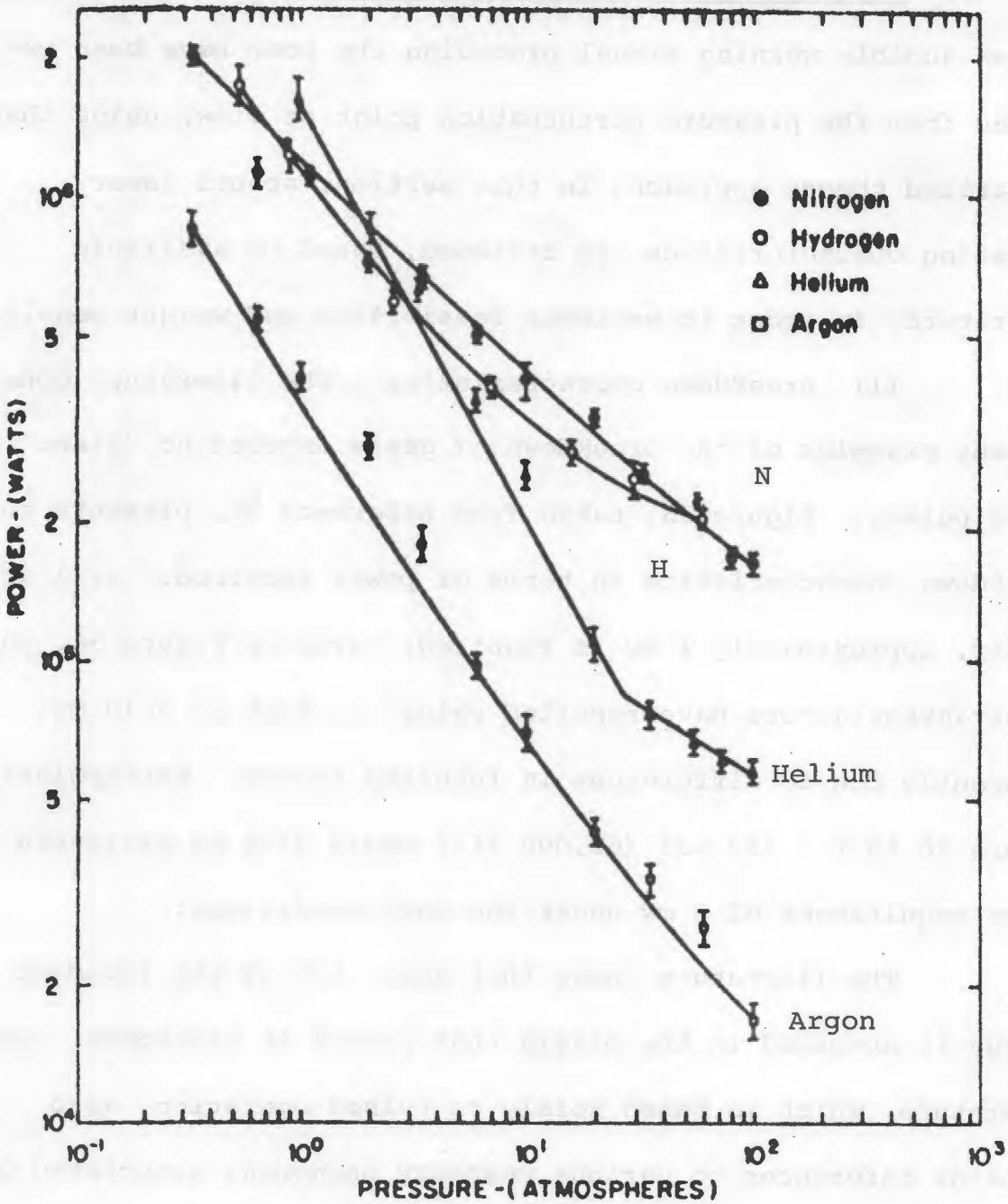

FIGURE 36 - Breakdown Characteristics of Various Gases at $\lambda \cong .7\ \mu$ (Reference 36)

Obviously both of these observations would have a bearing on the application of an airborne, moving, laser-powered warning system. The persistence would make a pulsed rather than cw mode of operation feasible for "quasi" steady ground signal, and the movement of the wave would affect the computation of the acoustic properties of the pulse. Finally, it should be mentioned that the power densities and thermal levels associated with breakdown are orders of magnitude higher than permitted for use with the linearized theory. In fact, the minimum breakdown strength becomes the primary factor determining the laser signal power requirement; the boom computation must follow a posteriori.

(2) Laser Beams and Focusing - In an ideal optical system, the radiance (power per unit area per unit solid angle) is preserved and can never be increased. This parameter is typically around 10^7 watts/cm^2/steradian for cw CO_2 lasers and 10^{15} watts/cm^2/steradian for pulsed solid-state lasers.

In addition to the source radiance, beam divergence must be considered. For a diffraction limited beam the divergence is given by

$$\theta = 1.22\ \lambda/D \qquad (26)$$

where λ is the wavelength and D is the numerical aperture, approximately the source diameter.

For the sonic boom precursor, it is desired to focus the energy at a point approximately 300 ft (100 m) from the aircraft. Assuming a 1 meter source diameter, then $\theta = 1.2 \times 10^{-6}$ radian and the minimum spot diameter for a CO_2 laser (10.6 μ) will be 1.3 mm. Based on the power density data of Reference 36 (4.4×10^{12} watts/cm^2), the laser output power required would be about 60 GW.

At shorter wavelengths (ruby ~ .69 μ) the spot size is substantially smaller, and the power required is reduced to around 250 MW.

In both cases, these requirements are substantially beyond the state-of-the-art and its current projections, even considering the 10^3 increase in pulse power that may be obtained from "Q-switching" a CO_2 cw laser. For example, a typical (short range) gas dynamic laser brightness value is 4×10^9 watts/cm^2 (Reference 37), and although breakdown has been achieved at atmospheric pressure and ranges of a few meters, the source brightness is insufficient for long ranges at low pressure.

With solid state lasers, the basic problem is efficiency; typically less than 1%, which would mean an enormous airborne electrical power requirement.

(E) Air Stream Compression. Some of the sonic boom alleviation schemes proposed by others rely on propulsive devices which produce an exhaust stream with (ρu) greater than (ρu) at the inlet, and also produce a net forward thrust. While this task is relatively straightforward at low subsonic flight speeds, this is not the case at supersonic speeds. An analysis was made of (non afterburning) turbojet engine cycles to determine the possible effect. The results are given in Figures 37 to 42.

Figure 37 presents the effect of various compressor pressure ratios on the minimun exhaust area achievable. The curves show that airstream compression is possible ideally with either low pressure ratios, in which case the engine produces drag instead of thrust, or at very high pressure ratios, generally beyond the anticipated state-of-the-art.

Figures 38 to 42 are based on a compression ratio of 10, and illustrate the effects of some of the other parameters. Figures 38 and 39 show the effect of turbomachine efficiency; Figures 40 and 41 γ_{exit} specific heat ratio; and Figure 42, overall pressure recovery. All of these effects tend to increase the exit area, so that the net conclusion is that no practical benefit may be obtained from this effect through the use of simple turbojet cycles. It is also interesting to note the close relationship of the minimum area and maximum I_f points.

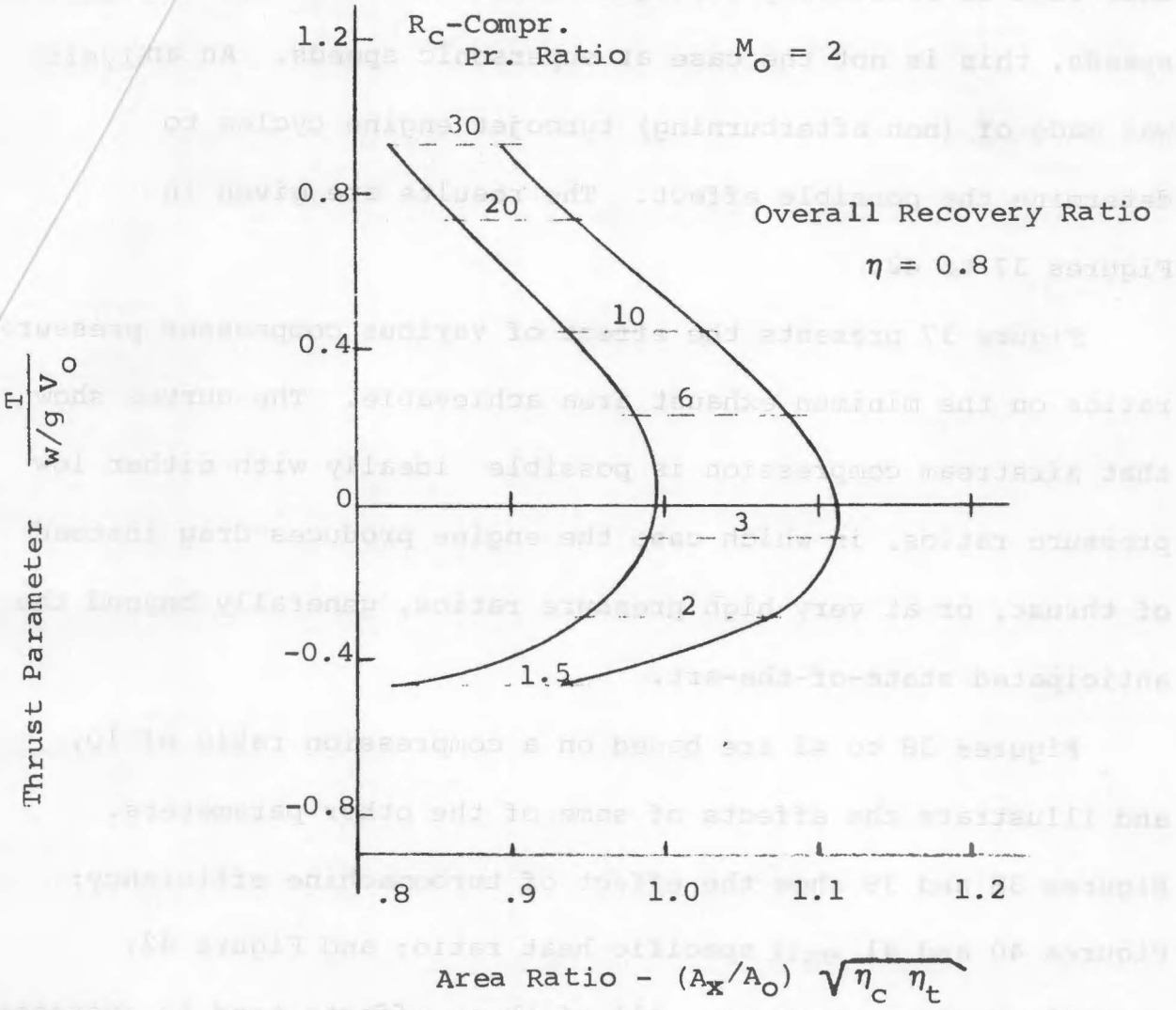

FIGURE 37 - Optimum Thrust/Area Relationship for Turbojet Cycle.

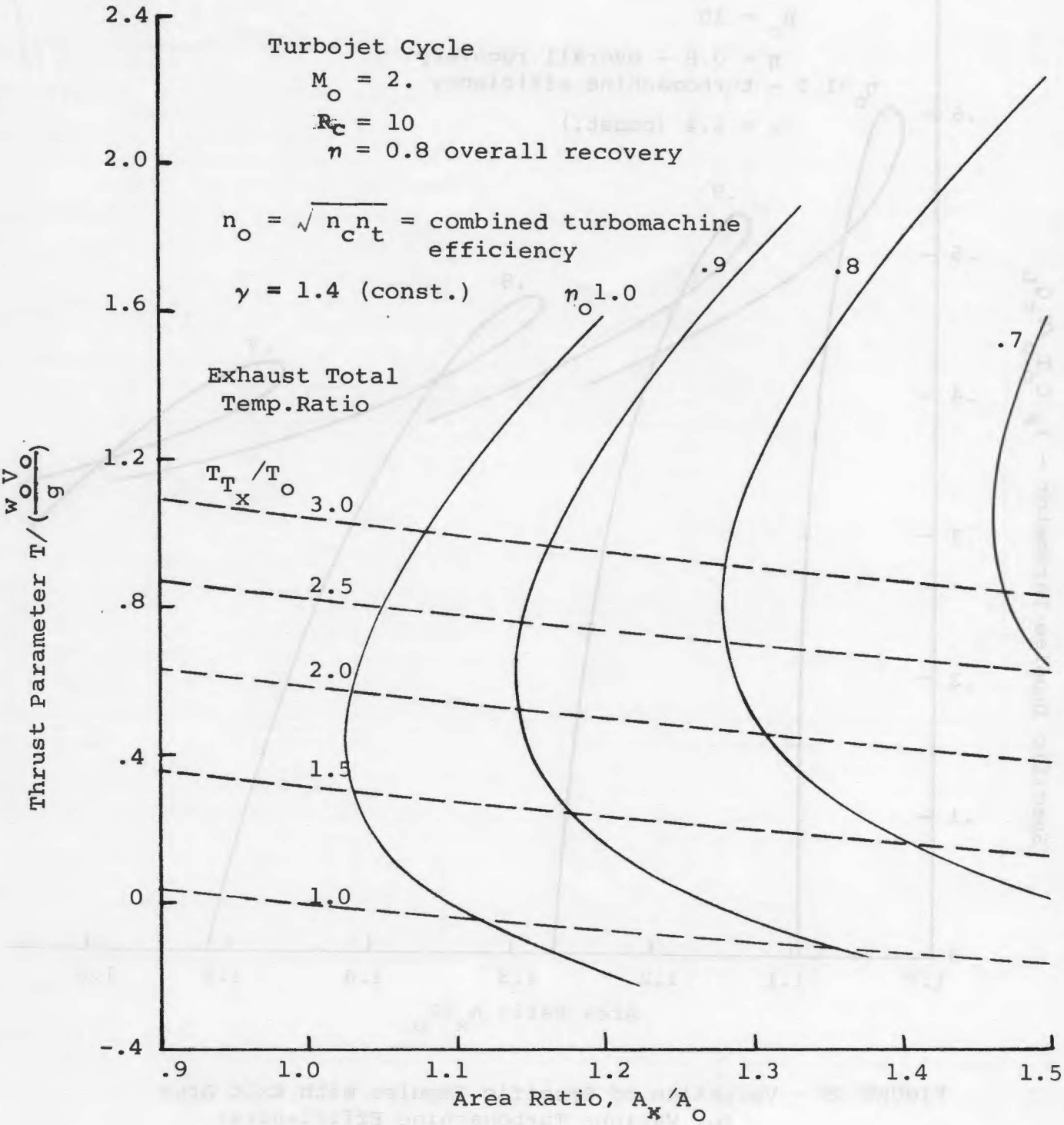

FIGURE 38 - Variation of Thrust with Exit Area for Various Turbomachine Efficiencies

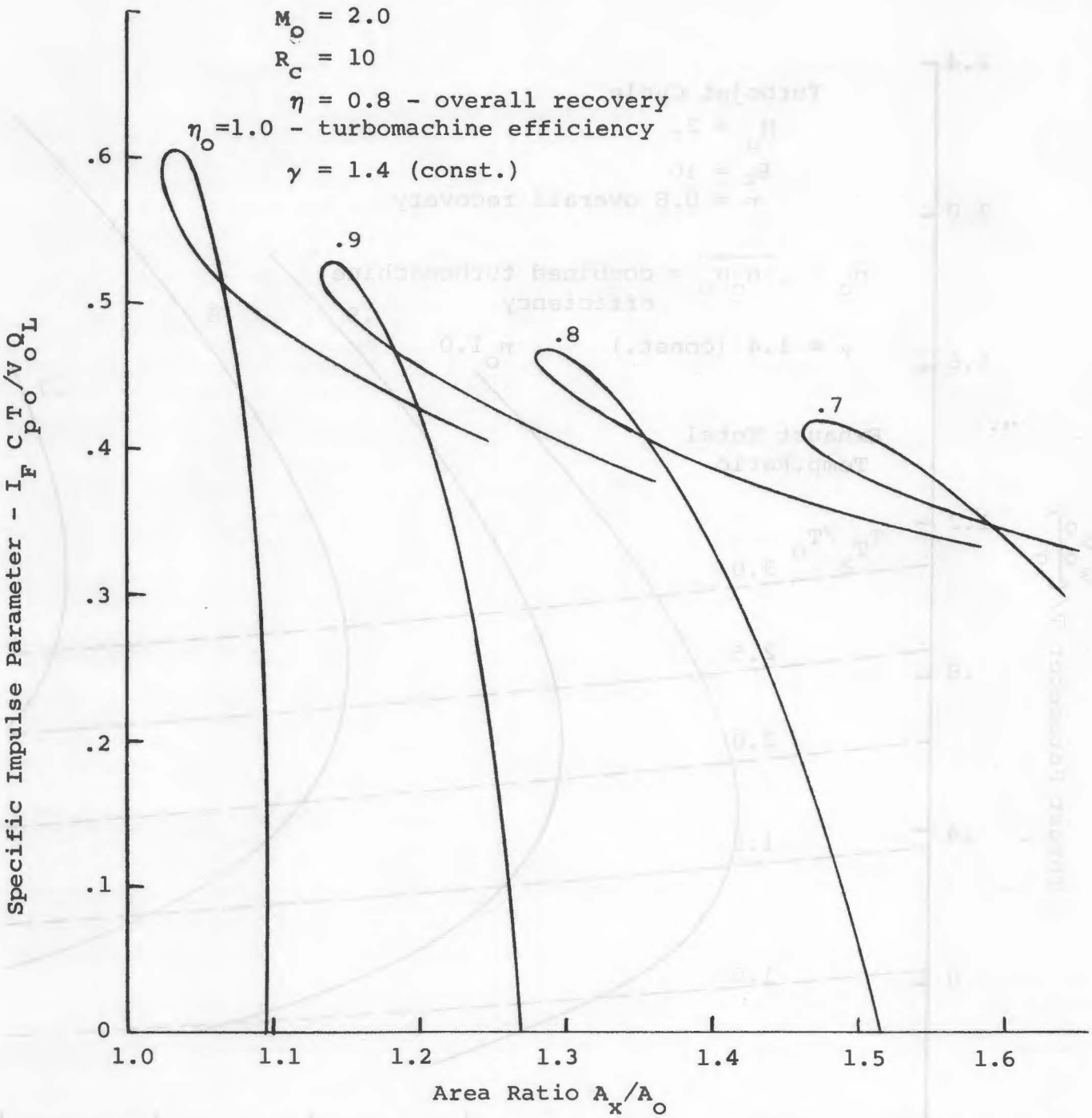

FIGURE 39 - Variation of Specific Impulse with Exit Area for Various Turbomachine Efficiencies

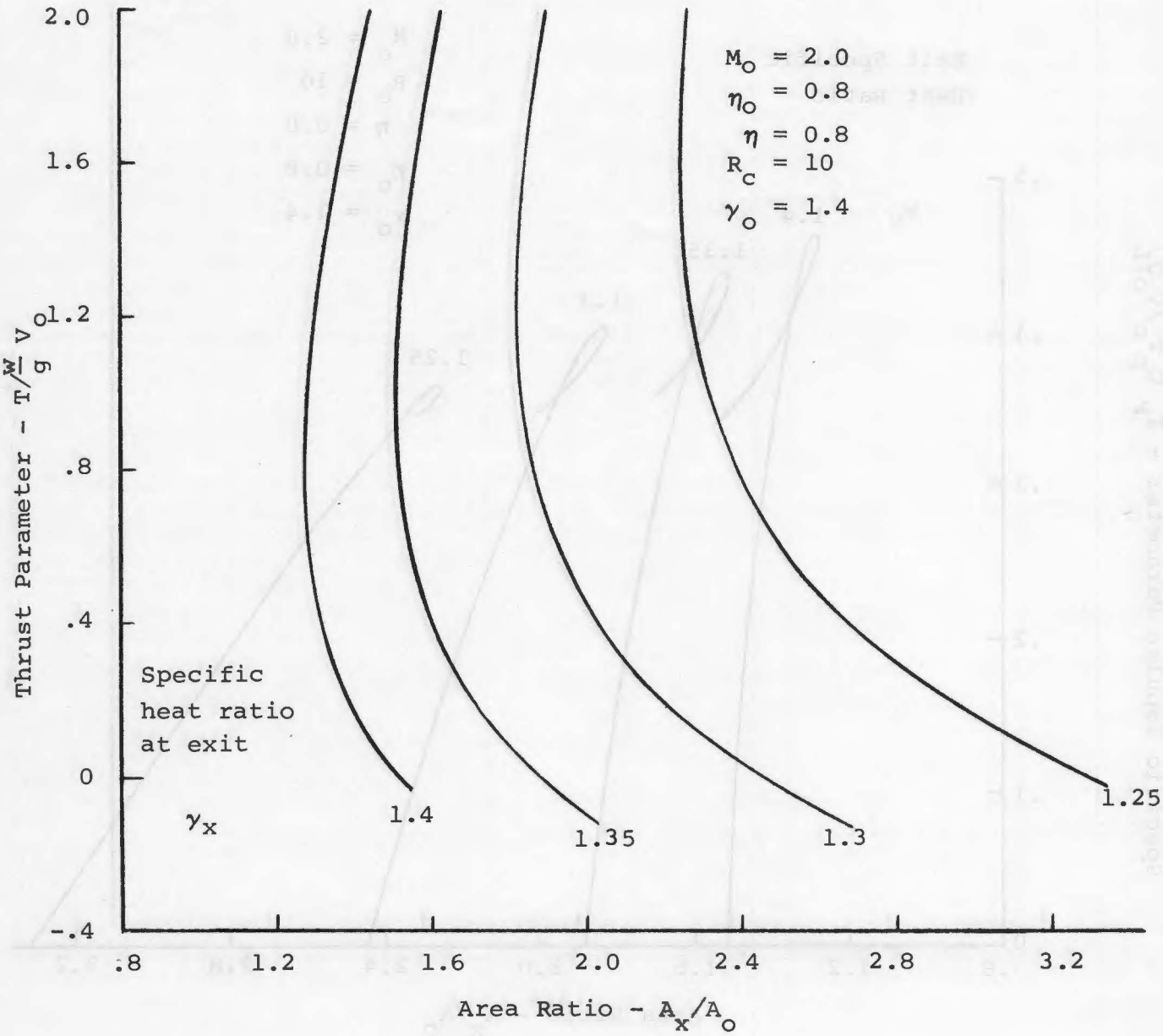

FIGURE 40 - Variation of Thrust with Exit Area for Various Exit Specific Heat Ratios

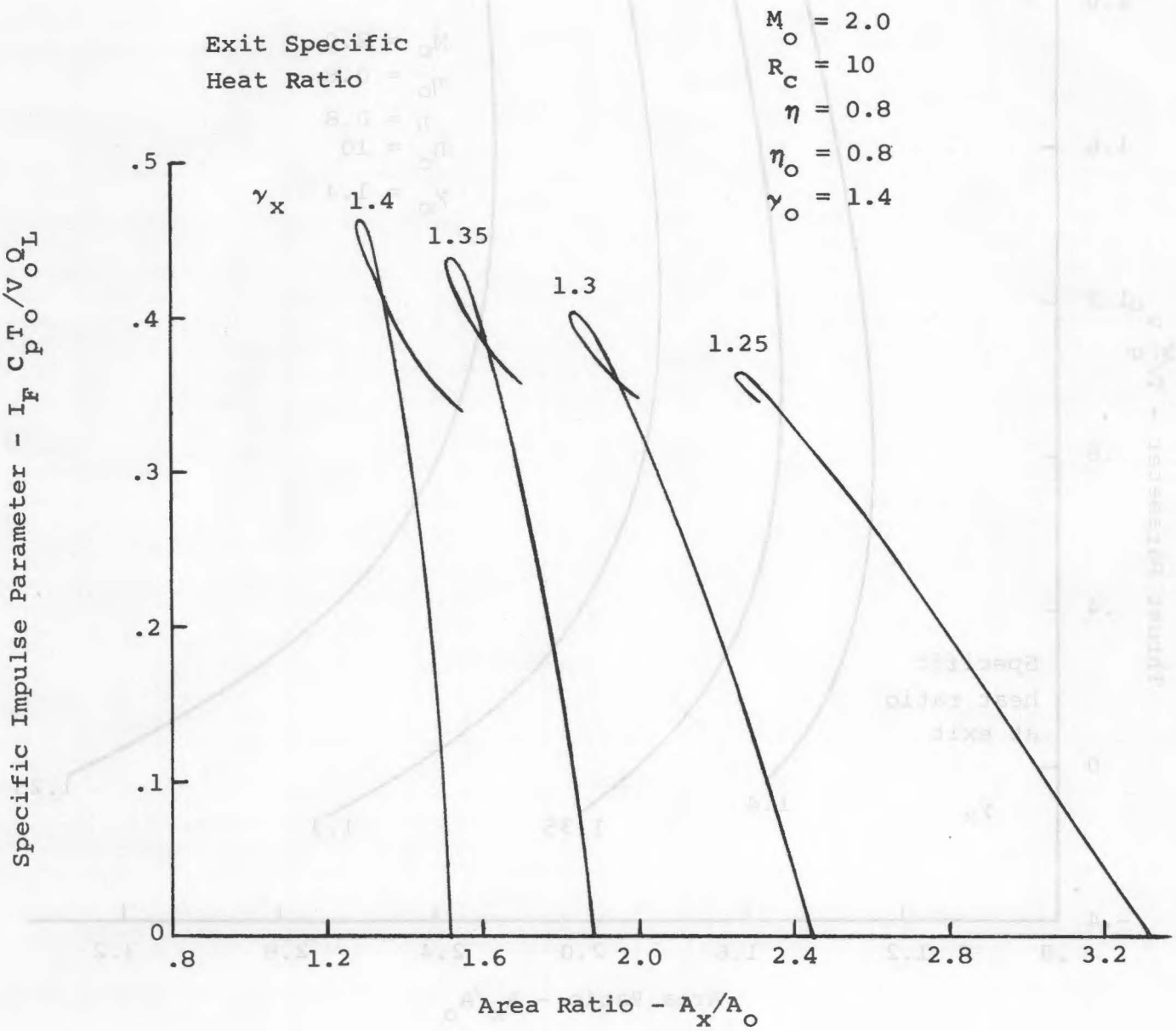

FIGURE 41 - Variation of Specific Impulse with Exit Area for Various Exit Specific Heat Ratios

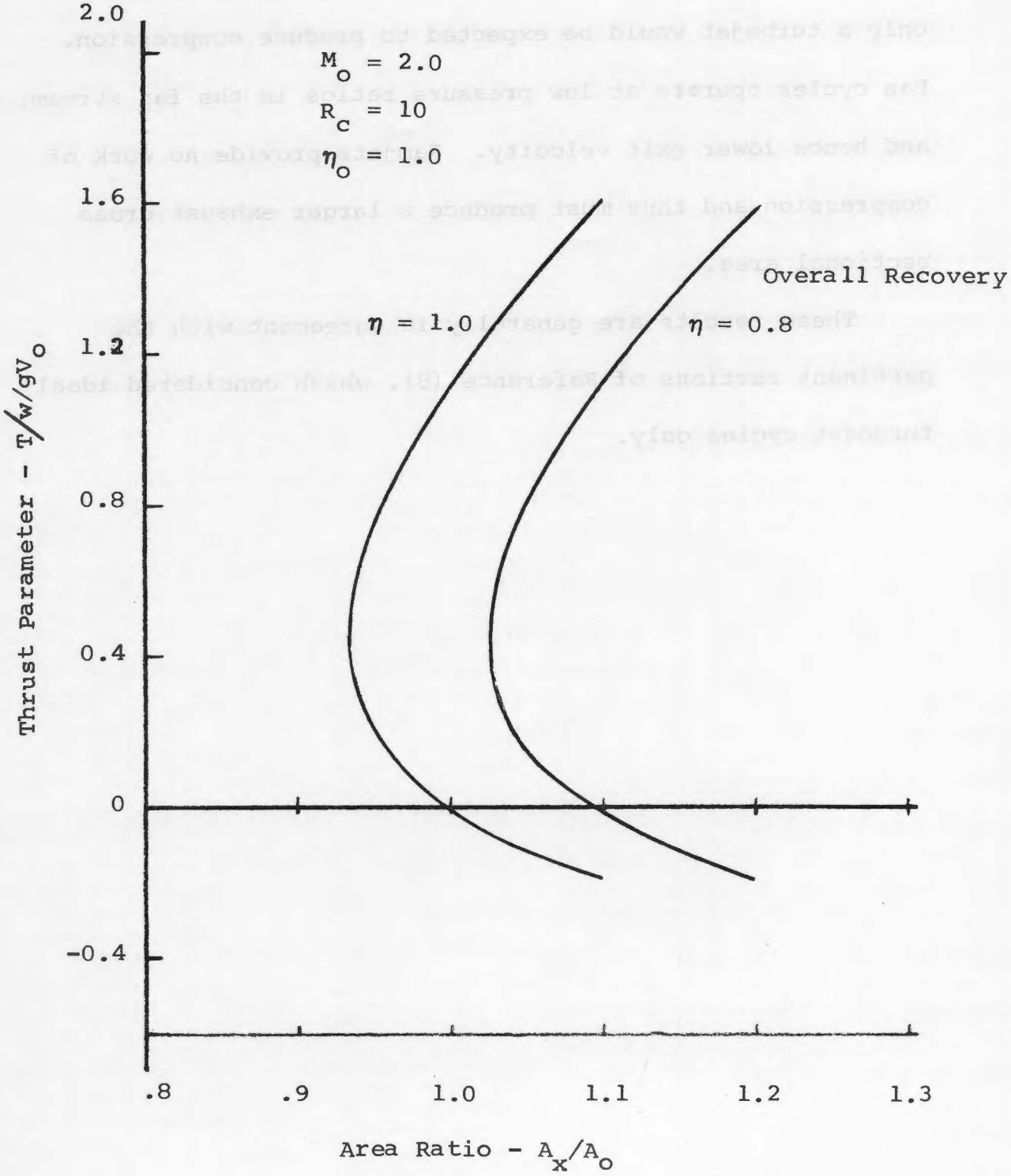

FIGURE 42 - Thrust/Area Relationship for Ideal Turbomachine Efficiency

Note also that, of the conventional engine cycles, only a turbojet would be expected to produce compression. Fan cycles operate at low pressure ratios in the fan stream, and hence lower exit velocity. Ramjets provide no work of compression and thus must produce a larger exhaust cross sectional area.

These results are generally in agreement with the pertinent sections of Reference (8), which considered ideal turbojet cycles only.

PENALTIES

It has been clear from the outset that any sonic boom alleviation scheme through air stream alteration would invoke some sort of penalty to the aircraft. Such a penalty could be in the form of reduced payload and/or range, i.e., a mission penalty, or alternatively, a penalty in terms of increased aircraft gross weight to perform the same mission. Since in many of these cases the weight penalties were an order of magnitude larger than the payload, the second approach was preferred. Moreover, if the sonic boom for the new, larger aircraft carrying the alleviation device were then recomputed, an assessment of the true merit of the device could be made in terms of sonic boom signature parameters alone.

Ground Rules - In order to estimate these penalties, the following assumptions were made:

(a)	mission time	5000 seconds
(b)	structural weight fraction	35%
(c)	specific fuel consumption	1.51 (hydrocarbon fuel) .65 (hydrogen fuel)
(d)	cruise L/D	7.3

The total weight penalty consists of the following increments:

- weight of consumables associated with boom alleviation

weight of additional structure required for both boom alleviation and additional propulsive fuel (assumption (b))

weight of additional propulsive fuel to overcome additional drag

The additional drag is composed of drag due to lift (due to additional weight), wave drag from the modified F-function, and ram drag from any air that was captured for combustion and/or mass addition.

Wave Drag Analysis - A detailed study of the analysis was made for several cases include the baseline, as follows

$$C_D = \frac{1}{S_{ref}} \int_0^{2\pi} \int_{-\infty}^{\infty} F(x,\varphi)\, dx d\varphi \qquad (27)$$

Dividing the F-function into two parts, F_A and F_L, due to volume and lift respectively, and integrating with respect to φ, we obtain

$$C_D = \frac{\pi}{S_{ref}} \int_{-\infty}^{\infty} (2\, F_A^2(x) + F_L^2(x))\, dx \qquad (28)$$

If airstream alleviation effects are present in an axisymmetric configuration, they may be included in F_A. Effects similar to lift with a $\cos\varphi$ dependence may be included in F_L.

For the baseline aircraft, the total drag, as obtained from the cruise L/D, was found to be dominated by wave drag (~ 63%). Of the wave drag, approximately 60% resulted from the volume F-function and 40% from lift.

The drag coefficient for analytic F-functions such as the finite rise time prescription

$$F_{(x)} = 15/16\ Kx$$

may be readily computed. In the case of prescribed $S'(x)$, the drag coefficient is given by

$$C_{D_1} = \frac{15\ \pi}{64}\ \frac{S'}{x_1}1 \qquad (29)$$

when referred to the (axisymmetric) equivalent area of the phantom nose. By comparison, the drag coefficient of the baseline aircraft, referred to its equivalent base area, is about .07, or nearly an order of magnitude larger than typical values for Eq. (29).

The use of phantom bodies thus has the following effects on drag: the wave drag due to volume tends to be increased only slightly, since the F-function values tend to be lower because of the integration over longer effective aircraft lengths (increased fineness ratios). The wave drag due to lift tends to be increased drastically, since according to the ground rules

chosen, all the weight penalty is borne by the same lifting length, and the drag increases as the square of F.

These effects showed a tendency for the L/D to remain roughly constant as the weight penalties were applied. As a simplification, this assumption was then adopted for the remaining cases. This allows the penalized aircraft to have larger dimensions in line with the increased gross weight.

Weight Calculations - The gross weight of the penalized aircraft is then given by

$$W_p = 600{,}000 + \Delta W_p$$

$$\Delta W_p = W_{boom} + .35(\Delta W_s) + \frac{SFC(\Delta W_p)}{L/D} \qquad (30)$$

Using the numerical values for SFC and L/D given above

$$W_p = 600{,}000 + \frac{w_{boom}}{.365} \qquad (31)$$

In order to arrive at estimates for the penalized aircraft from weight, relationships between w_{boom} and the required equivalent cross-sectional area increase are required for the various air-stream alteration methods. These are given in Table III, based on the previously derived results for heat and mass addition.

TABLE III

WEIGHT PENALTY - EQUIVALENT AREA FACTORS

Flow Field Modification Scheme		Weight Penalty, ΔW Hydrocarbon main Engine Prop. Fuel	Hydrogen Fuel
Free Combustion:	hydrocarbon	1465 ΔS	
	hydrogen	530 ΔS	366 ΔS
E/L Mass Addition:	ram air	1400 ΔS	
	hot hydrogen	780 ΔS	540 ΔS
Lift Distribution		156 ΔS (no penalty for device, which is self supporting)	

TABLE IV

SONIC BOOM SIGNATURE IMPROVEMENT PENALTIES

Signature Improvement	Add'l Eff. Area Req'd ft^2	Add'l Weight Penalty max	min	ΔP increase max	min
		10^6 lbs		psf	
front shock-just finite rise time	1043	1.43	.38	1.28	.37
front-rear shock-just finite rise time	1353	1.89	.50	1.43	.47
.040 sec. warning	244	.35	.09	.34	.09
two level jump ~ 1 psf	1000	1.40	.37	1.18	.35
.70 psf shock ΔP	1187	1.66	.43	1.46	.42

Since hydrogen (a pollution-free fuel) was considered for a mass injectant, it was also considered for direct combustion schemes in Table III. As a further improvement, the use of hydrogen fuel to supply propulsive power for the penalty drag was considered, which would revise Eq. (31) as

$$W_p = 600{,}000 + \frac{W_{boom}}{.527} \qquad (32)$$

The force field mechanism selected for comparison in Table III is a lift distribution, which of course has no direct weight penalty for the baseline aircraft since it is self-supporting. The penalty factor given in Table III is for the drag of the lift distribution, assuming L/D = 7.3. However, since this lift distribution is to be deployed along Mach lines ahead of the baseline aircraft, there may be a substantial control surface penalty invoked in order to maintain stability and overcome the moments involved. This could also be true for the vertical thermal fin of Reference (6),for example.

For this reason, the practical use of lift distributions in creating the area distributions required for signature improvement was limited to the penalty aircraft concept, described below.

Increased ΔP Calculations - To complete the penalty concept, the effect of the gross weight increase on the sonic boom must be taken into account. Baseline signatures were computed for various gross weights, by modifying the lift portion of the F-function, as shown in Figure 43. At the higher weights, the curve is asymptotic to the $\sqrt{w}$ relation, as predicted by theory. Figure 43 may thus be used to estimate increases in overpressure resulting from increased gross weight.

Figure 43 was generated by considering a fixed length aircraft with varying wing loading. The gross weight, penalty could also be considered to result in a scaled-up airplane, having the same area development and hence F-function but increased length. By Eq. (1), this would also result in a $\Delta p/p \sim \sqrt{w}$ relationship, in the far field.

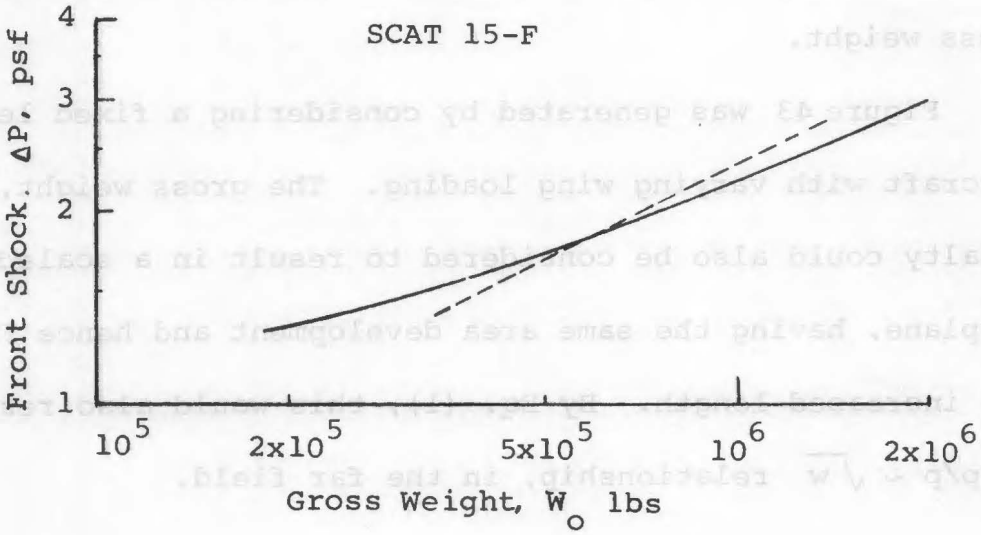

FIGURE 43- Variation of Baseline Front Shock ΔP with Gross Weight

In the case of matching a phantom body slope to a specific value of S' of the baseline, changes in the baseline lift distribution would change the value of S' for matching. This would have a strong bearing on the requirements for complete shock elimination, for example. An evaluation of this effect was made by deriving relationships for ΔS as a function of the S' match point

$$(\Delta S = 143\ S')$$

and for F as a function of W_o

$$(F/F_o = 1.4\ W_o/10^6)$$

and making the assumption

$$S'/S'_o = F/F_o\ .$$

This allows a closed form solution for the limiting* proportionality factor between ΔS and ΔW_o (Table III), which was found to be 625. Thus only the hydrogen-fueled air stream alteration schemes would be capable of finite rise times with the baseline aircraft carrying the weight penalty, to the limit of infinite gross weight. (In this connection it should be mentioned that this very crude penalty analysis takes no account of the hydrogen fuel volumetric storage requirements, which could

---

* gross weight tends to infinity

conceivably have a large effect on the aircraft volume distribution and thus effect additional boom penalties.)

Table IV then summarizes the penalties in terms of maximum ($\Delta W = 1400\ \Delta S$) and minimum ($\Delta W = 366\ \Delta S$) gross weights and ΔP increases for various types of signature modifications. These penalties are tolerable only for the "warning" concept. Note that the additional ΔP-due-to-gross-weight penalty tends to negate the pressure rise minimization schemes. Because of the strong effect of rise time on perceived noise (Figure 6), the ΔP penalty may not be important for finite rise time signatures. However, the magnitude of the gross weight penalty is a formidable challenge in any event.

Penalty Aircraft Concept - The foregoing discussion shows how assigning the weight penalty to the baseline aircraft generally results in a worsening rather than improvement of the sonic boom signature. However, if this weight penalty is borne by a separate aircraft flying near the baseline aircraft in its disturbance field, then the weight penalty may be distributed as lift, forming a portion of the effective area required for the alleviation scheme. This concept was intimated above in the discussion of the proper use of force fields.

While the design of such a penalty aircraft is generally beyond the scope of this effort, a rough estimate of the contributions of various portions of the total required effective area distribution was made, using the same aircraft, performance ground rules as above, as follows:

$$W_o = W_{boom} + .635\ W_o \qquad \text{(hydrocarbon fuel)}$$

$$W_{boom} = \Delta S_m \times 1400 \qquad \text{(mass addition of ram air)}$$

$$\Delta S = \Delta S_m + \Delta S_{lift} = \Delta S_m + W_o/554$$

$$\Delta S = 2.08 \times 10^{-3}\ W_o$$

This leads to penalty aircraft gross weights between 100,000 and 650,000 lbs., depending on the signature "improvement" selected, and based on the use of ram air as a mass injectant for the air stream alteration scheme. If hydrogen combustion were used for both boom alleviation and penalty aircraft propulsion, the gross weights would be reduced to 75,000 and 420,000 lbs., respectively. For the ram air concept, only about 13% of the required effective area is supplied by mass injection, the remainder being due to lift; for the hydrogen combustion concept, 44% of the required area is supplied by the combustion scheme.

In this concept, the penalty imposed on the baseline aircraft would only consist of that hardware (and weight) required for deployment and control of the penalty aircraft.

Since the size of the penalty aircraft approaches that of the baseline in many cases, a logical question arises as to the benefits to be gained from flying two baseline aircraft "in formation," one below and ahead of the other so that the two area developments combine into one F-function of generally lower magnitude. Investigation of this concept quantitatively was considered beyond the scope of this effort, but the advantage of the scheme may be seen qualitatively by considering the "figure of merit" given by Seebass in Reference (1). This relation postulates that increases in length that are accompanied by increases in weight in proportions less than $\ell^{3/2}$ will show a reduced overpressure. Since "formation" flying could in theory show a doubling in length at a cost of only doubling in weight, the overpressure could be reduced by a factor $\sqrt{2}$.

Area Distribution - All of the foregoing assumes that the precise desired equivalent area distribution may be obtained via the selected mechanisms, i.e., there is no "wasted" equivalent area. Since this will not in general be true for real situations, these results represent ideal or minimum levels.

CONCLUSIONS

Based on the analyses presented above, the following conclusions are suggested:

(a) Use of air stream alteration schemes to modify a complete sonic boom signature (i.e., complete shock elimination, substantial shock pressure rise reduction, etc.) will require gross weight penalties on the order of 100% of the baseline aircraft weight, and thus is not considered practical.

(b) A precursor signal warning of the arrival of the sonic boom may be generated through airstream alteration at substantially less gross weight penalty, and thus may be a practical scheme. The benefit to be derived from such a warning must be established through psychoacoustic studies of startle phenomena.

(c) The weight penalty (to the baseline aircraft) for boom alleviation may be substantially reduced through the concept of a separate penalty aircraft, the lift distribution of which is used to form part of the boom alleviation effective area. This concept may be extended to include payload-carrying penalty aircraft or two SST's flying "in formation" in such a way as to create favorable signature interference.

RECOMMENDATIONS - EXPERIMENTAL CONFIRMATION

One of the desired results of this program of investigation is recommendations for experimental research to substantiate the findings. Such recommendations of course hinge upon the conclusions, presented above, which point out the general impracticability of modifying the entire signature through flow field effects. It is not recommended that experimental research be conducted to verify this generally negative conclusion. Nor is it considered necessary to verify the basic sonic boom theory experimentally; this has been accomplished through many comparisons of flyover and wind tunnel data with theory.

Startle Effects - The concept of reducing startle phenomena by means of a precursor or warning signal appears worthy of further investigation. This should begin with psychoacoustic tests on human subjects in order to define the requirements for a warning signal (amplitude, time delay) to be effective in reducing startle.

The primary requirement for such an experimental program is realism, both in the environment and in the test signals. The ideal would be to use flyover tests, but unfortunately they are not only generally prohibitively expensive but suffer from lack of signal control. In particular, signal rise time may not be varied at will.

A simulator is thus required for precise control of the test signals. It should be capable of producing full scale wave forms and have a test section large enough for human subjects in a variety of modes: i.e., sleeping, performing psychomotor tests, etc. The simulator of Reference (38) meets these requirements; there may be others available as well. Both indoor and outdoor environments should be simulated.

Such an experimental program would produce data on perceived loudness and/or annoyance for various signatures, including precursor warnings. These data would allow precise evaluation of the aircraft penalties involved in producing the desired wave form, using the data of Table III.

Mass Addition Experiments - One of the more surprising results of the investigation was the relative attractiveness of mass addition as a flow-field-altering mechanism. This results from the large "amplification factor" when boundary layer blowing is used. This result appears worthy of experimental verification.

Such a program could be conducted in a wind tunnel using subscale models, in the manner of Reference (39). Wind tunnel sonic boom testing techniques are now quite well established, and particularly suitable for evaluating relative effects, rather than absolute overpressure levels. Boundary

layer blowing is also particularly suitable for such experiments, since it is well described by theory and thus may be scaled in size with a high degree of confidence. Note that this is generally not the case with combustion phenomena which may be controlled by chemical kinetics.

The verification program would consist of probing a model flow field at distances limited by the wind tunnel walls. Microphones would be used to record the small pressure disturbances. The model skin would be porous, and means would be provided to control the mass flow rate of fluid through the skin. The skin porosity distributions would be tailored to provide a given pressure signal, based on the theoretical methods of this report.

Changes in pressure signal would be correlated with changes in mass injection rate during a given run. At the same time, the model position in the wind tunnel would be carefully monitored to insure that no attitude or dimensional changes occurred as a result of flow rate changes. The resulting data would serve to verify Figure 28 and Eq. (22).

Penalty Aircraft Concept - A final recommendation, although not experimental in nature, concerns the concept of a separate "penalty aircraft" to carry the boom alleviating materiel, fuel, etc., and preclude penalizing the baseline or revenue aircraft.

This concept, discussed in more detail above, appears sufficiently attractive to warrant further investigation, from a theoretical and aircraft design standpoint. Aircraft superposition experiments, could of course,be carried out in a wind tunnel later as verification of the theoretical results, particularly as the separation between the two aircraft becomes significant.

REFERENCES

1. Seebass, A. R., "Sonic Boom Minimization,"Proceedings, 2nd Sonic Boom Symposium, Acoustical Soc. of America, Houston, 1970.

2. Cahn, M. S., and Andrew, G. M., "Electro-Aerodynamics in Supersonic Flow," AIAA Paper 68-24, 1968.

3. Cheng, S. I. and Goldburg, A., "An Analysis of the Possibility of Reduction of Sonic Boom by Electro-Aerodynamic Devices," AIAA Paper 69-38, 1969.

4. Chuan, R. L., "Sonic Boom Ameliorization," U. S. Patent 3510095.

5. Miller, D. S. and Carlson, H. W., "A Study of the Application of Heat or Force Fields to the Sonic Boom Minimization Problem," NASA TN D-5582, Dec. 1969.

6. Batdorf, S. B., "On Alleviation of the Sonic Boom by Thermal Means," AIAA Paper 70-1323, 1970.

7. Resler, E. S., "Lifting Aerodynamic Coefficients with No Sonic Boom," AFOSR-UTIAS Symp. on Aerodynamic Noise, Toronto, May 1968.

8. Galanis, N. T., "Power Plant Design for the Reduction of the Sonic Boom Generated by Supersonic Transport Aircraft," PhD. Thesis, Cornell University, June 1970.

9. Rethorst,S., et al., "Reduction of Shock Wave Strength by Means of Non-Uniform Flow," AFFDL-TR-69-62, Part I, 1969.

10. Hayes, W. D., et al., "Sonic Boom Propagation in a Stratified Atmosphere,with Computer Program," NASA CR-1299, April 1969.

11. George, A. R. and Plotkin, K. J., "Sonic Boom Waveforms and Amplitudes in a Real Atmosphere," AIAA J., 7, No. 10, p. 1968-1981.

12. McLean, F. E., "Some Nonasymptotic Effects on the Sonic Boom of Large Airplanes," NASA TN D-2877, June 1965.

13. Jones, L. B., "Lower Bounds for Sonic Bangs in the Far Field," Aeronautical Quarterly, Vol. XVIII, Feb. 1967.

14. Chu, B. T., "Pressure Waves Generated by Addition of Heat in a Gaseous Medium," NASA TN 3411, June 1955.

15. Tamagno, J., Slutsky, S. and Chu, B. T., "Research on Combustion Processes at High Speed," GASL TR-682, AFOSR 68-0467, 1968.

16. Kryter, K.D., "Laboratory Tests of Physiological Reaction to Sonic Booms," J. Acoustical Soc. of America, 39, No. 5, Part 2, 1966, pp. 565-572.

17. Nixon, C. W. and Borsky, P. N., "Effects of Sonic Boom on People," St. Louis, Mo., 1961-1962, J. Acoustical Soc. of America, 39, No. 5, Part 2, 1966, p. 557.

18. Lundberg, B., "The Economy and Sonic Boom of the Sea-Limited SST," BL Report No. 137, also presented at 7th Congress of the Int'l Council of Aeronautical Sciences, September 1970.

19. Wiggins, J. N., Jr., Effects of Sonic Boom, pub. by J.H.Wiggins Co., Palos Verdes Estates, California, 1967.

20. Lin, Sui, "Sonic Boom Analogues for Investigating Indoor Waves and Structural Response," UTIAS TN 158, November 1970.

21. Howell, C.S., et al., "Sonic Boom Consideration in Aircraft Design," Boeing Company Paper.

22. George, A. R., "Lower Bounds for Sonic Booms in the Midfield," AIAA J. 7, No. 8, 1969, pp. 1542-1545.

23. Hayes, W. D., et al., "Theoretical Problem Related to Sonic Boom," Pub. in Proc. 3rd Conference on Sonic Boom Research, NASA SP-255, 1971.

24. Seebass, A. R., "Sonic Boom Theory," J. Aircraft 6, No. 3, 1969, p. 181.

25. Leshowitz, B., "Measurement of the Two-Click Threshold," J. Acoustical Soc. of America, 49, Part 2, February 1971, p. 462.

26. Whitham, G. B., "On the Propagation of Weak Shock Waves," J. Fluid Mechanics, 1, 1956, p. 290-318.

27. Gerry, E. T., "Gasdynamics Lasers," AIAA Paper 71-23, January 1971.

28. Patel, C. K. N., "High Power Carbon Dioxide Lasers," Sci. Amer., August 1968.

29. Pimentel, G. C., "Chemical Lasers," Scientific American, 214, 1966.

30. Hertzberg, A., et al., "Photon Generators and Engines for Laser Power Transmission," AIAA Paper 71-106, Jan. 1971.

31. Handbook of Geophysics, U. S. Air Force, Publ. by McMillan Co., 1960.

32. Fernandez, F.L., and Zukoski, E.E., "Experiments in Supersonic Turbulent Flow with Large Distributed Surface Injection," AIAA J 7, No. 9, Sept. 1969.

33. Economos, C., "On The Applicability of Transformation Theory to Variable Property Turbulent Boundary Layers with Pressure Gradient and Heat and Mass Transfer," Sumposium on Compressible Turbulent Boundary Layers, Langley Research Center, NASA SP-216, Dec. 1968, Also GASL TR719, April 1969.

34. Edelman, R., and Fortune, O., "A Quasi-Global Chemical Kinetic Model for the Finite Rate Combustion of Hydrocarbon Fuels with Application to Turbulent Burning and Mixing in Hypersonic Engines and Nozzles," presented at the AIAA 7th Aerospace Sci. Meeting, Jan. 20-22, 1969, AIAA Preprint No. 69-85.

35. Lipfert, F.W., "Mixing Chamber Design Study," NASA CR 114286 (GASL TR 751) March 1971.

36. Minck, R.W., "Optical Frequency Electrical Discharge in Gases," J. Appl. Phys. 35, 1964, P. 252.

37. Sutton, George, Private Communication, July 1971.

38. Tomboulian, R., "Research and Development of a Sonic Boom Simulation Device," GASL TR-713, NASA CR-1378, Nov. 1968.

39. Carlson, H. W. and Morris, O. A., "Wind Tunnel Sonic Boom Testing Techniques," Presented at AIAA Aero. Testing Conference, Los Angeles, California, September 21-23, 1966.

ACKNOWLEDGMENT

The particular contributions of Drs. S. Slutsky and C. Ruger, and of Messrs. J. Schneider, R. Fort and A. Marino, are gratefully acknowledged, as well as those of other members of the GASL technical staff whose expertise was drawn upon in the course of this project.

In addition, the valuable consultation of Dr. A. R. Seebass is acknowledged.

ACKNOWLEDGEMENT

The particular contributions of Drs. S. Slutsky and C. Ruger, and of Messrs. J. Schneider, R. Fort and A. Marino, are gratefully acknowledged, as well as those of other members of the GASL technical staff whose expertise was drawn upon in the course of this project.

In addition, the valuable consultation of Dr. A. R. Seebass is acknowledged.